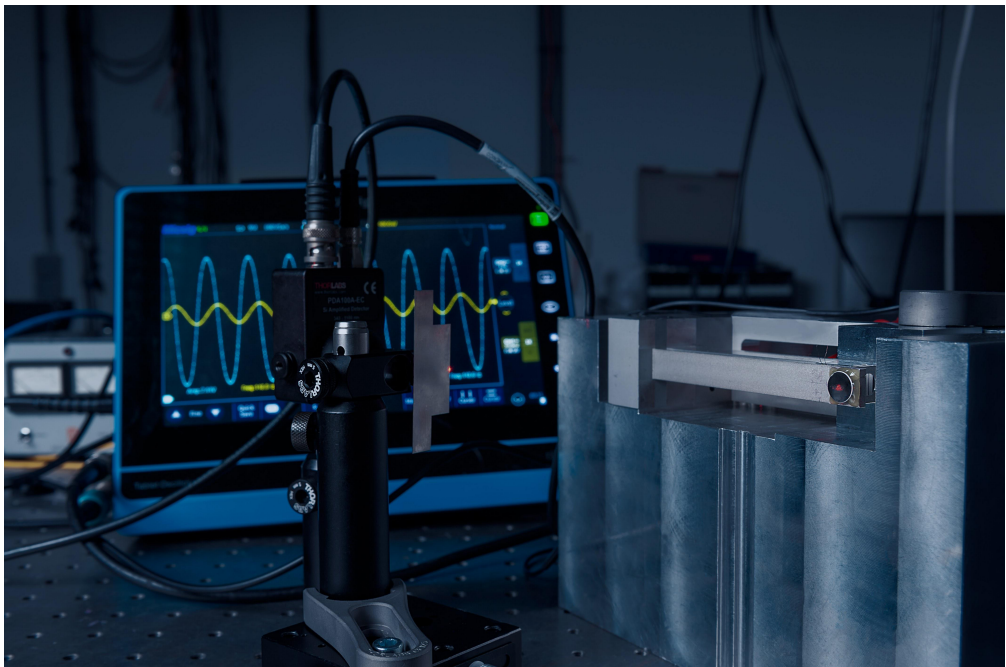


## Department of Precision and Microsystems Engineering

### Design of a Tunable Resonant Scanning Mirror

Jiajin Li

Report no : 2020.068  
Coach : Ir. J.P. Kappelhof  
Professor : Dr.ir. R.A.J. van Ostayen  
Specialisation : Opto-Mechatronics  
Type of report : Master Thesis  
Date : 17 December, 2020



# Design of a Tunable Resonant Scanning Mirror

By

**Jiajin Li**

in partial fulfilment of the requirements for the degree of

**Master of Science**

at the Delft University of Technology,  
to be defended publicly on Thursday December 17, 2020 at 13:30.

|                   |                            |                           |
|-------------------|----------------------------|---------------------------|
| Student number:   | 4898281                    |                           |
| Supervisor:       | Ir. J.P. Kappelhof         |                           |
| Thesis committee: | Dr.ir. R.A.J. van Ostayen, | TU Delft, chair           |
|                   | Ir. J.W. Spronck,          | TU Delft                  |
|                   | Ir. J.P. Kappelhof,        | TU Delft                  |
|                   | Prof. dr. G. Vdovin        | TU Delft, external member |

An electronic version of this thesis is available at <http://repository.tudelft.nl/>.

# SUMMARY

Scanning mirror is a widely used device in many optical systems to position the reflected beam. Existing products include galvanometer and resonant scanner. They are intended for accurate positioning at low frequency range and fast scanning at specified high frequency respectively. However, when a wide frequency range is involved, they might not be able to fulfill requirements. To solve this generic issue, Hittech starts to research new alternatives and attempt to cover a wide frequency range of 500 - 5k Hz.

To identify potential solutions, a welled-rounded literature review is conducted on resonant frequency tuning methods, scanner mechanism and dynamic balancing. However, no example of frequency tuning device is found for such a wide frequency range.

In this thesis, a novel solution is proposed, by tuning resonant frequency and exciting higher order modes to cover the intended frequency range. A flexure mechanism is designed, where the scanner contains a cantilever as resonator, and a cut-leafspring as hinge guiding to achieve 1 DoF resonant scan. Resonant frequency is tuned by clamping different positions of the cantilever by two surfaces with large radius of curvature, and sliding could be enabled by DLC coating. Concept and detailed design are evaluated by finite element modelling and a prototype is built. The test results show a good match with the simulation. The intended frequency range could be covered and the reflected beam could achieve a scanning angle of  $1\text{ mrad}$ . Unwanted motions of the mirror are verified and limited within the requirement with large margins, and hence could be negligible for operation.



# PREFACE

This project marks the end of my master study at TU Delft. Now looking back for the past two and a half years, this is really an amazing adventure. Still remember two and a half years ago, the first step into the Netherlands, a bit curious and a bit nervous. That was one of the most correct choices I have made, and I felt so lucky as a student at PME, where I made lots of friends and grew together, where I acquired impressive knowledge, and where I found my strong passions in the field of precision mechatronics. Every moment of life in Delft would become a precious experience and unforgettable memory in my life.

Hereby, I would like to express my sincere gratitude to my supervisor Pieter Kappelhof for providing me with such a great opportunity to work on this challenging project and to experience the Dutch working culture. Also many thanks to Lennino Cacace, you two really guide me into the field of Optomechatronics! Thanks for the countless inspirations and suggestions from the regular discussion to shape this project. I learn a lot from you two, not only technical knowledge but also the ways of thinking, the approach to deal with issues, and etc. You are the two most influential people in my study at Delft, and the time working with you would for sure become an invaluable experience for my future career. My appreciation also goes to Thomas Ooms who gives me numerous supports, especially in Optics; and to Ron van Ostayen for the very effective advice in consol simulation. Many thanks to Marc Buitenhuis and Casper van Wezel for the help in measurement and lab issues; Joep Jonker and Bradley But for the hardware and proto machining; Jos van Driel and Rob Luttjeboer for providing measurement equipment; Arjan Brand for the excellent photographs; and the Optomechatronics group for all the helpful inputs. Special thanks to Just Herder, Hassan HosseinNia, Danny de Gans, Jo Spronck, Volkert van der Wijk and Peter Steeneken, even we only had one or two discussions, those points and information are really critical; and Eveline Matroos, a kind and patient person who helps me deal with lots of problems in my study program.

I would also like to thank my beloved Ning Fang for accompanying me through this, we have a great time in the Netherlands! Last but not least, I am very grateful to my families, who always stand behind me with unlimited supports and love!

Student life in the Netherlands is like a sweet dream. Now to awake it, let me end with this thesis.

*Jiajin Li*  
*Delft, December 2020*



# CONTENTS

|          |   |           |
|----------|---|-----------|
| <b>1</b> | <b>Introduction</b>                                   | <b>1</b>  |
| 1.1      | Problem Statement . . . . .                           | 2         |
| 1.2      | Requirements . . . . .                                | 3         |
|          | References . . . . .                                  | 3         |
| <b>2</b> | <b>Literature Review</b>                              | <b>5</b>  |
| 2.1      | Review of resonant frequency tuning methods . . . . . | 6         |
| 2.1.1    | Introduction . . . . .                                | 6         |
| 2.1.2    | Changing Effective Length . . . . .                   | 7         |
| 2.1.3    | Changing Effective Mass . . . . .                     | 8         |
| 2.1.4    | Changing Transmission Ratio . . . . .                 | 10        |
| 2.1.5    | Adding Nonlinear Spring. . . . .                      | 12        |
| 2.1.6    | Adding Axial Load . . . . .                           | 15        |
| 2.1.7    | Changing Young's Modulus . . . . .                    | 18        |
| 2.1.8    | Changing Second Moment of Inertia. . . . .            | 20        |
| 2.1.9    | Discussion and Conclusion . . . . .                   | 20        |
| 2.2      | Review of Mechanisms of Resonant scanner . . . . .    | 24        |
| 2.2.1    | Cantilever Beam . . . . .                             | 24        |
| 2.2.2    | Torsional beam . . . . .                              | 25        |
| 2.2.3    | Crossed Flexure . . . . .                             | 27        |
| 2.2.4    | Notch Flexure . . . . .                               | 29        |
| 2.2.5    | Actuation . . . . .                                   | 30        |
| 2.2.6    | Discussion and Conclusion . . . . .                   | 33        |
| 2.3      | Review of dynamic balancing strategies. . . . .       | 35        |
| 2.3.1    | Reactionless Design . . . . .                         | 35        |
| 2.3.2    | Separated Balancing Mechanism . . . . .               | 36        |
| 2.3.3    | Connection Point . . . . .                            | 37        |
| 2.3.4    | Duplicate Mechanism . . . . .                         | 38        |
| 2.3.5    | Discussion and conclusion. . . . .                    | 38        |
|          | References . . . . .                                  | 40        |
| <b>3</b> | <b>Objective</b>                                      | <b>47</b> |
| 3.1      | Project Goal. . . . .                                 | 47        |
| 3.2      | Approach . . . . .                                    | 47        |
| 3.3      | Thesis Outline . . . . .                              | 48        |

---

|          |  |            |
|----------|--|------------|
| <b>4</b> | <b>Paper on Design of a Tunable Resonant Scanning Mirror</b> | <b>49</b>  |
| <b>5</b> | <b>Supplementary Material: Concept Design</b>                | <b>63</b>  |
| 5.1      | System concept . . . . .                                     | 63         |
| 5.2      | 1 DoF Resonant Scanner Mechanism . . . . .                   | 65         |
| 5.2.1    | Resonator . . . . .  | 65         |
| 5.2.2    | Guiding Hinge . . . . .                                      | 68         |
| 5.3      | Frequency Tuning Mechanism . . . . .                         | 72         |
| <b>6</b> | <b>Supplementary Material: Dimension Design</b>              | <b>75</b>  |
| 6.1      | Scanner Mechanism . . . . .                                  | 75         |
| 6.2      | Frequency Tuning Mechanism . . . . .                         | 79         |
| <b>7</b> | <b>Supplementary Material: Prototype and Test Setup</b>      | <b>87</b>  |
| 7.1      | Scanner Setup. . . . .                                       | 87         |
| 7.2      | Coil Design . . . . .  | 88         |
| 7.3      | Test Setup . . . . .   | 89         |
| <b>8</b> | <b>Supplementary Material: Test Result</b>                   | <b>91</b>  |
| 8.1      | Resonant scan and tuning performance test . . . . .          | 92         |
| 8.2      | Verification of unwanted motion . . . . .                    | 97         |
| <b>9</b> | <b>Conclusions and Recommendations</b>                       | <b>101</b> |
|          | <b>References</b>  | <b>103</b> |



# 1

## INTRODUCTION

Scanning mirror is often used in optical scanning device to change the direction of the beam in a scheduled way[1]. It is widely used in the applications of optical communications, material processing, microscope system, and etc[2, 3]. Conventional scanner is usually in a galvanometric configuration, shown as Fig. 1.1a. A mirror is mounted on a servo motor, and suspended by ball bearing or flexure[4]. With closed-loop control system, it could achieve angular positioning with high accuracy and resolution[4]. However, when operating at high frequency, high driving power is often needed, which means high energy consumption. And due to large rotational moment of inertia and nonlinear motion at high speed scanning, distortion in output could be expected[7, 8].

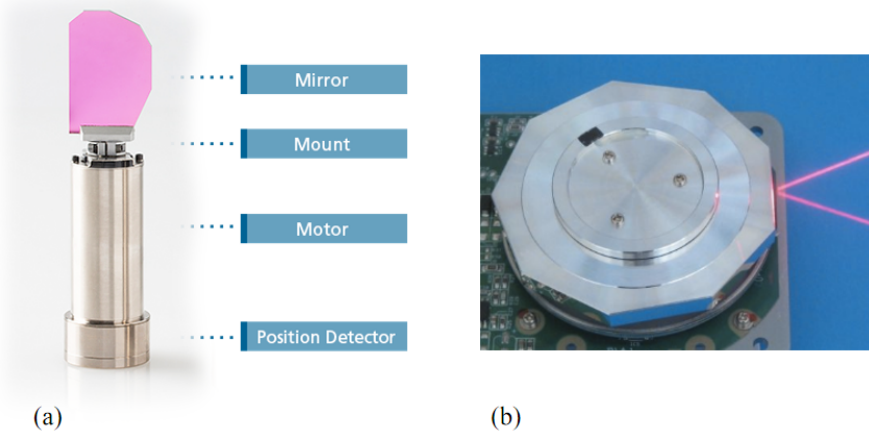


Figure 1.1: (a). A galvanometer scanner from Cambridge Technology[5] and (b) a polygon scanner from Precision Laser Scanning[6].

To achieve stable high frequency scanning, polygon scanner could also be an option, shown as Fig. 1.1b, which could reach a few kilo hertz, but scanning is discontinuous[9],

and when the mirror size is large but scanning angle is small, the corresponding polygon would be fairly large with many faces. Resonant scanner could be used as an alternative, which has distinguished features including high rigidity, low mass and high Q-Factor[10]. By making use of resonance, it is easy to achieve high frequency oscillation with low power input and simple electrical circuit[11]. However, most commercially available products are designed to operate at the specified frequency. Even some of their resonant frequency might be adjustable, but it is intended for error correction in a small range, which could be caused by manufacturing error, mechanical wear, change of working conditions and etc[12].

## 1.1. PROBLEM STATEMENT

In an application of electron scanning microscope, shown as Fig. 2.3, multiple electron beams serve as an excitation of fluorophore label in a biological sample, and fluorescence light would be generated at the illumination place. These light rays are captured by a lens system and then get focused. Between the last lens and the plane of focal points, a mirror is used to reflect the lights such that they get focused at the corresponding detector of each electron beam source. The scanning motion of the electron beam could deviate the reflected focal points, and thus the mirror should rotate to compensate for this such that each spot at the detector pinhole remains steady and does not wobble during the scanning process.

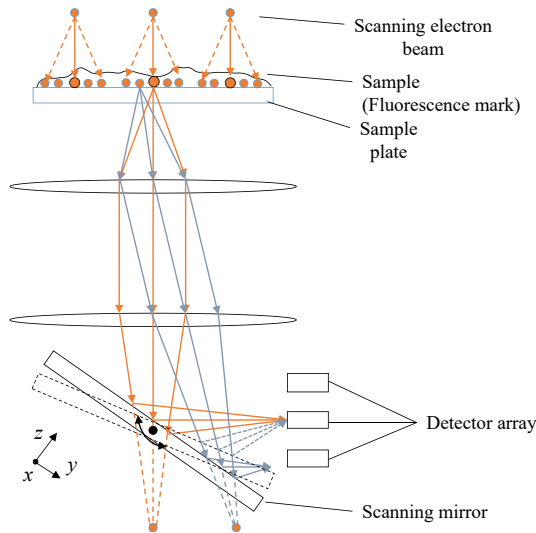


Figure 1.2: Basic system principle, application background of tunable resonant scanning mirror.

One of the most important components in traditional scanning microscopes is a scanning mirror, in which galvanometer-based scanning mirror system is often used[13].

However, performance of the galvanometer scanner limits the speed of image acquisition [14]. Since the speed of the galvanometer scanner is often slower than the speed of many physiological processes, it is difficult to achieve live-cell imaging [14–16]. In order to acquire image faster, traditional microscopes should be re-engineering and integrated with other advanced scanning devices such as resonant scanner to be able to capture and uncover intricate phenomena that occur in many biological processes.

There are many factors influencing imaging, such as scanning speed [17]. A high scanning speed could shorten the dwell time of each pixel, which would cause a loss of spatial information and decrease the signal-to-noise ratio. While a slow scanning speed could achieve a high resolution image, but an increase in exposure time might cause damage to the sample, and photobleaching issue [17]. Usually, to capture a large size image with high resolution of fixed fluorescent specimens, a scan rate of 2 frame/s is typically used for an area covered by  $512 \times 512$  pixels. While to realize live-cell imaging, 20–30 frame/s is often needed [18]. Therefore, an appropriate scanning frequency should be able to select by users in different applications with different purposes.

## 1.2. REQUIREMENTS

The goal of this thesis is to design a mechatronics system of a tunable resonant scanning mirror, and requirements in terms of range of working frequency, motion, size and etc. should be satisfied. Some major requirements are listed below:

- **Range of working frequency:** The resonant scanner should be able to achieve any frequency in the range of 500–5k Hz.
- **Range of motion:** The reflected beam should be able to scan an angle in the range of 0 - 1 *mrad*. Noting that this means 0 - 0.5 *mrad*  $R_x$  rotation of the mirror.
- **Mirror Motion in Unwanted DoF:** Translation along optical axis  $d_z$ : <100  $\mu m$ , rotation  $R_y$  (orthogonal to scanning motion): <25  $\mu rad$ .
- **Beam Size:** Scanning mirror should be able to cope with a beam size of 11 mm diameter.
- **Size:** The size of the device should fit into a space of  $70 \times 70 \times 150$  mm.

## REFERENCES

- [1] H. Cho, *Optomechanronics: Fusion of Optical and Mechatronic Engineering*, CRC Press, Boca Raton, USA, 0-8493-1969-2, 2006.
- [2] Zhou. et al, *Design of Fast Steering Mirror Systems for Precision Laser Beams Steering, 2008 International Workshop on Robotic and Sensors Environments*, 978-1-4244-2594-5, 2008.
- [3] M. Hafeza et al, *Design, simulations and experimental investigations of a compact single mirror tip/tilt laser scanner*, *Mechatronics*, 10, 741–760, 2000.

- [4] R. P. Aylward, *Advanced galvanometer-based optical scanner design*, *Sensor Review*, 23, 216-222, 2003.
- [5] Cambridge Technology, "Technology/ Galvanometer", accessed at 7/12/2019. <https://www.cambridgetechnology.com/laser-beam-technology>.
- [6] Precision Laser Scanning, "Products/ Polygon Scanner", accessed at 3/2/2020. <https://precisionlaserscanning.com/start-of-scan-sos-detection-for-polygon-scan-heads/>.
- [7] S. Xiang et al, *Study on fast linear scanning for a new laser scanner*, *Optics Laser Technology*, 42, 42-46, 2010.
- [8] J. Xiang et al, *The precision improvement of the scanner in optical scanning imaging system*, *Optics Laser Technology*, 30, 109-112, 1998.
- [9] Redmond P. Aylward, *Advances and technologies of galvanometer-based optical scanners*, *Proceeding of SPIE 3787, Optical Scanning: Design and Application*, Denver, CO, U.S., July 2, 1999.
- [10] G. F. Marshall and G. E. Stutz, *Handbook of Optical and Laser Scanning, Second Edition*, Boca Raton, USA: CRC Press, 978-1-4398-0880-1, 2012
- [11] M. Burdenko et al, "Resonant scanner.", *U.S. Patent 5,528,411*, issued June 18, 1996.
- [12] J. I. Montagu et al, "Tunable resonant mechanical system.", *U.S. Patent 4,874,215*, issued October 17, 1989.
- [13] N. S. Claxton "Microscopy, Confocal," in *Encyclopedia of Medical Devices and Instrumentation, Second Edition*, New York: Wiley, 2006, pp.453.
- [14] J. Sanderson, "Optical Sectioning and Confocal Microscopy," in *Understanding Light Microscopy, First Edition*, New York: Wiley, 2019, pp.437.
- [15] S.W. Paddock, *Principles and practices of laser scanning confocal microscopy*, *Molecular Biotechnology*, 16, 127-149, 2000.
- [16] S. Choi et al, *Development of a high speed laser scanning confocal microscope with an acquisition rate up to 200 frames per second*, *Optics Express*, 21, 23611-23618, 2013.
- [17] A. Hamdoun and K. Foltz, *Echinoderms Part B, First Edition*, Academic Press, Cambridge, Massachusetts, 9780128170731, 2019.
- [18] D. B. Murphy "Confocal Laser Scanning Microscopy," in *Fundamentals of Light Microscopy and Electronic Imaging*, New Jersey: Wiley, 2001, pp.218.

# 2

## LITERATURE REVIEW

According to the design requirements discussed above, a literature review is conducted in this chapter to show the state of the art in the field of resonant frequency tuning methods and resonant scanner mechanism. Dynamic balancing strategies are also included since resonance could lead to large reactions. For each method, the principle is explained and some examples from the literature are presented to discuss the detailed operation and performance in the reality. Noting that review is mainly based on the context of macro-scale, due to the beam size requirement, and thus system could not be miniaturized into MEMS device. At the end of review of each field, summary overview tables are presented, listing advantages, disadvantages, and other properties. This review could help to identify potential solutions, and serve as a reference for mechanical design with features of resonance motion, stiffness tuning and dynamic balancing. It is concluded that, in terms of resonant frequency tuning, changing effective length could be effective, but no example of resonant tuning for such a wide range up to an order of magnitude at high frequency ( $kHz$ ) is found. Regarding resonant scanning mechanism, it is possible to fix the rotational axis by flexure such as crossed and notch flexure, which gives accurate scanning, and resonance is generated by a separated resonator. But one should be aware of over-constrained design. As for dynamic balancing, separated balancing mechanisms or heavy mass suspended by air mount to absorb reactions are found more applicable on compliant mechanism with resonator.

## 2.1. REVIEW OF RESONANT FREQUENCY TUNING METHODS

### 2.1.1. INTRODUCTION

Resonant frequency is a one of the key factors in many engineering applications, from energy harvesters to tunable resonant scanner. And the tunability property could enhance the performance and enable them to work in different environment and for different purposes[1]. As for energy harvesters, their resonant frequencies are designed to match the environment vibration, and tunable ones could cover a certain range of spectrum for practical use[2]; regarding tunable resonant scanner, a high scanning speed could be achieved by resonance motion and tunability feature could enable different speed selection[3]. In some application, frequency tuning is also used to correct errors which could be induced by manufacturing and environment conditions such as temperature, to increase robustness[4, 5].

Resonant frequency could be defined as

$$f_c = \frac{1}{2\pi} \sqrt{\frac{k_{eff}}{m_{eff}}} \quad , \quad (2.1)$$

where  $k_{eff}$  and  $m_{eff}$  is effective stiffness and effective mass of the system respectively. Hence, to tune the resonant frequency, it is often achieved by changing effective stiffness or mass. An extensive review is conducted mainly focused on macro scale systems, and founded literature are classified based on these two groups. To adjust effective stiffness, one could change effective length, add nonlinear spring, add axial load, change Young's Modulus and change second moment of inertia; and to alter effective mass, one could change center of gravity (CoG). Noting that stiffness adjustment method changing transmission ratio could only change perceived stiffness but not resonant frequency, and it is also mentioned. For each of the methods, the basic principle is explained following with some examples in the literature to discuss detailed operation and performance. Following conditions are chosen as criteria for investigation:

- Untuned frequency: This is the original resonant frequency of the system without applying any tuning action.
- Tuning range: This factor implies the range of working frequency, which could be defined by the maximum  $f_{max}$  and minimum  $f_{min}$  achievable frequency.
- Frequency ratio: This parameter  $f_r$  is the ratio between maximum and minimum achievable frequency, which could imply the order of magnitude of tuning. Similar to [6], it could be defined as

$$f_r = \frac{f_{max}}{f_{min}} \quad . \quad (2.2)$$

Besides, advantages and disadvantages of each tuning method are listed as a summary table and finally discussions and conclusions are presented.

### 2.1.2. CHANGING EFFECTIVE LENGTH

Considering mechanical systems with cantilever beams and tip mass, a general schematic could be shown as Fig. 2.1a. Perceived stiffness at the end tip of this system is defined as

$$k = \frac{3EI}{l^3}, \quad (2.3)$$

where  $E$  is Young's Modulus and  $I$  is second second moment of inertia. According to Eq. 2.1, resonant frequency could be calculated as [7],

$$f_c = \frac{1}{2\pi} \sqrt{\frac{Ewh^3}{4l^3(m + 0.24m_c)}}. \quad (2.4)$$

Where  $w$  is width,  $h$  is thickness,  $m$  is mass of tip mass and  $m_c$  is mass of cantilever. It could be noticed that by changing the clamping position, length of cantilever  $l$  could be varied and hence change the resonant frequency  $f_c$ . Noting that  $f_c$  is inversely proportional to  $l^{3/2}$ , which means sensitive change in  $f_c$  could be achieved by changing effective length  $l$ .

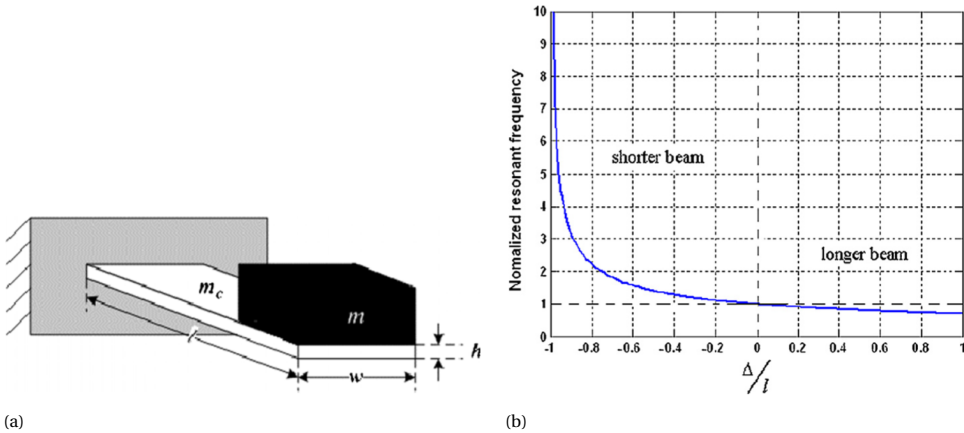


Figure 2.1: a. Schematic of cantilever with tip mass. b. Schematic of cantilever with tip mass[7].

Supposed that a change  $\Delta$  in length  $l$ , then the modified length  $l'$  could be expressed as  $l' = l + \Delta$ , and the mass of cantilever changes to  $m'_c = \rho whl'$ . Substituted  $l'$  and  $m'_c$  into Eq. 2.4, one could obtained[7],

$$f'_c = \frac{1}{2\pi} \sqrt{\frac{Ewh^3}{4(l + \Delta)^3\{m + 0.24[wh(l + \Delta)]\rho}}} \quad (2.5)$$

and the normalized resonant frequency could be expressed as[7],

$$\frac{f'_c}{f_c} = \sqrt{\frac{l^3(m + 0.24whl\rho)}{(l + \Delta)^3\{m + 0.24[wh(l + \Delta)]\rho}}} \quad (2.6)$$

and its relation with respect to normalized change in length  $\Delta/l$  is shown as Fig. 2.1b. It implies that an increase in length  $l$  ( $\Delta/l > 0$ ) would lower the resonant frequency  $f_c$  while shortening the length ( $\Delta/l < 0$ ) could increase it. Furthermore, one could notice that a more sensitive tuning could be achieved by shortening length, and ideally, as the length  $l$  approaches to zero, resonant frequency  $f_c$  approaches to infinity.

During implementation, an ideal case is to clamp the beam with plates, which could provide displacement and angle constraint, shown as Fig. 2.2a. In this way, the effective length is  $L$ . However, due to surface roughness with microscopic scale features, the actual surface contact area is much smaller than the nominal area, and it is also difficult to predict contact configuration[8]. This could cause the tuning process non-repeatable and complicated. Furthermore, two contact surfaces should be nicely polished, with high constrain force, and tuning action would require 2 DoF mechanism to release and reclamp, and change clamping position. While a more applicable way is to clamp with rollers, with tangent lines contact[9], shown as Fig. 2.2b. And a 1 DoF mechanism could change clamping position. But the effective length is not exactly  $L$  when distance between roller clamp and base is relatively large, since deformation between base and clamping would cause loss in stiffness. And approximate ideal clamping could be expected when it is close to base.

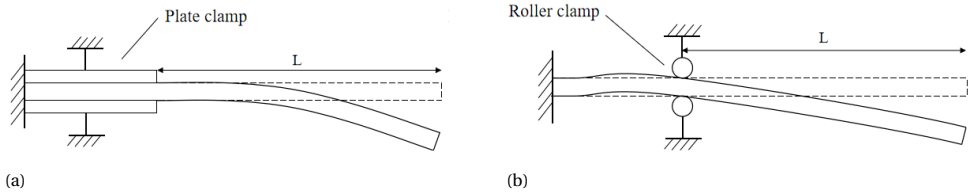


Figure 2.2: Schematic of cantilever with a. plate clamping and b. roller clamping.

This approach is widely used in variable stiffness actuator in robotic joint. An example is described by Esteveny et al. in [9]. To deal with this issue, slider mechanism with two roller clamps were proposed, and the principle is shown as Fig. 2.3. The parameter  $\delta$  defines the distance between two supports. When  $\delta$  decreases, two supports are getting closer and behavior of supports is tending towards ideal one; while  $\delta$  increases, support B is closing to base and slider behaves similarly to single support. It was reported that when  $\lambda$ , the distance between support C and base, is equal to  $0.65(r + p)$ , the worst case scenario in their design, with two supports, more than 93.5% of ideal stiffness could be achieved; while with one support, it decreases to 66%. A stiffness range 0.057-0.25  $Nm/deg$  was achieved.

### 2.1.3. CHANGING EFFECTIVE MASS

According to Eq. 2.1, resonant frequency could also be shifted by changing effective mass  $m_{eff}$  of oscillator. It could be rather difficult to change the actual mass, while an alternative is to change the position of center of gravity(CoG). Schaufuss et al. [10] reported a kinetic energy harvester with lever mechanism and auxiliary mass to realized this ap-



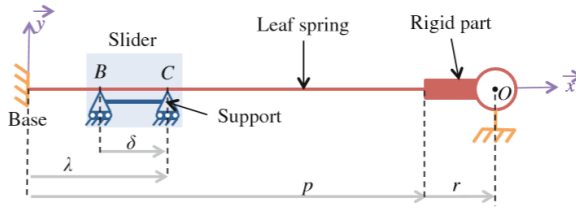


Figure 2.3: Schematic of slider mechanism with two roller clamps[9].

proach, with principle shown as Fig. 2.4. (A) is a conventional mass spring damper system, and comparing to it, their proposed design (B) replaced the mass with a lever, along which an auxiliary mass is able to slide. Resonant frequency could be calculated as

$$f_0 = \frac{1}{2\pi} \sqrt{\frac{K(L_1 + L_2)^2}{ML_1^2}} \tag{2.7}$$

where  $K$  is stiffness,  $M$  is mass of auxiliary mass,  $L = L_1 + L_2$  is total length of lever and  $L_1$  and  $L_2$  is the distance between CoG of mass and end effector to base. Eq. 2.7 could be re-written in to

$$f_0 = \frac{1}{2\pi} \sqrt{\frac{K}{M_{eff}}} \tag{2.8}$$

where

$$M_{eff} = M \frac{L_1^2}{L^2} \tag{2.9}$$

could define the effective mass of the system. By sliding the auxiliary mass from right end to left end (in configuration B), resonant frequency  $f_0$  could be shifted from 42 to 55 Hz.

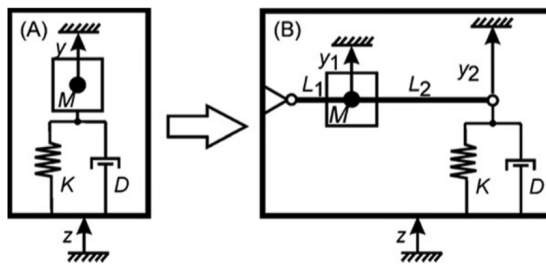


Figure 2.4: Comparison of schematics of mass spring damper system (A) of conventional and (B) with lever and auxiliary mass type[10].

Wu et al. presented a tunable vibration energy harvester with a movable mass, shown as Fig. 2.5a. The cantilever without mass has length of  $L$ , and its mass is negelectable the cylindrical rod has one degree of freedom of translation, with mass  $m_i$  and distance  $l_i$

between CoG and end of cantilever. And the fixed block has mass of  $m_o$ , with distance  $l_o$  between CoG and the end of cantilever. Resultant mass  $M = m_o + m_i$  and CoG position of the tuning mechanism  $l$  is calculated as

$$l = \frac{m_o l_o + m_i l_i}{M}. \quad (2.10)$$

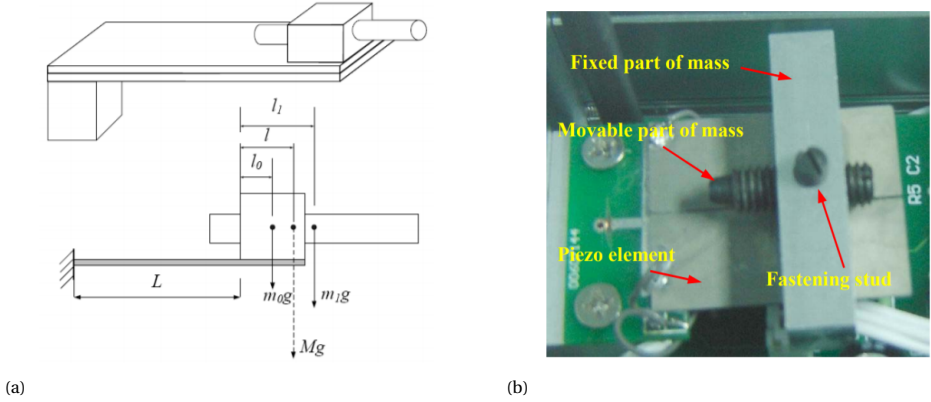


Figure 2.5: a. Schematic of cantilever with movable mass and b. experiment prototype[11].

An approximation of resonant frequency could be expressed as[19]

$$f_c \approx \frac{1}{2\pi} \sqrt{\frac{EI}{ML^3} \frac{6a^2 + 6a + 2}{8a^4 + 14a^3 + 10.5a^2 + 4a + \frac{2}{3}}} \quad (2.11)$$

where  $a = l/L$ ,  $E$  is Young's Modulus, and  $I$  is second moment of inertia. Fig. 2.5b shows the hardware, where the movable mass is realized by a screw with length of  $30mm$  and radius of  $6mm$ , and a fastening screw is used to lock the position of movable screw after tuning. The resonant frequency could be adjusted between  $130Hz$  and  $180Hz$ , by moving the screw from right end to left end, shown as Fig. 2.6.

#### 2.1.4. CHANGING TRANSMISSION RATIO

Transmission converts input motion to output motion, and for an ideal transmission, there is no power loss, which means all input power are converted to output power[12]. For system with stiffness element involved, transmission ratio  $i$  could be defined as[12]

$$i = \frac{d_F}{d_k} \quad (2.12)$$

where  $d_F$  is displacement of force application and  $d_k$  is displacement of stiffness element, and perceived stiffness at force application point is

$$k_p = \frac{k}{i^2} \quad (2.13)$$

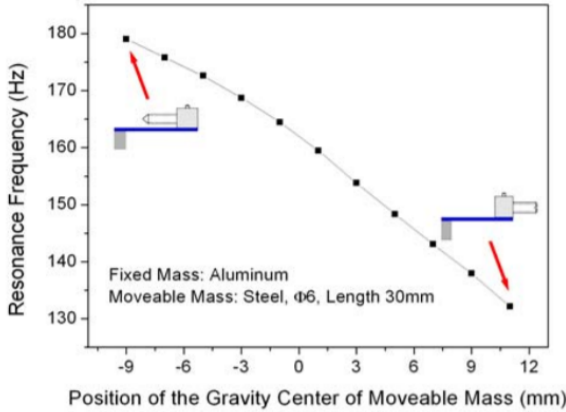


Figure 2.6: Experiment result of tuned resonant frequency with respect to position of CoG of moveable mass[11].

where  $k$  is stiffness of element. Considering a case shown as Fig. 2.7, where a spring with stiffness  $k_s$  is connected to lever, with length  $L$ , at point  $A$  with distance  $L_k$  to pivot, and force is applied at point  $B$  on lever with distance  $L_F$  to pivot. Transmission ratio could be calculated as  $i = L/L_k$ , and hence perceived stiffness is  $k_p = k/i^2$ . Thus, for a lever mechanism with stiffness element attached, different position of pivot, force application and stiffness element connection could change transmission ratio and hence tune stiffness. One could notice that as force application point is approaching pivot, perceived stiffness is growing to infinity, and as stiffness connection point is approaching pivot point, stiffness is dropping to zero. This tuning approach is widely used in adjustable stiffness actuator design for robotics.

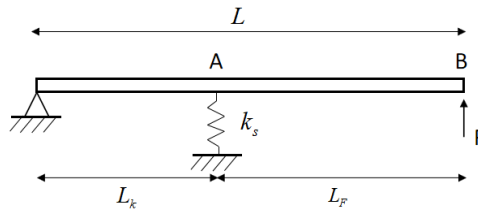


Figure 2.7: Effect of transmission on perceived stiffness.

A. Jafari et al.[13] used two springs, one side of which were connected to an intermediate link and the other side were connected to an output ring. A motor was used to control the position of the springs. B. Kim and J. Song[14] proposed a hybrid dual actuator unit to control position of two springs independently on a guiding link, whose center point was connected to an output shaft. These correspond to the principle shown as Fig. 2.8a. Examples of moving pivot (Fig. 2.8b) including [15–17]. In [15] and [16], an intermediate link was developed to guide the pivot and its position was controlled by a motor. [17] proposed a

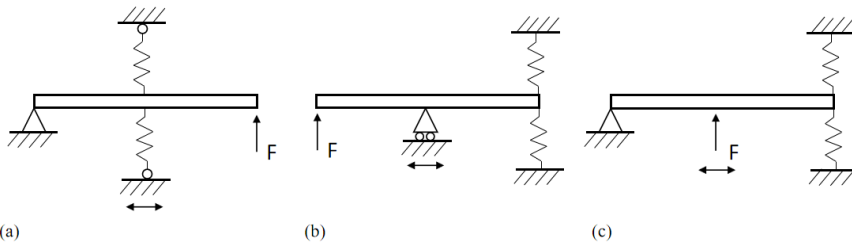


Figure 2.8: Schematics of stiffness tuning method by changing transmission ratio through movable (a). springs, (b). pivot and (c). applied force.

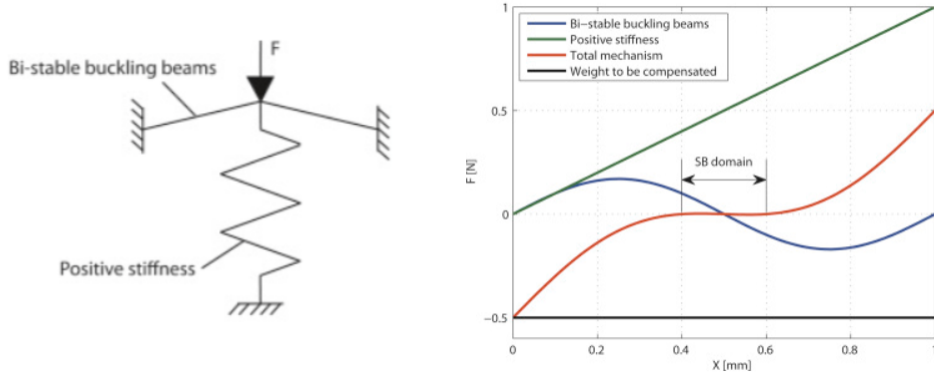
design where pivot position was adjusted by planetary gears system to achieve straight-line movement. Concept of moving force application point (Fig. 2.8c) was analytically studied by L. C. Visser[18]. It should be pointed out that transmission ratio could only adjust the perceived stiffness while resonant frequency is still unchanged. If the mass of bar is considered, then it is similar to changing effective mass.

### 2.1.5. ADDING NONLINEAR SPRING

The stiffness of a system could be changed by adding other stiffness, and one widely used application is to add nonlinear stiffness[20]. This could be achieved by bi-stable buckling beam, which has two stable position. Its negative stiffness (NS) behavior is extensively used in compliant mechanism to compensate the positive stiffness (PS) and hence realize statically balancing with a finite range of zero stiffness, which has benefit of low actuation force[20, 21]. A general configuration of these mechanism could be shown as Fig. 2.9a. When applying a force from shown position, force displacement relation is shown as Fig. 2.9b, where the green line represents linear spring with positive stiffness and blue line stands for bi-stable buckling beams with nonlinear stiffness. These two could add up and resultant stiffness is as red line shown, in which a certain band has zero stiffness.

Plenty of example are found in literature, where bi-stable buckling beams were design properly to compensate one fixed positive stiffness and achieved zero stiffness. Dunning et al. [22] developed a zero stiffness six DoF compliant positioning stage, and its zero stiffness in 3 out-of-plane motion was realized by bi-stable buckling beams. N.Tolou et al. proposed a set of criteria which defined statically balancing mechanism[21]. A.Staple and J.L.Herder reported a feasibility study of a fully compliant statically balancing laparoscopic grasper[23], and J. Lassooij et al. developed this prototype and achieved 2 DoF[24]. N.Tolou et al. presented statically balancing concepts applicable to MEMS device and simulation results confirmed their performance[25]. P.J. Pluimers et al. achieved zero stiffness with an ON/OFF mechanism to activate buckling state[26].

The end of bi-stable buckling beams could be released and connected to actuators, which can apply different axial load to control the nonlinearity of beams. In this way, the amount of compensation to the positive stiffness could be controlled and hence adjust



(a) (b)  
 Figure 2.9: a. General configuration of statically balanced compliant mechanism and b. Figure of stiffness of linear spring, bi-stable buckling beam and total stiffness of system[20].

the stiffness. Yalcin et al. [27] reported a variable negative stiffness actuation based on this principle, with model shown as Fig. 2.10. Leaf springs were connected to the moving base end effector with clamped-clamped boundary conditions, which were intended to create variable stiffness. Tensioning linear actuators were used to change the applied axial compression and tension on the leaf springs, which was to change their transverse stiffness. Linear sliders were used to support motion of end effector and guide the movement of tensioning actuators. Leaf springs started to buckle at axial load of 53.2N, and stiffness tuning from -5 to 12.5N/mm was observed. While the stroke for constant stiffness region would also change, which was 7mm at 12.5N/mm and 2mm at -5N/mm.

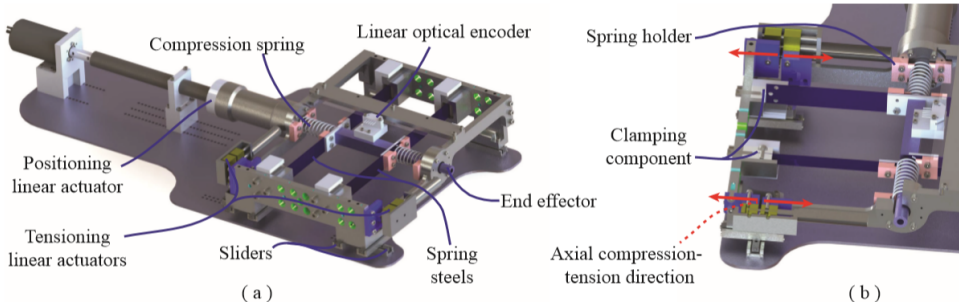


Figure 2.10: Experiment result of tuned resonant frequency with respect to position of CoG of moveable mass[27].

Churchill et al. [28] achieved manipulating stiffness of bi-stable buckling beams through spring force generated by displacement, as shown in Fig. 2.11.  $k_3$  was positive stiffness of plate spring, and negative stiffness was contributed by snap-through mechanism and a horizontal spring ( $k_2$ ) together. A piezoelectric actuator was used to control the displacement of horizontal spring ( $k_2$ ) and hence adjust the preload applied to the snap-through

mechanism. Total stiffness of the system could be expressed as

$$k_t = k_3 - \frac{2k_2}{L} x_0 \quad (2.14)$$

where  $L$  is length of bi-stable buckling beams, and  $x_0$  is displacement by piezo actuator that deforms spring  $k_2$ . Plate spring had a positive stiffness  $k_3 = 100N/mm$ , and negative stiffness could be varied in the range of  $10N/mm$  to  $-100N/mm$ , corresponding to displacement  $x_0 = \pm 0.25mm$ . Experiment results showed the resonant frequency could be changed 10 times, from 16 to 160Hz, which corresponds to 100 times change in stiffness. It was reported that damping would also change during tuning process, which could be observed from  $Q$  factor. It was approximately proportional to resonant frequency with a slope of  $m/c$  ( $c$  the damping coefficient) when above 20Hz. But at extreme tuning, increased damping from unknown sourced were measured, which could be induced by power supply of actuator or friction from joint.

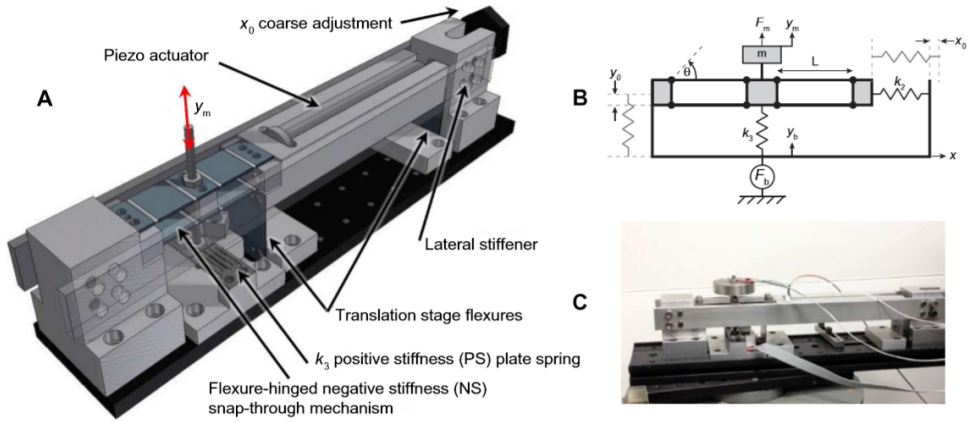


Figure 2.11: A. CAD design, B. schematic and C. experimental set up of dynamically variable negative stiffness structure[28].

Wu et al. directly applied displacement to end of preloaded curved beams to adjust stiffness, and realized approximately linear stiffness tuning[29]. Two types of curved beams were investigated, one was pinned beams with semicircular shape and the other was fixed beams obtained from shape optimization with 3 arcs. It was reported from experiment that pinned beams could reach large stiffness tuning range ( $11.82N/mm$ ) with good linearity while  $6.5N/mm$  was obtained by fixed beams. Stroke of  $11mm$  could be achieved in both cases.

Another way to create nonlinear stiffness is to use magnetic force. Force between two cylindrical magnets could be approximately expressed as[30]

$$F = \left[ \frac{B^2 A^2 (l+r)^2}{\pi \mu_0 l^2} \right] \left[ \frac{1}{d^2} + \frac{1}{(d+2l)^2} - \frac{2}{(d+l)^2} \right] \quad (2.15)$$

where  $B$  is flux density of magnet,  $A$  is common area,  $l$  and  $r$  is length of magnet,  $d$  is distance between two magnets, and  $\mu_0$  is permeability of medium. Stiffness could be calculated as  $k = \partial F / \partial d$ , and example of force and absolute stiffness with respect to distance is shown as Fig. 2.12. One could notice that it is nonlinear and position dependent. Furthermore, when moving two magnets towards each other, repulsive force creates positive stiffness and attractive force generate negative one, and vice versa. This could be added to a system to adjust the effective stiffness. It should be pointed out that magnets should be separated with a distance such that magnetic force is smaller than force produced by mechanism during range of motion to avoid snap-through, which could change the boundary conditions or system configuration.



Figure 2.12: An example of force and absolute stiffness between two magnets with respect to distance in log-log scale[30].

V. R. Challa et al.[30] used this approach to develop a tunable energy harvester, with a cantilever beam and two magnets at both side of its tips, shown as Fig. 2.13a. Distance between two pairs of magnets was adjusted to tune stiffness. Range of resonant frequency of 22 to 32Hz was achieved with untuned one 26Hz. Increase in damping was also observed when increasing tuning stiffness. They proposed another configuration[31] shown as Fig. 2.13b, in which one pair of magnets was used, and they were mounted at the tip of a pair of cantilevers. By changing the position of movable cantilever, distance between two magnets were adjusted and hence tuned stiffness. Range of resonant frequency of fixed beam and movable beam was 22-32Hz and 23.5-34Hz respectively.

### 2.1.6. ADDING AXIAL LOAD

Stiffness of a structure could be changed by applied axial load. Considering transverse vibration of a beam, under compressive axial load  $P$ , its natural frequency of first mode  $f'_0$  could be approximated as[32]

$$f'_0 = f_0 \sqrt{1 - \frac{P}{P_c}}, \quad (2.16)$$

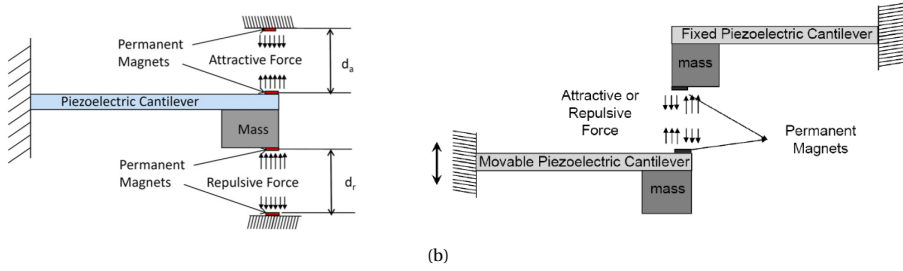


Figure 2.13: Schematics of a tunable energy harvester using magnets for tuning from a.[30] and b.[31].

where  $f_0$  is original natural frequency of uncompressed beam,  $P_c$  is Euler's critical load for buckling. Noting that positive  $P$  represents compression and negative one signifies tension. Fig. 2.14 shows the relation of normalized natural frequency with axial load, and one could notice that it is more sensitive to tune resonant frequency by applying compression.

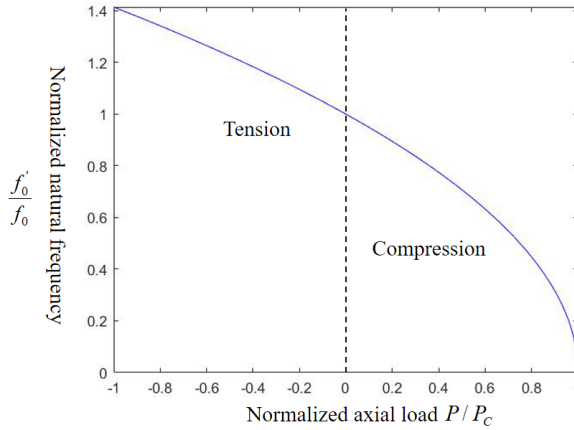


Figure 2.14: Change in normalized natural frequency with respect to normalized axial load.

Lots of studies have been conducted about relation between dynamic behavior of beams and axial load, including theoretical and numerical (e.g. [35–37]), and experimental (e.g. [33, 34]). An experimental study performed by Laux[33] could show the insensitive tuning by tension, where tensile load with magnitude 8 times larger than Euler's critical load was applied to an aluminium beam, natural frequency of first mode shifted 60%. Analysis conducted by C.L. Amba-Rao[37] reported that for beam configuration with some different boundary conditions, their unloaded bending stiffness are different, and when axial compression equals Euler's critical buckling load, resonant frequency would drop to zero for all cases. Hence, by choosing different boundary conditions, different range of resonant frequency could be covered by applying a certain range of axial compressive



load.

E. S. Leland and P. K. Wright[38] presented a tunable piezoelectric vibration energy generator, whose resonant frequency was tuned by applying axial compression. As shown in Fig. 2.15a, schematic was based on clamped-clamped beam configuration, with a proof mass at the center. Experimental set up is shown as Fig. 2.15b, where generator was held by a steel vise, and axial compressive load was applied by micrometer head then measured by force sensor. Two proof masses were used in testing, and results reported resonant frequency reduced from 250 to 200 Hz and from 190 to 160 Hz with proof mass of 7.1 g and 12.2 g respectively. Failure occurred at bimorph material then load was larger than 65 N, and an increase in damping of 67% was observed as axial load was applied from 0 to 60 N.

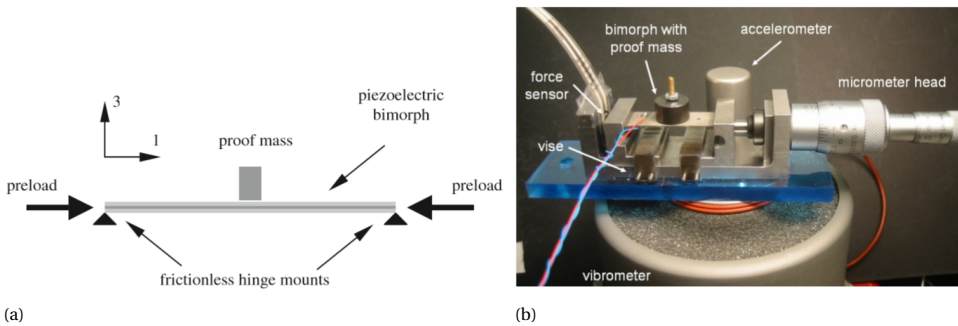


Figure 2.15: a. Schematic and b. experimental set up of resonant frequency tunable piezoelectric bimorph vibration energy scavenger[38]

Damping effects and dynamical behavior of a piezoelectric bimorph due to axial preload was also analytically studied by Y. Hu et al.[39]. Proposed design is shown as Fig. 2.16, a bolt passed through the whole layer and was fixed at left-side wall, and a capping plate was connected to right-end of beam. By clockwise and counter-clockwise rotating, compression and tension load can be applied respectively. Tuning range of 58.1 to 169.4 Hz was achieved by adjusting axial load from tension 50 N to compression 50 N. Resonant frequency at unloaded condition was 129.3 Hz, which is consistent with more sensitive tuning by compression. Furthermore, results reported that compared to unloaded case, axial compression would result in lower power output while tensile load could increase it. This corresponds to change of  $Q$  factor at resonance, which implies change of damping under axial tension and compression.

C. Eichhorn et al.[40, 41] achieved axial load tuning on a cantilever beam. As shown in Fig. 2.17, device included a cantilever, two additional arms, a spring and a tuning screw. By rotating screw, deformation would occur at spring. A force could be generated and applied axially to the tip of cantilever through two arms. Noting that the force is linear to the position of screw. By introducing a notch at the wing, shown as Fig. 2.17a, a more sensitive tuning and wider range was realized. Results showed that a frequency

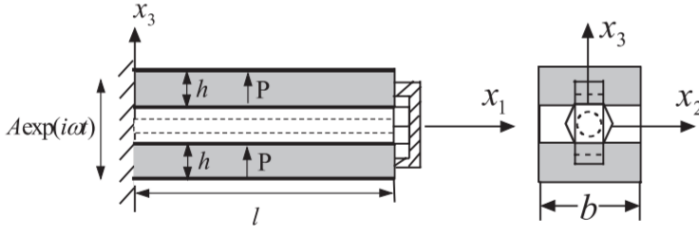


Figure 2.16: Schematic of an approach to apply an axial preload to a piezoelectric bimorph.[39]

shift of 22% (380-290Hz) was obtained by compression load of 22.75N, and from another experiment, 4% (440-460Hz) shift occurred by applying about the same amount of tension. They suggested an improvement of auto and real time tuning, which could be achieved by combining screw for coarse adjustment and piezoelectric actuator for fine tuning. Reduction and increase in damping was observed under tension and compression respectively.

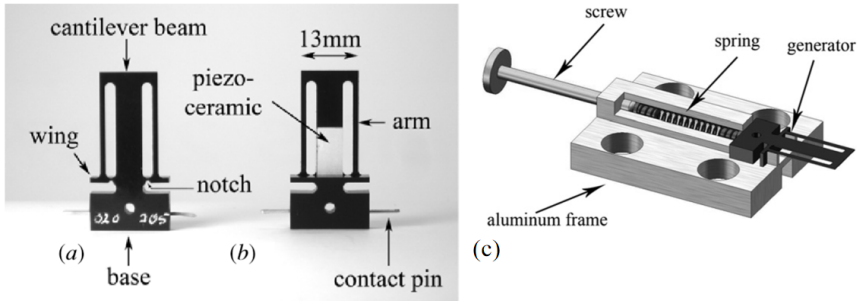


Figure 2.17: Generator structure (a). with notch and (b). without notch at arm. (c) CAD design of device[40, 41].

Another approach to produce axial load is using magnetic force. D. Zhu et al.[42] presented a frequency tunable energy harvester device by using this method. As shown in Fig. 2.18, a magnet was mounted at the tip of a cantilever. There was another movable magnet which had DoF of translation along cantilever. This pair of magnet could generate tuning force at axial direction of cantilever. By varying distance, and pole position, attractive and repulsive force could be produce with different magnitude, corresponding to tension and compression respectively. Experimental results showed a frequency range of 1.2 to 68Hz by applying tension load of 26N or compression load of 2.8N (unloaded frequency 27Hz).

### 2.1.7. CHANGING YOUNG'S MODULUS

Stiffness of a structure depends on Young's Modulus of material. It is reported that some shape-memory alloys (SMA) (e.g. Nitinol) have the property of temperature dependent Young's Modulus, which is caused by two different types of crystal structure, austen-

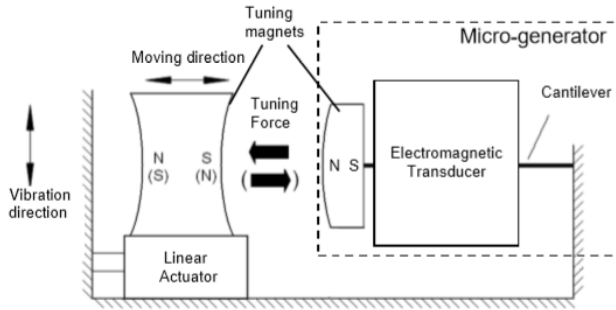


Figure 2.18: Schematic of a tunable energy harvester with axial load applied by magnetic force[42].

ite and martensite state, corresponding to "hot" and "cold" state[43–45]. In martensite state, materials have corresponding low Young's Modulus and yielding stress. When subjected to thermal heat, they could change to austenite state, where both Young's Modulus and yielding stress increase. And this process is reversible[45]. An application of SMA materials is in vibration control device, such as vibration absorber, whose anti-resonant frequency should be tuned to match the frequency of ambient vibration.

C. Rogers and C. Liang[43, 44] studied behavior of shape-memory alloys in terms of both mechanics and dynamics, and proposed two concepts in tuning of vibration absorber, one of which was using different amount of heat to change Young's Modulus. They also experimentally validate the feasibility of this approach.

K. Williams et al. [45] developed a vibration absorber using three segments of SMAs, and each of them could be independently controlled. Schematic is shown as Fig. 2.19, where SMAs were combined with steel in parallel connection. This could remarkably increase stiffness of the absorber. Temperature of SMAs were manipulated by input current manually, which adjusted Young's Modulus and hence stiffness. High magnitude of current was applied to change temperature in order to achieve fast response and then it was shifted to low magnitude to maintain temperature level. Testing showed that resonant frequency shifted from 83.55 with all three SMAs in "cold state", to 98Hz, with all SMAs in "hot state".

E. Rustighi et al. [46] used a beam that was made from SMA material to design a vibration absorber, shown as Fig. 2.20. Several analysis were conducted theoretically and experimentally, where hysteresis were observed between temperature and tuning frequency and in transient behavior of device during heating and cooling, while it did not affect response time. They also pointed out that damping did not change evidently during tuning process. An increase in natural frequency of 21.4% from 63.9 to 76.4Hz, corresponding to change of 47.5% in Young's Modulus from 40 to 100 Gpa.

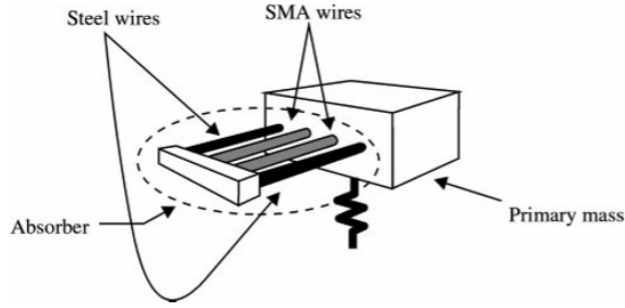


Figure 2.19: Schematic of a tunable vibration absorber with steel and SMAs in parallel[45].

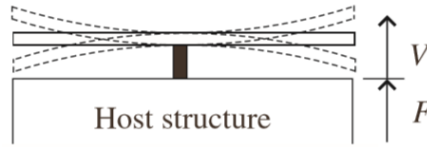


Figure 2.20: Schematic of a tunable vibration absorber with beam made from SMA[46].

### 2.1.8. CHANGING SECOND MOMENT OF INERTIA

According to Eq. 2.3, bending stiffness of a cantilever beam could be altered by changing second second moment of inertia. For any arbitrary shape in 2 dimension, second second moment of inertia with respect to  $x$  axis could be expressed as

$$I_x = \iint_A y^2 dx dy, \quad (2.17)$$

where  $A$  is area. It is not applicable to change dimension of cross section but change of geometrical shape of it could realized this. C. Peter[47] demonstrated tuning resonant frequency of an energy harvester by using this method, with schematic shown as Fig. 2.21. Two piezoelectric actuators were used, where one was clamped and the other was free. They were connected by three flexure hinges, and the free one had the DoF of rotation about the shown axis. When electric potential was applied to clamped actuator, it would deform as Fig. 2.21c described, and a stiffer structure could be obtained. A spacer was inserted at the middle hinge to have an initial deformation at  $0V$ , which could make use of positive and negative tuning voltage and hence increase the tuning range. By applying voltage of  $\pm 5V$ , resonant frequency was tuned from  $66$  to  $89Hz$ , with untuned (no voltage but with deformation) resonance at  $78Hz$ . Another application could be found in a MEMS tunable AFM device[48], where piezoelectric elements were used to manipulate its cross section.

### 2.1.9. DISCUSSION AND CONCLUSION

In this section, various resonant frequency SMA tuning methods for macro scale devices are reviewed, and tuning is achieved by varying stiffness of effective mass. Discussion of

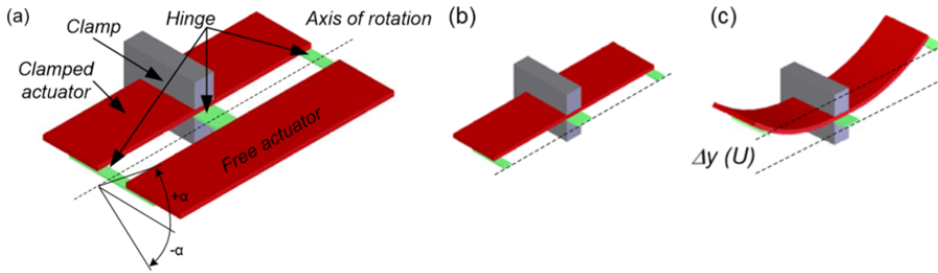


Figure 2.21: Schematic of (a). a tunable energy harvester by changing second moment of inertia, (b). untuned mode and (c). stiff mode[47].

each tuning methods is listed below.

- Change Effective Length:** This is effective to achieve large tuning range, since beam length  $L$  is related to resonant frequency with power of  $3/2$ . Noting that it is also possible to activate higher order eigenmodes to further cover a wide range. However, this method requires additional movable mechanism with large stroke to clamp different position, and the contact between clamping and beam would also cause issues such as mechanical wear and stiction. While in application, it is found that most designers would choose roller clamp rather than plate clamp. Roller clamp is easier to implement with slider, but deflection between fixed base and clamp would lead to loss of stiffness. Furthermore, Hertz contact stiffness between roller and beam should also be considered, such that it does not effect dynamic of system. While a novel design with two roller clamps in a small separated distance shows a promising result to maintain bending stiffness close to ideal one. Further investigations could be conducted to study its dynamic behavior and Hertz contact stiffness.
- Change Effective Mass:** This method is easy to implement with slider, even large stroke movable mechanism may still needed for a relatively wide range tuning. One important advantage is that it does not effect damping. But limited range of tuning might be obtained, and a relatively heavy mass would require, since mass  $m$  is related to resonant frequency with power of  $1/2$ .
- Change Transmission Ratio:** This is widely used to design variable stiffness joints and actuators in robotics field. A large stiffness range could be obtained, but large stroke moving mechanism is needed. One should notice that, different transmission only change the perceived stiffness but not resonant frequency of the system. If the mass of lever is considered, resonant frequency would change because of change in effective mass.
- Add Nonlinear Spring:** Numerous applications of nonlinear spring are found in zero stiffness mechanism, where buckling effect of these springs are utilized to add negative stiffness. It is possible to achieve monolithic design, which could get rid of mechanical contact problems. Stiffness of system could even be tuned

| Tuning Method            | Reference | Untuned Frequency(Hz)  | Tuning Range(Hz)                | Frequency Ratio $f_r$ |
|--------------------------|-----------|------------------------|---------------------------------|-----------------------|
| Effective Length         | [9]       | N/A                    | (stiffness)<br>0.057-0.25Nm/deg | N/A                   |
| Effective Mass           | [10]      | N/A                    | 42-55                           | 1.31                  |
|                          | [11]      | 160                    | 138-180                         | 1.30                  |
| Nonlinear Spring         | [27]      | (stiffness)<br>1500N/m | (stiffness)<br>-5000-12500N/m   | N/A                   |
|                          | [28]      | N/A                    | 16-160                          | 10                    |
|                          | [30]      | 26                     | 22-36                           | 1.64                  |
|                          | [31]      | 22.5                   | 22.5-32                         | 1.42                  |
|                          | [31]      | 23                     | 23-34                           | 1.48                  |
|                          | [38]      | 250                    | 200-250                         | 1.25                  |
| Axial Load               | [38]      | 190                    | 160-190                         | 1.19                  |
|                          | [39]      | 129.3                  | 58.1-169.4                      | 2.92                  |
|                          | [40]      | 380                    | 290-380                         | 1.31                  |
|                          | [41]      | 440                    | 440-460                         | 1.05                  |
|                          | [42]      | 27                     | 1.2-68                          | 56.67                 |
| Young's Modulus          | [45]      | 83.55                  | 83.55-98                        | 1.17                  |
|                          | [46]      | 63.9                   | 63.9-76.4                       | 1.20                  |
| Second Moment of Inertia | [47]      | 78                     | 66-89                           | 1.35                  |

Table 2.1: Summary of device with tunable resonator

to negative. A sensitive tuning could be achieved, since a small displacement applied to one end could generate large stiffness change, but limited range could be obtained. As stiffness of these springs is linearly added to system stiffness, influence on high stiffness system would be minor. Furthermore, control of nonlinear stiffness would be difficult, and complex design could be expected.

- **Add Axial Load:** This is a simple way to realize resonant frequency tuning, and easy to implement. Compact device could be expected, without large stroke moving mechanism. Axial load could be compressive and tensile. Regarding compression, tuning is sensitive and could cover a wide range till buckling, and negative stiffness could be obtained when compressive load is larger than critical buckling load, but compression would increase damping. In terms of tension, tuning is insensitive and limited by yielding stress, but damping would drop. Hence, tension could be suitable for fine tuning.
- **Change Young's Modulus:** Young's Modulus of some shape-memory alloys such as Nitinol could be altered by applying current which induces temperature. This is a simple way and device could be compact without extra moving mechanism. But limited tuning range and hysteresis between temperature and tuned frequency are reported from literature. Since it is tuned by thermal load, response time would be

generally slow, and energy is needed to maintain stiffness.

- **Change Second second moment of inertia:** This method is often realized by changing cross section area of a vibrator. One energy harvester device and one MEMS AFM tuned by this approach are found in literature. Piezoelectric actuator are used to activate change in cross section configuration. Compact size but limited tuning range could be expected.

| Tuning Method                   | Advantages   | Disadvantages  |
|---------------------------------|--|--|
| Change Effective Length         | <ul style="list-style-type: none"> <li>• Large tuning range</li> <li>• Effective</li> </ul>  | <ul style="list-style-type: none"> <li>• Mechanical contact cause wear and stiction problems</li> <li>• Need extra large stroke moving mechanism</li> </ul>              |
| Change Effective Mass           | <ul style="list-style-type: none"> <li>• Easy to implement</li> <li>• does not effect damping</li> </ul>   | <ul style="list-style-type: none"> <li>• Limited tuning range</li> <li>• need extra large stroke moving mechanism</li> </ul>   |
| Add Nonlinear Spring            | <ul style="list-style-type: none"> <li>• Design could be monolithic</li> <li>• Able to achieve negative stiffness</li> <li>• Sensitive tuning</li> </ul>   | <ul style="list-style-type: none"> <li>• Limited tuning range</li> <li>• Difficult to control nonlinear stiffness</li> <li>• Complex design</li> </ul>                   |
| Add Axial Load                  | <ul style="list-style-type: none"> <li>• Simple design</li> <li>• Easy to implement</li> <li>• compact size</li> <li>• Sensitive(Compression)</li> <li>• Relatively large tuning range(Compression)</li> <li>• Reduce damping (Tension)</li> </ul> | <ul style="list-style-type: none"> <li>• Insensitive(Tension)<sup>1</sup></li> <li>• Limited tuning range (Tension)</li> <li>• Increase damping (Compression)</li> </ul> |
| Change Young's Modulus          | <ul style="list-style-type: none"> <li>• No extra moving mechanism is needed</li> <li>• Easy to implement</li> <li>• Compact size</li> </ul>   | <ul style="list-style-type: none"> <li>• Require energy to maintain stiffness</li> <li>• limited range of tuning</li> <li>• slow response time</li> </ul>                |
| Change Second Moment of Inertia | <ul style="list-style-type: none"> <li>• Compact size</li> <li>• Sensitive tuning</li> </ul>   | <ul style="list-style-type: none"> <li>• Limited tuning range</li> </ul>   |

Table 2.2: Summary of advantages and disadvantages of different tuning methods

These technologies are widely applied in various field, such as tunable energy harvesters, variable stiffness joint and tunable resonant scanner. Table 2.1 provides an overview of performance of tunable devices, and Table 2.2 summarizes and compares different tuning methods. For large tuning range of resonant frequency at high frequency more than

<sup>1</sup>Note that insensitive feature could be advantageous for fine tuning.

an order of magnitude, changing effective length is effective, and for small range fine tuning, axial load especially tension is recommended. When damping is an issue, effective mass and tensile axial load could be considered. When compact and simple design is preferred, changing Young's Modulus, second second moment of inertia, adding axial load and nonlinear spring could be options. One should keep in mind that several methods could be integrated together to achieve desired performance.

## 2.2. REVIEW OF MECHANISMS OF RESONANT SCANNER

To generate mechanical resonance, mechanisms contain elastic elements which provide stiffness, and masses are needed. In this section, a review based on mechanisms that produce tilting motion is conducted, since this is the desired motion of scanning mirror that steers beam. Many high frequency scanning device are designed in MEMS, which could achieve a typical resonant frequency of a few tens of kilo hertz[49]. In macro scale mechanisms, it is found that resonance in tilting motion could be generated by cantilever beam, torsional beam and crossed flexure, while some mechanisms with low rotational stiffness such as crossed flexure and notch flexure could be added as suspension to maintain rotational center. Furthermore, most of the resonant scanners in the literature or commercially available are designed to operate at one fixed resonant frequency, though some of them have tunable feature, it is intended to be tuned within a small range to correct errors induced by manufacturing or change in conditions. In the end of this section, evaluations of each type of mechanism in terms of parasitic motion, ease of implementing stiffness tuning, and other advantages and disadvantages are discussed.

### 2.2.1. CANTILEVER BEAM

Free vibration in transverse direction of a uniformed cantilever beam without considering damping could be described as[50]

$$EI \frac{\partial^4 v(x, t)}{\partial x^4} + \bar{m} \frac{\partial^2 v(x, t)}{\partial t^2} = 0 \quad (2.18)$$

where  $\bar{m}$  is mass per unit length and  $v(x, t)$  is displacement field. Natural frequency could be derived as[51]

$$f_i = \frac{\lambda_i^2}{2\pi L^2} \left( \frac{EI}{\bar{m}} \right)^{1/2} ; \quad i = 1, 2, 3 \dots \quad (2.19)$$

where  $\lambda_i$  is a parameter varied from different boundary conditions which could be found in [51], and  $i$  represents order of modes. Boundary conditions of sliding, hinge and free could give angular deflection, which is out-of-plane tilting motion while clamping constrains all motions.

An example of resonant scanner in cantilever beam configuration is presented by L. B. Kheng et al.[52], shown as Fig. 2.22. A mirror was mounted orthogonally to the axial direction, and a magnet was placed near the tip of cantilever, actuated by coil. It was reported that system was operated only at the first bending mode at resonant frequency



of  $44\text{Hz}$  with large angular deflection of approximately  $38^\circ$ . But angular deflection was achieved by large parasitic translation as well, and hence scanning mirror did not have a fixed rotational center.

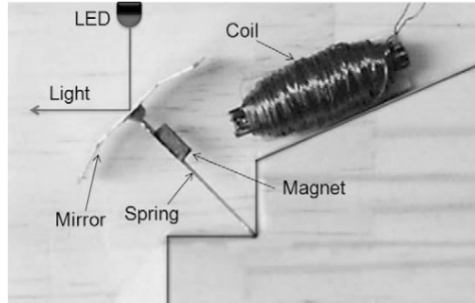


Figure 2.22: A resonant scanner in cantilever configuration[52].

### 2.2.2. TORSIONAL BEAM

Free torsional vibration of a beam without damping could be expressed as[53]

$$I_p \ddot{\alpha} + K_t \alpha = 0 \quad (2.20)$$

where  $I_p$  is polar moment of inertia,  $K_t$  is torsional stiffness and  $\alpha$  is angular deflection. And natural frequency could be derived as[51]

$$f_i = \frac{\lambda_i}{2\pi} \left( \frac{K_t}{\bar{m} L I_p} \right)^{1/2} \quad (2.21)$$

where torsional stiffness could be expressed as

$$K_t = \frac{CG}{L} \quad (2.22)$$

where  $C$  is torsional constant, related to cross sectional area, could be found in [51] and  $G$  is shear modulus which could be calculated as  $G = E/2(1 + \nu)$ , with  $E$  and  $\nu$  the Young's Modulus and Poisson's ratio respectively. Torsional beam in clamp-clamp boundary condition could provide a rather fixed rotational axis, which means less parasitic translation. J. I. Montagu[54] adopted this configuration with drive torque provided by magnetic induction. Shown as Fig. 2.23a, when current was applied to coil, a magnetic flux would be generated through the iron loop, this flux could then induce current in the wire loop, whose one edge was attached to the mirror. This wire loop could interact with permanent magnet and hence generate a torque at torsional beam. By using shaped-memory alloy Nitinol, resonant frequency could be tuned from  $745$  to  $830\text{Hz}$  with a temperature change from  $40$  to  $100^\circ\text{C}$ . L. Koay et al.[55, 56] used two voice coil actuators to apply a force couple to two end of an arm symmetrically, which resulted

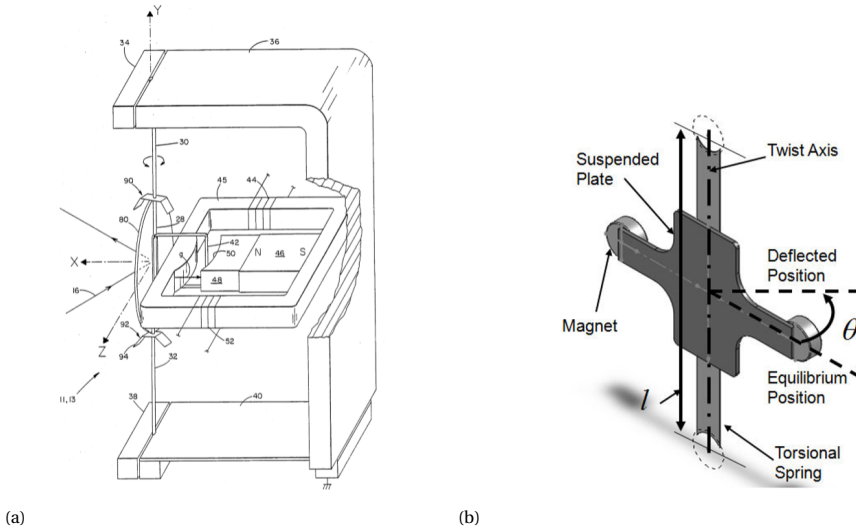


Figure 2.23: Schematics of resonant scanner in torsional configuration from [54] and [56].

in a torque at torsional beam, shown as Fig. 2.23b. Beam dimension design and actuation position was obtained by optimization to minimize maximum stress and energy consumption. While a fixed resonant scanning frequency of  $44\text{ Hz}$  was achieved.

For a torsional beam, it also has other DoF besides rotation about torsional axis, and thus it would have other eigenmodes including torsional mode. To avoid energy coupling, other modes should separate with the torsional mode in frequency spectrum. H. Urey et al. [57] considered this issue and in their design, torsional mode had frequency of  $16.5\text{ kHz}$  while the closest two modes had frequency of  $10.77$  and  $29.33\text{ kHz}$  respectively. Shown as Fig. 2.24c. mirror had high magnetic permeability, suspended by a torsional beam. Two ends were mounted on magnet, such that magnetic flux would be generated between mirror and coil. By applying alternative current, a torque could be produced to tilt mirror. They also reported an issue of mirror deformation caused by large acceleration force during scanning motion, as shown in Fig. 2.24b. The maximum deformation could be approximated as

$$\delta_{\max} = 0.217 \frac{\rho f^2 D^5 \theta}{E t_m^2} \quad (2.23)$$

where  $\rho$  and  $E$  is material density and Young's Modulus,  $f$  is scanning frequency,  $D$  and  $t_m$  is mirror diameter and thickness, and  $\theta$  is scanning angle. This maximum deformation should be less than  $\lambda/10$ , where  $\lambda$  is wavelength, to remain within the diffraction limit of reflected light beam. By introducing a notch underneath mirror, as shown in Fig. 2.24c deformation could be reduced to an acceptable level with  $4.5^\circ$  scanning angle.

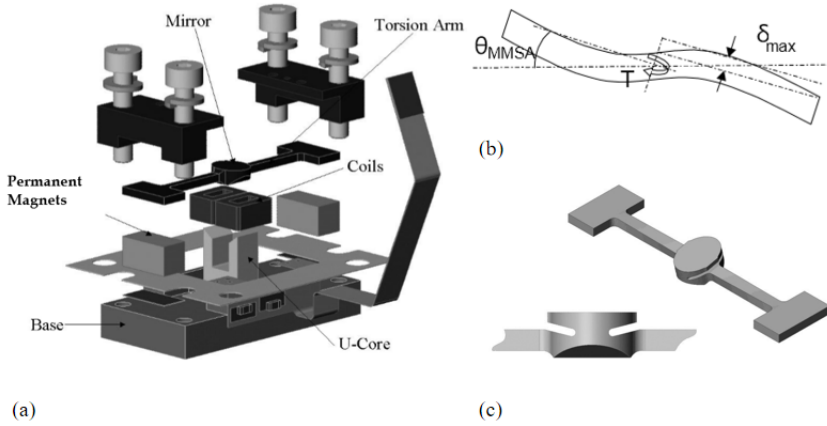


Figure 2.24: (a). A resonant scanner device in torsional configuration. (b). Schematics of mirror deformation due to acceleration force. (c). Notch feature underneath mirror[57].

### 2.2.3. CROSSED FLEXURE

For traditional devices with ball bearing suspension, issues such as mechanical wear could happen, which limits the lifetime [67, 69]. While its oil lubrication would further limit the application in vacuum environment. Compliant mechanisms such as crossed flexure could be alternatives, which transfer force, movement and energy by elastic deformation instead of rigid body interaction. This could enable devices to get rid of bearing and lubrication, which reduces virtual play, backlash and friction, and hence increase precision. With the absence of bearing, these mechanisms could be maintenance free and vacuum friendly, even with infinite lifetime[22].

A general configuration of crossed flexure could be shown as Fig. 2.25, where two flexural beam are oriented in "X" shape. The intersection line is the rotation axis. Crossed flexure has one DoF of rotation, with high rigidity in other DoF. However, its rotational center would shift during deflection, resulting parasitic motion at end effector. Lots of researchers have analytically studied the behavior of center shift[58–64], though each of them proposed different model, it could be concluded that trajectory of center shift is similar to a quadratic function, and it is predictable[65]. H. Zhao and S. Bi[59] and R. A. DeBoalt[60] found that when  $A = 12.7322\%L$  or  $87.2678\%L$ , center shift is minimal and when  $A = B$ , it is maximal. E. G. Merriam et al.[65] numerically investigated this center shift by FEA, and reported that for a  $15^\circ$  rotation, shift of axis in horizontal direction is much smaller than that in vertical direction, and both of them are smaller than beam length  $L$  by a factor with order of magnitude of  $10^{-3}$ .

In the case of  $\alpha = 90^\circ$ , rotational stiffness could be estimated as[60]

$$K = k(1 + 3e^2) \quad (2.24)$$

where  $k = 2EI/L$  and  $e = (A - B)/L$ .

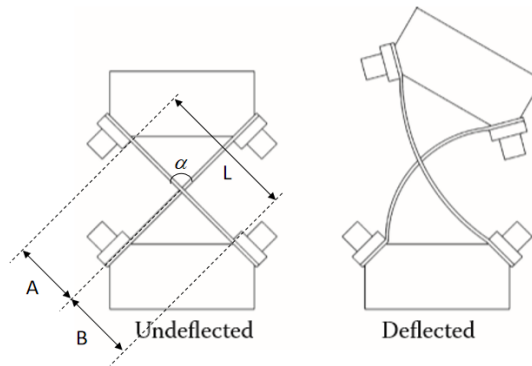


Figure 2.25: A general configuration of crossed flexure.

There are mainly two types of applications of crossed flexure in resonant scanner device. The first one is to use the resonance generated by crossed flexure itself. Additional mechanism would be needed to mount the mirror and locate it at the intersection of crossed flexure, such that the rotational center is at the mirror. W. Reimels[66] described a resonant scanning device where mirror was mounted on a support tube, and the tube was actuated by galvanometer, shown as Fig. 2.26. Resonant frequency of  $400\text{ Hz}$  was achieved, and center shift induced by  $10^\circ$  of rotation was approximately  $0.5$  and  $0.005\text{ mm}$  in direction of normal and parallel to mirror plate respectively, which was negligible. Other examples could be found in [60] and [67].

Another type is to use it as suspension, and resonance is provided by other separated oscillator. In this configuration, rotational stiffness of flexure suspension should be low, while radial and axial stiffness should be high, such that its dynamic separates a distance with resonance of oscillator. An example is called "Bendix Pivot", as shown in Fig. 2.27. M. Burdenko[69] adopted this method to develop a resonant scanner, where a "Bendix Pivot" was placed close to mirror, which acted as suspension to maintain rotational center, and a torsional bar was connected to the mirror to generate resonance.

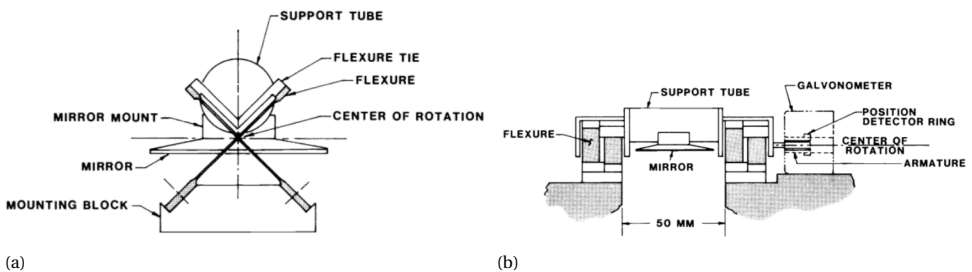


Figure 2.26: (a). Side view and (b). front view of a crossed flexure resonant scanner device[66].



Figure 2.27: A Bnedix Pivot[68].

#### 2.2.4. NOTCH FLEXURE

It should be noted that notch flexure hinge could also be used as suspension to maintain rotational center. Plenty of studies have been conducted on its behavior including stiffness, stress, rotational center and etc. in different notch profile. Relations between stiffness and different design parameters in different notch profile were studied by N. Xu et al.[70]. They analyzed four types of notch: elliptic, circular, parabolic and hyperbolic hinge, and design parameters were defined as shown in Fig. 2.28. Furthermore, shift of rotational center was indicated by two translation stiffness in  $x$  and  $y$  directions, and performance was implied by ratio between two translation stiffness and rotational stiffness. Their results showed that increase in parameter  $t$ ,  $h$  and  $b$  could heighten rotational stiffness and reduce center shift, while increase in  $l$  would generate opposite outcome. Performance is inversely related to  $t$  and  $h$  but insensitive to  $b$  and  $l$ . With same value in all parameters, hyperbolic notch profile is the least compliant in rotation but the most stiff in translation to maintain rotational center, while opposite behavior was reported for elliptic profile.

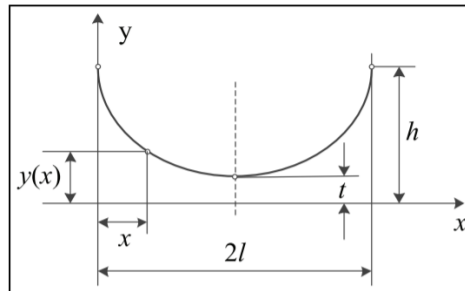


Figure 2.28: Parameters define half of symmetrical notch flexure[70].

Application examples of notch hinge in scanner could be found in [71], where notch hinges were used as suspension to support mirror, and in[72, 73], where they were used as replacement for rigid joint connection.

### 2.2.5. ACTUATION

To generate motion, actuator should be selected correctly based on different application. In a tunable resonant scanner, moving parts might include scanner and tuning mechanism. Regarding tilting motion of scanner, galvanometric, piezoelectric and voice coil actuator [74] could be used, where galvanometric and voice coil actuator produce force and piezoelectric actuator provides displacement. For some of tuning methods that require moving parts, positioning mechanism would be often needed and this could be realized by screw with motor or Lorentz actuator.

#### SCANNER

##### Galvanometric Actuator

This is commonly used in available galvanometer scanner in the market, which is often placed at the rotational axis of mirror with position detector, and generate torque to actuate scanning motion with high accuracy. The basic principle is interaction of magnetic field created by permanent magnet and wire coil with current. According to structure, it could be mainly divided into three categories, which are moving iron, moving magnet and moving coil type [75], as shown in Fig. 2.29a, 2.29b and 2.29c respectively. Moving iron type could provide a relatively high torque constant but might be limited to low speed because of magnetic saturation of iron. Moving coil one is generally sensitive and could achieve high torque to inertia ratio due to the use of high flux and low inertia coil. Its high positioning accuracy could also provide high level short and long term repeatability. Moving magnet type has the highest cut off frequency, due to high stiffness of moving magnet. While it could also achieve high torque to inertia ratio.

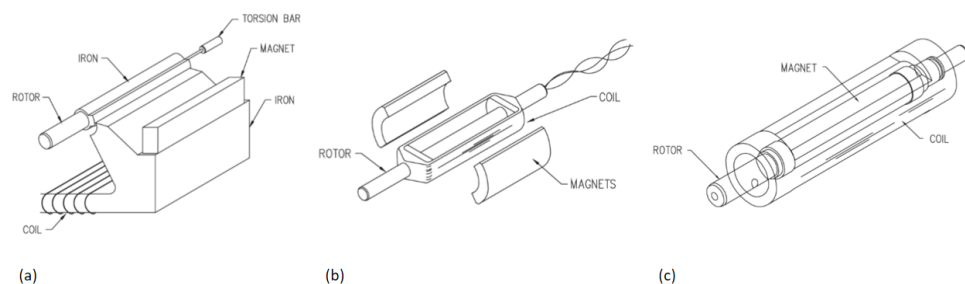


Figure 2.29: Schematic of galvanometric actuator in (a). moving iron (b). moving coil and (c). moving magnet configuration[75].

##### Piezoelectric Actuator

Piezoelectric effect could be divided into direct and inverse, where direct refers to electric potential generated in material when being compressed; and inverse refers to displacement produced by material when applying current[92]. Thus it could be used as a transducer between mechanical and electrical energy. As an actuator, it could provide high accuracy displacement with fine resolution up to sub-nanometer, while stroke is

often limited to micro-meter scale[74, 92]. To realize larger tilting angle, mechanical amplifier or other compliant mechanisms could be used to magnify piezoelectric actuator displacement. Furthermore, piezoelectric materials often have high mechanical resonant frequency up to a few tens of kilo Hertz, while creep, aging and hysteresis would be drawbacks of them.

T. Chen et al.[76] presented a compliant mechanism that transfers linear piezo displacement to rotation as output and hence realize scanning. The mechanism could be also miniaturize into MEMS device, and with  $40\mu m$  input displacement,  $\pm 12^\circ$  scanning angle was achieved.

S. Xiang et al.[77] used two piezoelectric actuators mounted on mechanical amplifier, where amplification ratio depends on length and height of it. Two actuator with amplifier mechanisms were in parallel connection to scanning mirror, and with same magnitude but opposite direction (shortening and extension), tilting motion of mirror was realized. In closed-loop control,  $\pm 12 mrad$  scanning angle with bandwidth  $250 Hz$  was achieved.

### Voice coil Actuator

Voice coil actuator is one of Lorentz actuator, where Lorentz force would be produced by supplying current to coil in magnetic field generated by permanent magnet. It has low connection stiffness between stationary and movable parts, which means external vibration from environment would less influence system (low transmissibility). Therefore, it is often used in high precision positioning application. Compared to galvanometric actuator, voice coil actuator is often used to generates linear motion. One widely used version of voice coil is moving coil type used on loudspeaker[92], with a general schematic shown as Fig. 2.30. It is rotation symmetrical, where a coil is inserted in to a magnetic field pointing towards center, created by a round magnet. In this way, the coil could be completely encircled by magnetic field and thus realize a high efficiency.

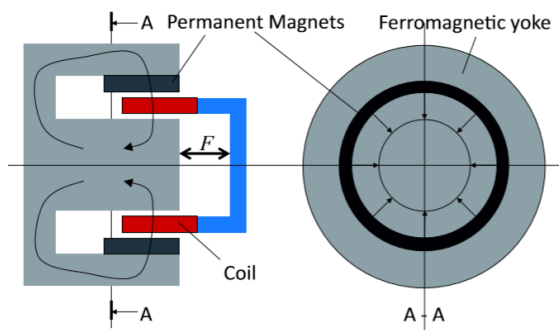


Figure 2.30: Schematic of galvanometric actuator in (a). moving iron (b). moving coil and (c). moving magnet configuration[92].

Q. Zhou et al. [73] connected two voice coil actuators in parallel to two edge of mirror,

and mirror center was suspended by a notch hinge. Same amplitude but different direction driving force were input to rotate mirror. A bandwidth of  $260\text{Hz}$  was achieved by closed-loop.

## 2

## TUNING MECHANISM

## Ball Screw

Ball screw is a widely used linear actuator which could transfer rotation into translation. Combined with stepper motor, it could generally achieve precision positioning. However, its accuracy is often limited to (sub)micro meter level. To realize higher resolution up to nanometer level, other precision linear actuators such as Lorentz and piezoelectric actuators would be combined, where ball screw is used for large stroke movement and other actuators are for small stroke adjustment [78, 79]. To eliminate backlash between screw and end effector, often preload spring would be used [12].

## Lorentz Actuator

Lorentz actuator is inherently favorable for high precision positioning, and to realize long stroke movement, more magnets and coil segments could be added. Fig. 2.31 shows a schematic of moving coil three phase large stroke Lorentz actuator, where magnets part is consist with a set of even number alternatively magnetized permanent magnets, and coil is divided into three equal parts. In this way, force factor  $Bl$  of each coil is sinusoidal function of position, with spatial phase difference  $120^\circ$ . The net force factor of three coil is almost constant, shown as black curve.

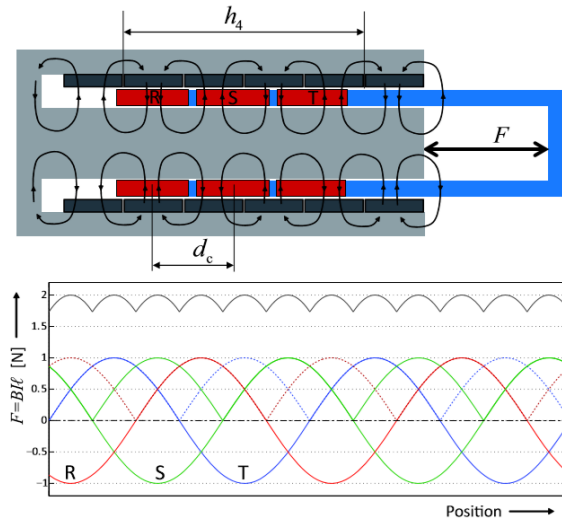


Figure 2.31: Schematic of galvanometric actuator in (a) moving iron (b) moving coil and (c) moving magnet configuration [92].



### 2.2.6. DISCUSSION AND CONCLUSION

In this section, several mechanisms used to design resonant scanner are reviewed. Discussion are listed below.

- **Cantilever beam:** Cantilever beam in clamp-free configuration is a simple way to achieve resonant tilting motion. Its resonant frequency could be easily tuned by changing effective length, and even activating higher order eigenmodes. When beam length is shortened, to have the same magnitude of tilting angle at tip, smaller deflection is needed. However, an obvious drawback is parasitic translation of tip, and hence the mirror does not have fixed rotational center. Other hinge mechanisms could be used to constraint translation, but their eigenfrequency should not close to that of the beam.
- **Torsional beam:** The rotational center of a torsional beam is rather fixed, and it is a common solution for resonant scanners in literature and commercial products. However, if tuning method of changing effective length is used, magnitude of angular deflection would be lower when beam length is shortened. For some boundary conditions such as clamp-clamp, beam length should be symmetrically changed, which means more tuning mechanism.
- **Crossed Flexure:** Crossed flexure has low rotational stiffness in its DoF while high stiffness in other DoFs. Rotational center could be remained, with negligible parasitic deviation. Resonant frequency of the flexure itself could be tuned, while the flexure could also be used as suspension. It should be noted that to be qualified as suspension, its rotational stiffness should be low and eigenmodes does not occur in the tuning range of resonator. One should notice that, crossed flexure itself is over-constrained, and to realize statically determined design, notch could be introduced to release some DoFs.
- **Notch Flexure:** A notch flexure could be used as a hinge suspension to constraint translation and release rotation, however, one should be aware of number of constraint of notch to avoid over-constrained. Notch could also be introduced to mechanism to release rotation, as a solution to over-constrained design. Though its resonant frequency is rather difficult to tune, the design is simple and easy to manufactured. Noting that its dynamic should be investigated such that it does not effect motion of resonator.
- **Actuation:** Regarding actuation of scanner which might include resonator and suspension, actuator selection should base on scanning mechanism design. When rotational axis is fixed by suspension, a moment could be applied, and this could be generated by single motor or pair of piezoelectric or voice coil actuator. Regarding tuning mechanism, selection should base on tuning accuracy. Noting that some tuning methods such as axial load, which could be sensitive but might not require a large stroke movement, piezoelectric and voice coil actuator could be considered for precision small stroke adjustment.

Table 2.4 summarizes advantages and disadvantages of different mechanisms for resonant tilting motion. It should be noted that some mechanisms are suitable for both resonator and suspension. It is possible to integrate resonator whose stiffness could be tuned for a wide range, with suspension that could maintain rotational center, and hence develop a tunable resonant scanning mirror with wide working range. Noting that for resonator, eigenmode of desire resonance should separate a distance with other modes in frequency spectrum for the whole tuning range in order to avoid energy coupling. And dynamics of suspension should not occur in the working range of resonator as well.

| <b>Mechanism</b> | <b>Advantages</b>   | <b>Disadvantages</b>   |
|------------------|---|--|
| Cantilever beam  | <ul style="list-style-type: none"> <li>•Simple</li> <li>•Easy to implement tuning</li> </ul>  | <ul style="list-style-type: none"> <li>• No fixed rotational center</li> </ul>   |
| Torsional beam   | <ul style="list-style-type: none"> <li>•Fixed rotational center</li> </ul>  | <ul style="list-style-type: none"> <li>•Difficult to avoid energy coupling</li> <li>•More tuning mechanisms may need</li> <li>•Low magnitude of angular deflection for short beam</li> </ul> |
| Crossed flexure  | <ul style="list-style-type: none"> <li>•Fixed rotational axis with almost negligible deviation</li> <li>•Low rotational stiffness, could be used as suspension</li> </ul> | <ul style="list-style-type: none"> <li>•Dynamic at high frequency could effect motion of resonator</li> <li>•Over-constrained</li> </ul>   |
| Notch flexure    | <ul style="list-style-type: none"> <li>•Simple, easy to manufacture</li> <li>•Fixed rotational center, could be used as suspension</li> </ul>                             | <ul style="list-style-type: none"> <li>•Dynamic at high frequency could effect motion of resonator</li> <li>•Difficult to tune resonant frequency</li> </ul>                                 |

Table 2.3: Summary of advantages and disadvantages of different mechanisms

## 2.3. REVIEW OF DYNAMIC BALANCING STRATEGIES

To move an object, a force or moment is needed, and an equal and opposite reaction would be generated simultaneously. In a machine especially high-speed ones, this reaction would transmit to base frame and other components, leading to issues such as unwanted vibration, wear and fatigue[80]. A mechanism that is designed in a way such that reaction force and moment are eliminated is dynamically balanced[81]. The basic principle is that reaction force is balanced when linear momentum is constant during movement, which is often achieved by counter mass or fixed position of center of mass (CoM). Reaction moment is eliminated when angular momentum is constant, which could be achieved by counter rotation.

In the resonant scanner device, resonance and reactions are generated by elastic flexure elements. A brief review on reaction force and moment compensation is conducted. Numerous studies are focusing on dynamic balancing of rigid body interaction by ideal joints[80], while limited researches in the field of compliant mechanism are found. Following contents would briefly summarize and compare different methods.

### 2.3.1. REACTIONLESS DESIGN

To achieve reactionless, each individual movable element could be balanced and hence the total mechanism is reactionless. It is found that this could be realized by adding counter mass and rotation, or inherently dynamically balanced mechanism. Noting that a key common feature is fixed CoM during motion.

Lots of studies were carried out on the balancing of rigid 4-bar linkages with revolute joints, where counter mass or parallelogram were added to maintain CoM and counter rotation were used to balanced moment[82–85]. S. K. Agrawal and A. Fattah [86] proposed two concepts of reactionless space robot manipulators. The first one is open-chain with 3 linkages in series connection where each linkage was balanced by a counter mass; and for the second one, CoM was fixed by auxiliary parallelograms. Reaction force were balanced by connecting CoM to base, while reaction moment could only be balanced by restricting to a certain trajectory. E. S. Papadopoulos and A. A. Abed[87] developed a 3 DoF manipulator, where within certain work space, inertia force between linkages could compensate each other and hence achieve fixed CoM, while reaction moment was eliminated by following certain trajectories. This "reaction less" work space is fairly small compared to total reachable work space. V. van der Wijk[88] presented a synthesis method of inherently dynamically balanced mechanisms based on principle vector linkage. This could achieve reaction force balance since CoM is fixed, while it was claimed that moment balance was still challenging to solve. He proposed that it might be possible to combine force balanced linkages such that they are counter rotate and eliminate reaction moment.

This principle could be applied on compliant mechanisms to balance flexible elements. S. Martinez1 et al.[89] presented a flexible 4-bar linkage mechanism with rigid coupler. They proposed a method for force balancing on a flexible beam with tip mass, which is

adding a counter mass connected with another flexible beam, as shown in Fig. 2.32a. Criterion is constant linear momentum and equal eigenfrequency for both sides, corresponding to fixed CoM and same oscillation pattern of flexible beams. Therefore, conditions for force balancing could be derived as[89]

$$m_1 l_1 = m_2 l_2, \quad l_1^2 \rho_1 A_1 = l_2^2 \rho_2 A_2, \quad \frac{E_1 I_1}{l_1^2} = \frac{E_2 I_2}{l_2^2}. \quad (2.25)$$

where  $m$  is tip mass,  $\rho$  is material density,  $A, l, E, I$  is cross sectional area, length, Young's Modulus and second moment of inertia of beam. Revolute joints were also replaced by compliant butterfly hinges, which has low rotational stiffness, rather fixed CoM, and symmetrical mass distribution, shown as Fig. 2.32b. Results showed that 93% force reduction was obtained by revolute joint and 97.3% by compliant butterfly hinge. While reaction moment was still unbalanced.

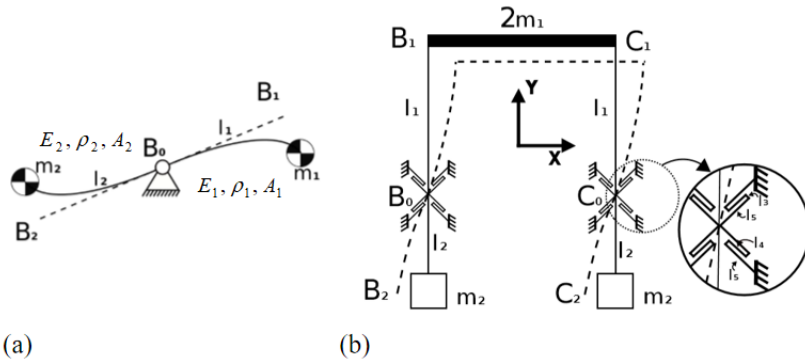


Figure 2.32: Schematic of (a). dynamic balancing on a flexible beam and (b). a dynamically balanced compliant 4 bar linkage with rigid coupler[89].

### 2.3.2. SEPARATED BALANCING MECHANISM

One could also separate counter mass or rotation, which is often used to balance mass with linear motion. Balancing mechanism could be actuated actively to generate equal but opposite reaction to compensate. Counter mechanism could be added to existing system, without changing original configuration. Noting that in terms of force compensation, reaction force generated by counter mechanism and moving object should exert at a same line, otherwise a moment would be generated. While for moment balancing, this does not matter.

S. Song and M. Zhang[90] presented a 3 DoF reactionless parallel platform to actively balance reaction force for robot movement on a spacecraft. Reaction force was balanced by moving a mass, with approximately same value as robot, in same amplitude but opposite direction with respect to robot, while moment was balanced by a counter rotating wheel on the spacecraft.

R. Schmidt[91, 92] described the balancing design in modern lithography machine, where a  $80\text{kg}$  wafer stage was balanced by a  $500\text{kg}$  mass. Balanced mass was suspended by air bearing or compliant guiding with low stiffness and actuated by Lorentz actuator. A much heavier balancing mass could lead to shorter relative movement, which could get rid of large stroke linear motor.

P. Sebek[93] developed a 3 DoF dynamically balanced fully compliant stage for scanning microscope. A sample holder stage was suspended by three folded leaf springs for 3 DoF motion, and balancing masses were connected to the stage by lever, to produce opposite momentum with respect to movement of sample stage, shown as Fig. 2.33a. In this way, CoM of the whole system does not move. Reaction force was reduced by a factor of 50, reported from testing. He also proposed an issue caused by internal stress, shown as Fig. 2.33b. Even net force acting on a compliant element is zero, displacement field is not zero, and hence the connection point between this element to other parts should have zero displacement in order to isolate reaction forces.

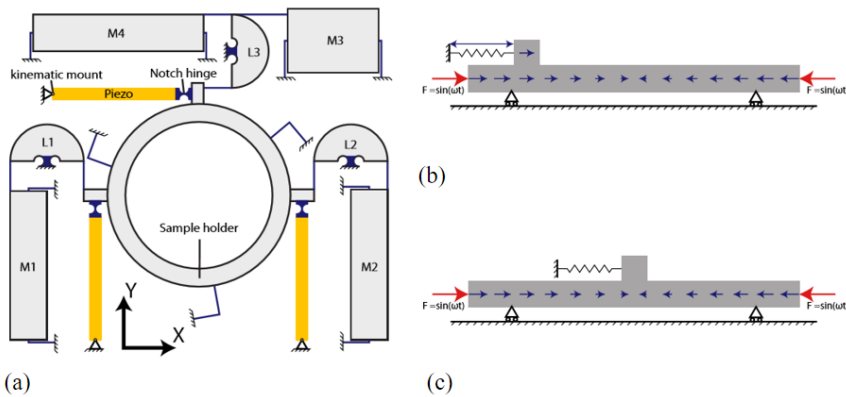


Figure 2.33: (a). Schematic of a dynamically balanced fully compliant scanning stage. Connection point of a compliant element under zero net force (b). with displacement and (c). with zero displacement[93].

### 2.3.3. CONNECTION POINT

Regarding compliant mechanism, during movement, flexible elements would deform, and this deformation could exert force and moment to suspension or base which causes unwanted vibration. When the connection points of this element are nodes of eigenmode of deformation configuration, then reactions could be reduced.

J. P. Meijaard and V. van der Wijk[94] analytically studies supporting of flexible beam as a coupler in a 4-bar linkage (other bars were assumed rigid) for dynamic balancing. Two counter rotation wheels were added to the connection joints between bars and ground, and each rigid bar was balanced mass. In this way, reactions were only produced by the flexible beam. A trade off between force and moment balance were found. Compared to hinge at two end of the beam, hinge at two node of first bending mode could achieve

force reduction by a factor of 20 and moment reduction of 2. To further consider balancing for the first, third and fifth mode, two points that could result in the least movement of CoM of the beam at these modes were chosen, force reduction by a factor of 200 was achieved but reaction moment increased.

2

#### 2.3.4. DUPLICATE MECHANISM

It is intuitive that two identical mechanisms move with same amplitude but out of phase could compensate reaction. As discussed in [81], axial and mirror symmetric duplicate mechanisms could completely eliminate reaction force and moment and all mechanisms are balanced each other together.

Considering a double pendulum, its rotation about pivot would generate reaction forces and moment. A mirror mechanism could be added to counter rotate with it. Reaction moment and reaction at horizontal direction are eliminated, while reaction force at vertical direction are doubled. An axial mirror mechanism could then be added such that this reaction force is compensated, shown as Fig. 2.34.

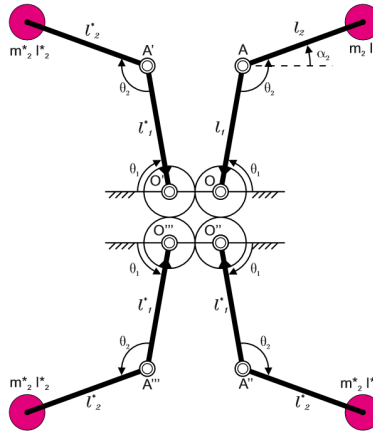


Figure 2.34: Dynamically balanced double pendulum by duplicate mechanism[81].

#### 2.3.5. DISCUSSION AND CONCLUSION

A brief review on dynamic balancing methods is conducted, mainly focusing on methods applicable to compliant mechanism. Discussion are presented below.

- Reactionless design could be used to balance flexible beam, with counter mass suspended by another flexible beam, and connected to moving object by some flexure hinge. This could achieve advantageous balancing on reaction force, but moment is still unable to balance, since it could be hard to apply counter rotation on compliant mechanism. Furthermore, balancing mass could also be difficult to connect to some resonators such as cantilever with fixed clamp to base ground.

- Separated balancing mechanism could be added to the existing system without modification to original moving parts. This could also be able to implemented on compliant mechanism, with certain connections to moving parts. Added balancing mechanism could also be used to absorb reactions, which are generated by original moving parts and transmitted to base ground. These reactions would activate the added balancing mechanisms, and it is possible that reactions generated by balancing mechanisms could achieve compensation. Another simple way is to mount mechanism on a heavy mass suspended by air bearing and the reactions would be absorbed by the mass.
- When connection points of flexible element are nodes of eigenmode, then reaction force and moment could be reduced. While for situation such as resonator with fixed clamp boundary condition, the connection point to the base is forced to be a node, and this would still generate reactions. Noting that during the tuning process, eigen modeshape would change and hence position of nodes.
- Duplicate mechanism could achieve that four mechanisms are balanced together, but in compliant mechanism design, it might lead to complex design that would occupy large space, since one end effector needs 3 extra same mechanism to balance.

| Strategy                      | Advantages   | Disadvantages   |
|-------------------------------|--|---|
| Reactionless Design           | <ul style="list-style-type: none"> <li>• advantageous balancing on reaction force</li> </ul>   | <ul style="list-style-type: none"> <li>• Difficult to balance moment</li> <li>• Difficult to implement on clamped B.C.</li> </ul>                             |
| Separated Balancing Mechanism | <ul style="list-style-type: none"> <li>• Without large modification on original mechanism</li> <li>• Could balance flexible element with clamped B.C.</li> </ul> |   |
| Connection Point              | <ul style="list-style-type: none"> <li>• Could balance reaction force and moment</li> </ul>  | <ul style="list-style-type: none"> <li>• Trade off between force and moment reduction</li> <li>• Nodal position could change during tuning process</li> </ul> |
| Duplicate Mechanism           | <ul style="list-style-type: none"> <li>• Could balance reaction force and moment</li> </ul>  | <ul style="list-style-type: none"> <li>• Would occupy large space</li> </ul>  |

Table 2.4: Summary of advantages and disadvantages of different mechanisms

Regarding a tunable resonant scanner device, which could consist flexure resonator, suspension and tuning mechanism, it could be challenging to implement dynamic balancing, since balancing flexure mechanism should remain same linear momentum and

eigenfrequency as the resonator during the wide range tuning. Noting that for compliant cantilever beam, reaction force could be balanced by another added beam, but moment would still exist, and added beam should be aligned at the same line as the resonator beam. While for torsional flexible beam, both reaction force and moment could be eliminated by adding another torsional beam. And even they are not aligned at the same line, reaction moment could still be compensated. Another promising balancing way is to mount the flexure mechanism on a heavy platform suspended by air bearing. In this way, reaction is hardly transmitted.

## REFERENCES

- [1] S. W. Ibrahima et al., *A review on frequency tuning methods for piezoelectric energy harvesting systems*, *Journal of Renewable Sustainable Energy*, vol. 4, 2012.
- [2] J. Twiefel and H. Westermann, *Survey on broadband techniques for vibration energy harvesting*, *Journal of Intelligent Material Systems*, vol. 24, pp. 1291–1302, 2013.
- [3] D. B. Murphy, "Confocal Laser Scanning Microscopy," in *Fundamentals of Light Microscopy and Electronic Imaging*, New Jersey: Wiley, 2001, pp. 218.
- [4] M. d. Laat et al., *A review on in situ stiffness adjustment methods in MEMS*, *Journal of Micromechanics and Microengineering*, vol. 26, 2016.
- [5] J. I. Montagu et al., "Tunable resonant mechanical system.", U.S. Patent 4,874,215, issued October 17, 1989.
- [6] M.F. Winthrop et al., *A variable stiffness device selection and design tool for lightly damped structures*, *Journal of Sound and Vibration*, Vol. 287, pp. 667-682, 2005.
- [7] D. Zhu et al., *Strategies for increasing the operating frequency range of vibration energy harvesters: a review*, *Measurement Science and Technology*, vol. 21, 2010.
- [8] J. A. GREENWOOD et al., *Contact of nominally flat surfaces*, *Proceedings of the Royal Society of London. Series A, Mathematical and Physical Sciences*, vol. 295, pp. 300-319, December 6, 1996.
- [9] L. Esteveny et al., *Variable Stiffness Mechanism in Robotized Interventional Radiology*, in *"New Trends in Medical and Service Robots. Mechanisms and Machine Science"*, vol. 39, Springer, 2016, pp. 45-58, 978-3-319-30673-5.
- [10] J. Schaufuss et al., *New approach of frequency tuning for kinetic energy harvesters*, *2 Sensors and Actuators A: Physical*, vol. 171, pp. 352-360, 2011.
- [11] X. Wu et al., *A Frequency Adjustable Vibration Energy Harvester*, *Proceedings of PowerMEMS 2008+ microEMS2008*, Sendai, Japan, November 9-12, 2008.
- [12] H. Soemers, *Design for Stiffness*, in *"Design Principle for Precision Mechanism"*, 978-90-365-3103-0, 2010.



- [13] A. Jafari et al., *A Novel Actuator with Adjustable Stiffness (AwAS)*, *The 2010 IEEE/RSJ International Conference on Intelligent Robots and Systems, Taipei, Taiwan*, October 18-22, 2010.
- [14] B. Kim et al., *Hybrid Dual Actuator Unit: A Design of a Variable Stiffness Actuator based on an Adjustable Moment Arm Mechanism*, *2010 IEEE International Conference on Robotics and Automation Anchorage Convention District, Anchorage, Alaska, USA*, May 3-8, 2010.
- [15] A. Jafari et al., *A New Actuator With Adjustable Stiffness Based on a Variable Ratio Lever Mechanism*, *IEEE/ASME Transaction on Mechatronics*, vol. 19, No. 1, 2014.
- [16] S. S. Groothuis et al., *The Variable Stiffness Actuator vsaUT-II: Mechanical Design, Modeling, and Identification*, *IEEE/ASME Transaction on Mechatronics*, vol. 19, No. 1, 2014.
- [17] N. G. Tsagarakis et al., *A New Variable Stiffness Actuator (CompAct-VSA): Design and Modelling*, *2011 IEEE/RSJ International Conference on Intelligent Robots and Systems, San Francisco, CA, USA*, September 25-30, 2011.
- [18] L. C. Visser et al., *Modeling and Design of Energy Efficient Variable Stiffness Actuators*, *2010 IEEE International Conference on Robotics and Automation Anchorage Convention District, Anchorage, Alaska, USA*, May 3-8, 2010.
- [19] L. M. Roylance et al., *A batch-fabricated silicon accelerometer*, *IEEE Transactions on Electron Devices*, vol. 26, pp. 1911 - 1917, 1979.
- [20] A. G. Dunning et al., *Bistable Compliant Mechanisms: Corrected Finite Element Modeling for Stiffness Tuning and Preloading Incorporation*, *Journal of Mechanical Design*, vol. 134, 2012.
- [21] N. Tolou et al., *A Breakthrough in Precision Engineering*, *Mikroniek*, No. 6, 2010.
- [22] A. G. Dunning et al., *A compact low-stiffness six degrees of freedom compliant precision stage*, *Precision Engineering*, vol. 37, pp. 380-388, 2013.
- [23] A. Stapel and J. L. Herder, *Feasibility Study of a Fully Compliant Statically Balanced Laparoscopic Grasper*, *Proceedings of DETC'04 ASME 2004 Design Engineering Technical Conferences and Computers and Information in Engineering Conference, Salt Lake City, Utah, USA*, Sept. 28 -Oct. 2, 2004.
- [24] J. Lassoij et al., *A statically balanced and bi-stable compliant end effector combined with a laparoscopic 2DoF robotic arm*, *Mechanical Science*, vol. 3, pp. 85-93, 2012.
- [25] N. Tolou et al., *Statically Balanced Compliant Micro Mechanisms (SB-MEMS): Concepts and Simulation*, *Proceedings of the ASME 2010 International Design Engineering Technical Conferences and Computers and Information in Engineering Conference.*, August 15-18, 2010. pp. 447-454. ASME.

- [26] P. J. Pluimers et al., *A Compliant On/Off Connection Mechanism for Preloading Statically Balanced Compliant Mechanisms*, *Proceedings of the ASME 2012 International Design Engineering Technical Conferences & Computers and Information in Engineering Conference*, Chicago, IL, USA, August 12-15, 2012.
- [27] M. Yalcin et al., *VNSA: Variable Negative Stiffness Actuation based on Nonlinear Delection Characteristics of Buckling Beams*, *2013 IEEE/RSJ International Conference on Intelligent Robots and Systems (IROS) Tokyo, Japan*, November 3-7, 2013..
- [28] C. B. Churchill et al., *Dynamically variable negative stiffness structures*, *Science Advance*, vol. 2, 2016.
- [29] Y. S. Wu and C. C. Lan, *Linear Variable-Stiffness Mechanisms Based on Preloaded Curved Beams*, *Journal of Mechanical Design*, vol. 136, 2014.
- [30] V. R. Challa et al., *A vibration energy harvesting device with bidirectional resonance frequency tunability*, *Smart Material and Structure* vol. 17, 2008.
- [31] V. R. Challa et al., *High efficiency energy harvesting device with magnetic coupling for resonance frequency tuning*, *Proceedings SPIE 6932, Sensors and Smart Structures Technologies for Civil, Mechanical, and Aerospace Systems 2008* April 8<sup>th</sup>, 2008.
- [32] D. F. Pilkington and J. B. Carr, *Vibration of Beams Subjected to End and Axially Distributed Loading*, *Journal Mechanical Engineering Science*, Vol 12, No.1, 1970.
- [33] S. Laux, *Estimation of Axial Load in Timber Beams using Resonance Frequency analysis (Master thesis)*, *Chalmers University of Technology*, Gothenburg, Sweden, 2012.
- [34] G. Rebecchi et al., *Estimate of the axial force in slender beams with unknown boundary conditions using one flexural mode shape*, *Journal of Sound and Vibration*, vol 332, pp.4122-4135, 2013.
- [35] A. Bokaian, *Natural frequencies of beams under compressive axial loads*, *Journal of Sound and Vibration*, vol 126, pp.49-65, 1988.
- [36] L. Šnirc et al., *Axial force and bending stiffness*, *Journal of Sound and Vibration*, vol 126, pp.49-65, 1988.
- [37] C.L. Amba-Rao, *Effect of End Conditions on the Lateral Frequencies of Uniform Straight Columns*, *The Journal of the Acoustical Society of America*, vol 42, pp. 900, 1967.
- [38] E. S. Leland and P. K. Wright, *Resonance tuning of piezoelectric vibration energy scavenging generators using compressive axial preload*, *Smart Materials and Structures*, vol 15, pp. 1413-1420, 2006.
- [39] Y. Hu et al., *A piezoelectric power harvester with adjustable frequency through axial preloads*, *Smart Materials and Structures*, vol 16, pp.1961–1966, 2007.

- [40] C. Eichhorn et al., *A Frequency Tunable Piezoelectric Energy Converter Based on a Cantilever Beam*, *Proceedings of PowerMEMS 2008+ microEMS2008*, Sendai, Japan, November 9-12, 2008, pp.309-312.
- [41] C. Eichhorn et al., *Bidirectional frequency tuning of a piezoelectric energy converter based on a cantilever beam*, *Journal of Micromechanics and Microengineering*, vol. 19, 2009.
- [42] D. Zhu et al., *Frequency Tuning Vibration Energy Harvesters using Compressive and Tensile Axial Loads*, *PowerMEMS 2011*, 15 - 18 Nov 2011.
- [43] C. Rogers et al., *Behavior of shape memory alloy reinforced composite plates. I - Model formulations and control concepts*, *30<sup>th</sup> Structures, Structural Dynamics and Materials Conference*, Mobile, AL, U.S.A., April 3-5, 1989.
- [44] C. Liang et al., *Behavior of shape memory alloy reinforced composite plates. II - Results*, *30<sup>th</sup> Structures, Structural Dynamics and Materials Conference*, Mobile, AL, U.S.A., April 3-5, 1989.
- [45] K. Williams et al., *Adaptive-Passive Absorbers using Shape-Memory Alloys*, *Journal of Sound and Vibration*, vol. 249, no. 5, pp. 835-848, 2002.
- [46] E. Rustighi et al., *A shape memory alloy adaptive tuned vibration absorber: design and implementation*, *Smart Materials and Structures*, vol. 14, pp. 19-28, 2005.
- [47] C. Peter et al., *Novel Electrically Tunable Mechanical Resonator for Energy Harvesting*, *Proceedings of PowerMEMS 2008+ microEMS2008*, Sendai, Japan, November 9-12, 2008.
- [48] Y. Kawai et al., *Piezoelectric Actuator Integrated Cantilever with Tunable Spring Constant For Atom Probe*, *19th IEEE International Conference on Micro Electro Mechanical Systems*, January, pp.778-781, IEEE, 2006.
- [49] S. T. S. Holmström et al., *MEMS Laser Scanners: A Review*, *Journal of Microelectromechanical system*, vol. 23, 2014.
- [50] R. Clough and J. Penzien, "Analysis of Undamped Vibration", in *Dynamic of Structures*, 3<sup>rd</sup> edition, Berkeley, 2003, pp. 377.
- [51] R. D. Blevins, *Formulas for Natural Frequency and Mode Shape*, ISBN: 0442207107, 1979.
- [52] L.B. Kheng et al., *Design optimization and fatigue testing of an electronically-driven mechanically-resonant cantilever spring mechanism*, *Materials and Design*, vol. 31, pp. 4023-4028, 2010.
- [53] J. Chen et al., *Dynamic Macromodeling of MEMS Mirror Devices*, *International Electron Devices Meeting*, Washington, DC, USA, December 2-5, 2001.
- [54] J. I. Montagu et al, "Tunable resonant mechanical system.", *U.S. Patent 4,874,215*, issued October 17, 1989.

- [55] L. Koay and H. Gitano, *Design and Optimization of Mechanically Resonant Torsional Spring Mechanism for Laser Light Dispersion Applications*, *Journal of Mechanical Design*, vol. 133, 2011.
- [56] L. Koay and M. Ratnam, *Magnet Position Variation of the Electromagnetic Actuation System in a Torsional Scanner*, *International Journal of Computer and Information Engineering*, vol. 8, pp. 1357-1366, 2014.
- [57] H. Urey et al, *Optical scanners for high resolution RSD systems*, *Proceedings of SPIE, AeroSense, Orlando, U.S.*, vol. 4711, August 5, 2002.
- [58] W. H. Wittrick, *The theory of symmetrical crossed flexure pivots*, *Australian Journal of Chemistry*, vol. 1, pp. 121-134, 2002.
- [59] H. Zhao and S. Bi, *Accuracy characteristics of the generalized cross-spring pivot*, *Mechanism and Machine Theory*, vol. 45, pp. 1434-1448, 2010.
- [60] R. A. DeBoalt, "Method for Tuning the Resonant Frequency of Crossed-Flexure Pivot Galvanometers.", *U.S. Patent 6,265,794 B1*, issued July 24, 2001.
- [61] S. Zelenika and F. De Bona, *Analytical and experimental characterisation of high-precision flexural pivots subjected to lateral loads*, *Precision Engineering*, vol. 26, pp. 381-388, 2002.
- [62] W. E. Young, *An investigation of the cross-spring pivot*, *Journal of Applied Mechanics*, vol. 11, pp. 113-120, 1944.
- [63] J. A. Haringx, *The cross-spring pivot as a constructional element*, *Applied Scientific Research*, vol. 1, pp. 313-332, 1949.
- [64] H. Troeger, *Considerations in the application of flexural pivots*, *Automatic Control*, vol. 17, pp. 41-46, 1962.
- [65] E. G. Merriam et al., *compound joints: Behavior and benefits of flexure arrays*, *Precision Engineering*, vol. 145, pp. 79-89, 2016.
- [66] W. Reimels, *Low Wobble Resonant Scanners*, *Proceeding SPIE 0390, High Speed Read/Write Techniques for Advanced Printing and Data Handling, Los Angeles, U.S.*, September 20, 1983.
- [67] J. S. Gadhok, *Self Resonant Scanning Device*, *U.S. Patent 4,732,440*, issued March 22, 1988.
- [68] *Office of Research at Utah State University, "Technology Transfer Services"*, accessed at 30/1/2020. <https://research.usu.edu/techtransfer/monolithic-like-flexures/>.
- [69] M. Burdenko, *Resonant Scanner*, *U.S. Patent 5,528,411*, issued June 18, 1996.
- [70] N. Xu et al., *Analysis and design of symmetric notch flexure hinges*, *Advances in Mechanical Engineering*, vol. 9, pp. 1-12, 2017.

- [71] Q. Zhou et al., *Design of Fast Steering Mirror Systems for Precision Laser Beams Steering*, *IEEE International Workshop on Robotic and Sensors Environments*, Ottawa, Canada, October 17-18, 2008.
- [72] S. Xiang et al., *Study on fast linear scanning for a new laser scanner*, *Optics & Laser Technology*, vol. 42, pp. 42-46, 2010.
- [73] N. He et al., *Design and mechanism analysis of a novel type compact single mirror laser scanner*, *Sensors and Actuators A: Physical*, vol. 125, pp. 482-485, 2006.
- [74] L. Koay and N. Rahim, *Reviews: Torsional spring mechanism resonant scanner's technology*, *Journal of Mechanical Science and Technology*, vol. 30, pp. 1781-1798, 2016.
- [75] R. P. Aylward, *Advanced galvanometer-based optical scanner design*, *Sensor Review*, vol. 3, pp. 216-222, 2003.
- [76] T. Chen et al., *12° design rule for single crystal silicon curved beam compliant mechanisms with large deformation*, *IEEE 23rd International Conference on Micro Electro Mechanical Systems (MEMS)*, Wanchai, Hong Kong, China 24-28 Jan. 2010.
- [77] S. Xiang et al., *Study on fast linear scanning for a new laser scanner*, *Optics & Laser Technology*, vol. 42, pp. 42-46, 2010.
- [78] B. A. Awabdy et al., *Nanometer Positioning of a Linear Motion Stage Under Static Loads*, *IEEE/ASME Transaction on Mechatronics*, vol. 3, pp. 113-119, 1998.
- [79] J. Chen and I. Dwang, *A ballscrew drive mechanism with piezo-electric nut for preload and motion control*, *International Journal of Machine Tools and Manufacture*, vol. 40, pp. 513-526, 2000.
- [80] V. H. Arakelian and M. R. Smith, *Shaking Force and Shaking Moment Balancing of Mechanisms: A Historical Review With New Examples*, *Journal of Mechanical Design*, vol. 127, pp. 334-339, 2005, ASME.
- [81] V. van der Wijk et al., *Comparison of Various Dynamic Balancing Principles Regarding Additional Mass and Additional Inertia*, *Journal of Mechanisms and Robotics*, vol. 1, 2009, ASME.
- [82] Bagci. C., *Complete Shaking Force and Shaking Moment Balancing of Link Mechanisms Using Balancing Idler Loops*, *Transaction of ASME*, vol. 104, pp. 482-493, 1982, ASME.
- [83] z. Ye, and M. R. Smith, *Complete Balancing of Planar Linkages by an Equivalence Method*, *Mechanism and Machine Theory*, vol. 29, pp. 701-712, 1994.
- [84] R. S. Berkof, *Complete Force and Moment Balancing of Inline FourBar Linkages*, *Mechanism and Machine Theory*, vol. 8, pp. 397-410, 1973.

- [85] G. Feng, *Complete Shaking Force and Shaking Moment Balancing of 17 Types of Eight-Bar Linkages Only With Revolute Pair*, *Mechanism and Machine Theory*, vol. 26, pp. 197-206, 1991.
- [86] S. K. Agrawal and A. Fattah, *Reactionless space and ground robots: novel designs and concept studies*, *Mechanism and Machine Theory*, vol. 39, pp. 25-40, 2004.
- [87] E. Papadopoulos and A. A-Abed, *Design and Motion Planning for a Zero-Reaction Manipulator*, *Proceedings of the 1994 IEEE International Conference on Robotics and Automation, San Diego, California*, May 8-13, 1994.
- [88] V. van der Wijk, *Methodology for analysis and synthesis of inherently force and moment-balanced mechanisms - theory and applications*, *Ph.D. Thesis*, 2014.
- [89] S. Martinez<sup>1</sup> et al., *On the Shaking Force Balancing of Compliant Mechanisms*.
- [90] S. Song and M. Zhang, *A Study of Reactional Force Compensation Based on Three-Degree-of-Freedom Parallel Platforms*, *Journal of Robotic Systems*, vol. 12, pp. 783-794, 1995.
- [91] R. M. Schmidt, *Ultra-precision engineering in lithographic exposure equipment for the semiconductor industry*, *Philosophical Transaction of the Royal Society A*, vol. 370, pp. 3950-3972, 2012.
- [92] R. M. Schmidt et al., *"Precision Positioning in Wafer Scanners"*, in *The Design of High Performance Mechatronics*, pp. 687-732, 2011, Delft University Press, ISBN 978-1-60750-825-0.
- [93] P. Sebek, *Dynamically balancing a flexure-based scan stage inside a scanning electron microscope*, *Master Thesis*, 2015.
- [94] J. P. Meijaard and V. van der Wijk, *"On the Dynamic Balance of a Planar Four-Bar Mechanism with a Flexible Coupler"*, in *Advances in Mechanism and Machine Science*, pp. 3037-3046, 2019, Springer.

# 3

## OBJECTIVE

### 3.1. PROJECT GOAL

The literature part summarizes a variety of eigenfrequency tuning methods, scanner mechanisms and dynamic balancing approach, with lots of examples in each category. However, no literature has been found about resonant frequency tunable device for such a wide range in macro-scale applications. And regarding the resonant scanner, some designers attempted to make resonant frequency tunable, but it is intended for error correction in a small range, to cope with manufacturing error, mechanical wear, change of working conditions and etc. Based on this, the objective of this thesis is to:

*Design a tunable scanner system that could achieve scanning motion in resonance, with a novel tuning method to cover a wide frequency range of 500 to 5k Hz.*

### 3.2. APPROACH

The project is divided into the following parts based on V-Model

- 1. System Concept: Select a tuning method and investigate the feasibility of the novel tuning method to cover the intended frequency range.
- 2. Subsystem Concept: Propose concepts to implement resonance and tuning method according to the chosen system concept.
- 3. Detail Design: Design dimension and detail features for individual component and combine with finite element modelling and analysis to validate performance.
- 4. Testing: Integrate the setup and design experiment to validate performance.

### 3.3. THESIS OUTLINE

The thesis is organized in the following structure:

Chapter 1 is a brief introduction for the background information and requirements, Chapter 2 provides a well-rounded literature review. This Chapter states the project goal and design approach. The core design flow, simulation study and test results would be presented in a paper format in Chapter 4. After that, some supplementary materials including concept design, dimension design, test setup and detailed results would be shown in the following Chapters. Lastly, conclusions and recommendations are presented in Chapter 9.



# 4

## PAPER ON DESIGN OF A TUNABLE RESONANT SCANNING MIRROR

# Design of a Tunable Resonant Scanning Mirror

Jiajin Li<sup>a,b</sup>

<sup>a</sup>*Delft University of Technology*

*Department of Precision and Microsystem Engineering, Mekelweg 2, Delft, 2628 CD, Netherlands*

<sup>b</sup>*Hitech Multin BV*

*Laan van Ypenburg 60, 2497 GB, The Hague, Netherlands*

---

## Abstract

Scanning mirror is a widely used device in many optical systems to position the reflected beam. Existing products include galvanometer and resonant scanner. They are intended for accurate positioning at low frequency range and fast scanning at the specified high frequency respectively. However, when a wide frequency range is involved, they might not be able to fulfill requirements. In this paper, a novel solution is proposed, by tuning resonant frequency and exciting higher order modes to cover the intended frequency range of 500 - 5k Hz. A flexure mechanism is designed, where the scanner contains a cantilever as resonator, and a cut-leavespring as hinge guiding to achieve 1 DoF resonant scan. Resonant frequency is tuned by clamping different positions of the cantilever by two surfaces with large radius of curvature, and sliding could be enabled by DLC coating. Concept and detailed design are evaluated by finite element modelling and a prototype is built. The test results show a good match with the simulation. The intended frequency range could be covered and the reflected beam could achieve scanning angle of 1mrad, although at high frequency range, gain of frequency response is relatively low. This could be partly due to the cutoff frequency of the reluctant actuator in the test setup. Unwanted motions of the mirror are verified and limited within the requirement with large margins, and hence could be negligible for operation.

*Keywords:* Flexure mechanism, Resonance, Tunable, Scanning mirror, Frequency variable, Modal analysis.

---

## 1. Introduction

Scanning mirror is an important device in many optical systems to change the direction of the beam in a scheduled way [1]. It is widely used in the applications of optical communications, material processing, microscope system, and etc [2,3]. Conventional scanner is usually in a galvanometric configuration with closed-loop control system. It could achieve angular positioning with high accuracy and resolution [4]. However, when operating at high frequency, high driving power is often needed, which means high energy consumption. And due to large rotational moment of inertia and nonlinear effect at high speed scanning, especially outside bandwidth, distortion in output could be expected [5,6]. To achieve stable high frequency scanning, resonant scanner could be used, which has distinguished features including high rigidity, low mass and high Q-Factor [7]. By making use of resonance, it is easy to achieve high frequency oscillation with low power input and a simple electrical circuit [8]. However, most of them are designed to operate at the specified frequency. In some applications, such as to achieve live-cell imaging and high resolution imaging from a scanning microscope, it needs both high frequency scanning (a few kilo Hertz) by resonance and low frequency scanning (a few hundred Hertz) [9]. Therefore, making use of resonance to achieve high frequency and tuning it to cover a certain frequency range would be preferable.

To generate mechanical resonance, mechanisms should contain elastic elements which provide certain stiffness. L. B.Kheng

et al. [10] presented a resonant scanner in a clamped-free cantilever beam configuration, where a mirror was mounted at the tip, orthogonally to the axial direction. But the scanning motion does not have a fixed rotational axis. L. Koay et al. [11] and H.Urey et al. [12] achieved resonant scanning by torsional beam, with the rotational axis at the twist axis. W. Reimels [13] described a resonant scanning device in a crossed flexure configuration, and the resonance was generated by the crossed flexure itself. M. Burdenko [14] used crossed flexure as a guiding, and resonance was provided by an extra torsional resonator. Even the rotational axis of the crossed flexure would shift during scanning, but it is rather negligible for small deflection [13]. However, these resonant scanners are not tunable, which means they could only be operated at one intended resonant frequency. Some designers attempted to make resonant frequency adjustable, but it is intended for error correction in a small range, to cope with manufacturing error, mechanical wear, change of working conditions and etc [15].

### 1.1. Application Background

In an application of a scanning microscope system, a scanning mirror is needed. The basic principle is shown as Fig. 1. Some biological sample marked by fluorescent substance is placed on a sample plate. On top of that, there are multiple scanning electron beams, each of which would scan its corresponding region. Once the electron beam hits the sample, fluorescent light would be generated and captured by an optical system and get focus on each corresponding detector. One could notice that the

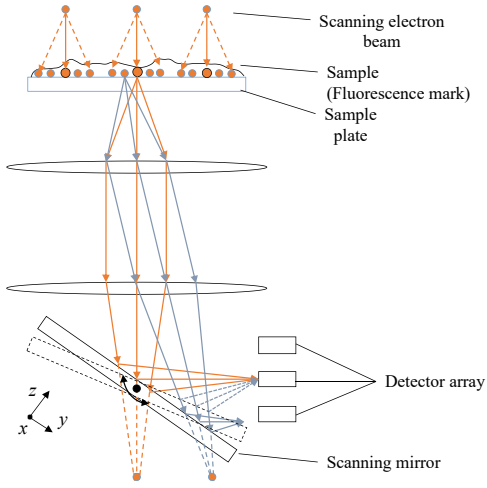


Figure 1: Basic system principle, application background of tunable resonant scanning mirror.

scanning motion of the electron beam could deviate the optical beam path (from orange one to gray one), and therefore the mirror should rotate to compensate for this beam motion such that the focus point would always stay still at each of the detector during scanning. To be able to achieve both high resolution scanning and live-cell imaging, a wide frequency range needs to be coped with.

### 1.2. Objectives and Design Requirements

The goal of this paper is to design a tunable resonant scanner, which fulfills the following requirements:

- **Frequency Range:** Resonant frequency of the scanner could be tuned in the range of 500 - 5k Hz
- **Range of Motion:** The reflected beam should be able to scan an angle in the range of 0 - 1 mrad. Noting that this means 0 - 0.5 mrad rotation  $R_x$  of the mirror.
- **Mirror Motion in Unwanted DoF:** Translation along optical axis  $d_z$ : <100  $\mu\text{m}$ , rotation  $R_y$  (orthogonal to scanning motion): <25  $\mu\text{rad}$ .
- **Beam Size:** Scanning mirror should be able to cope with a beam size of 11 mm diameter.
- **Size:** The size of the device should fit into space of 70×70×150 mm.

No literature has been found about resonant frequency tunable device for such a wide range in macro-scale applications. This paper presents a flexure-based mechanism to meet all the above criteria, and a new way to tune resonant frequency for a

wide range. The end application of this device is to be integrated into a scanning microscope system in Fig. 1.

The rest of the paper is structured as follow: in Section 2, the design scheme and detailed design of the mechanism is described, followed by FEM analysis. A prototype is built and the measurement setup is shown in Section 3. Results and discussion are presented in Section 4 and finally conclusions are made in Section 5.

## 2. Design and Analysis

### 2.1. Concept

The desired range of frequency change is an order of magnitude, which corresponds to two orders of magnitude change in stiffness if the mass is unchanged. This is quite difficult if only considering one resonance mode. Therefore, the basic concept to cover a wide frequency range is to combine tuning action with exciting higher order modes. Fig. 2 shows an example of frequency tuning for a given range between  $f_1$  to  $f_2$ . By applying tuning action, the system response curve would shift from the original one (blue) to the right. One could notice that the second and third peaks of the green curve have passed the third and fourth peak of the blue curve, and the first peak of the red curve is coincident with the second peak of the blue curve. Therefore, the whole intended frequency range  $[f_1, f_2]$  could be covered from original to tuning action 2.

The design of a tunable resonant scanner consists of two parts, a resonant scanner to provide 1 degree of rotation in resonant motion, and a frequency tuning mechanism. The resonator inside the scanner mechanism is a cantilever beam, and the tuning action is to change its effective length by clamping at different positions.

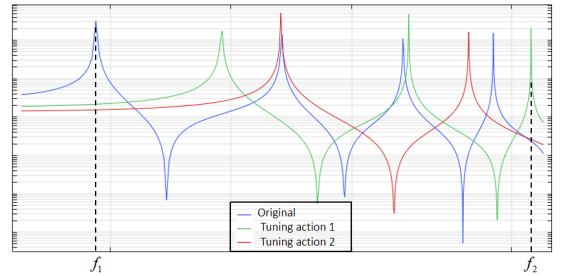


Figure 2: Concept of using higher order modes for wide frequency tuning.

### 2.2. Resonant Scanner Mechanism

To achieve 1 DoF resonant scanning, one could use some mechanisms that have 1 degree of rotation, such as crossed flexure or notch flexure as guiding with low rotational stiffness and high rigidity in other DoF, and resonance is provided by a separated "resonant actuator". But based on the resonator configuration and chosen tuning method, this design scheme might lead to a complicated mechanism. Alternatively, one

could treat the cantilever as a leaf spring which constrains 3 DoF, and synthesize a mechanism by freedom and constraint topology (FACT) method [16,17]. In this way, the mechanism is equivalent to a clamped-hinged cantilever. The proposed design model is shown as Fig. 3, where the hinge is a leaf spring. Also a cut at its middle to further increase its first eigenfrequency so that it would not interfere resonance motion of the cantilever. At the same time, this could reduce the rotational stiffness of the guiding hinge and over-constrain effect of the whole mechanism, which is preferable. The cantilever beam resonator is designed with a dimension of  $12\text{mm} \times 1\text{mm} \times 90\text{mm}$  such that the eigenfrequency of 1<sup>st</sup> to 4<sup>th</sup> bending modes is close to or stay in the range between 500 and 5k Hz.

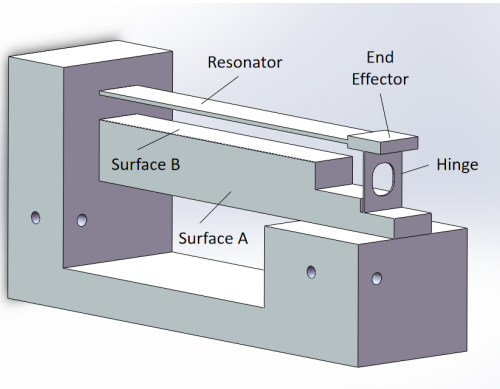


Figure 3: Design CAD model of resonant scanner mechanism.

### 2.3. Frequency Tuning Mechanism

To change the effective length of a cantilever, one can use two clamping members to clamp at different locations of the cantilever, with one fixed and the other preloaded by spring, and if the reaction force at clamping position is less than the preload force, clamping members would stay in position. To make sure clamping would function well, Hertzian contact should be considered as well, that it is preferable to have high Hertzian contact stress ( $<$  yielding stress of material), which gives low hysteresis clamping [18], and high contact stiffness. This means a small contact area with high preload force would be favourable, and large radius of curvature if curved surface involves. In this sense, clamping plate (Fig. 4(a)) might lead to microslip, even the effective length  $L$  is equal to the length between clamping end and the end effector. Clamping with Hertzian line contact would be more suitable, shown as Fig. 4(b), and standard roller bearing can give line contact, but this would lead to tight tolerance in assembly (see Chapter 5.3). Furthermore, large radius of curvature could lead to a bulky device.

The proposed design has two parts, the first one is an "E-shaped" block, as shown in Fig. 5(a). It adopts two clamping curved surfaces with large radius of curvature, coated with Diamond-like carbon (DLC) coating to enable sliding. Preload of clamping is applied by two springs (Bore A) through a notch

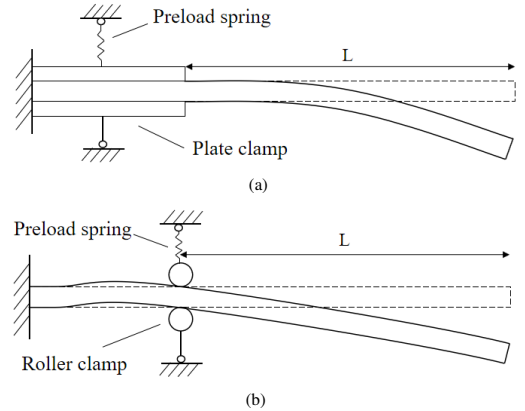


Figure 4: Schematic of cantilever with (a). plate clamping and (b). roller clamping.

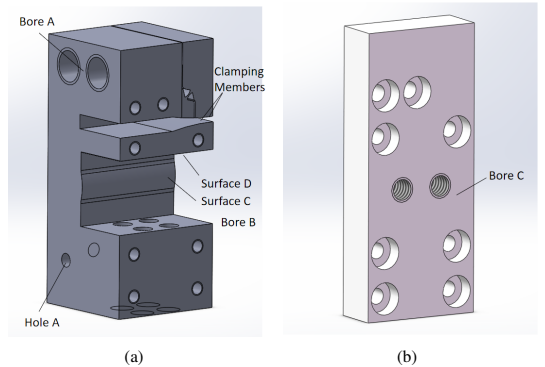


Figure 5: CAD model of (a). "E-shaped" block and (b). closing unit.

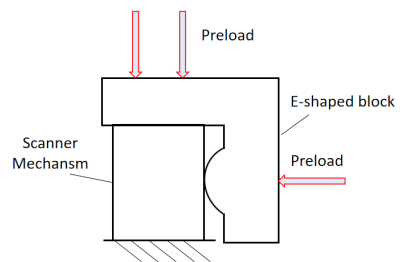


Figure 6: Contact configuration between scanner mechanism and "E-shaped" block in an exact-constrained way to define clamping position.

flexure, and the notch flexure is oriented in accordance with the direction of reaction force. Between the second and third arm of the "E", there is a curved surface C which would be in contact with the plane surface A at the side of the scanner mechanism, and the plane surface D would contact the surface B. In this way, these surface contact constrain 5 DoF of "E-shaped" block,

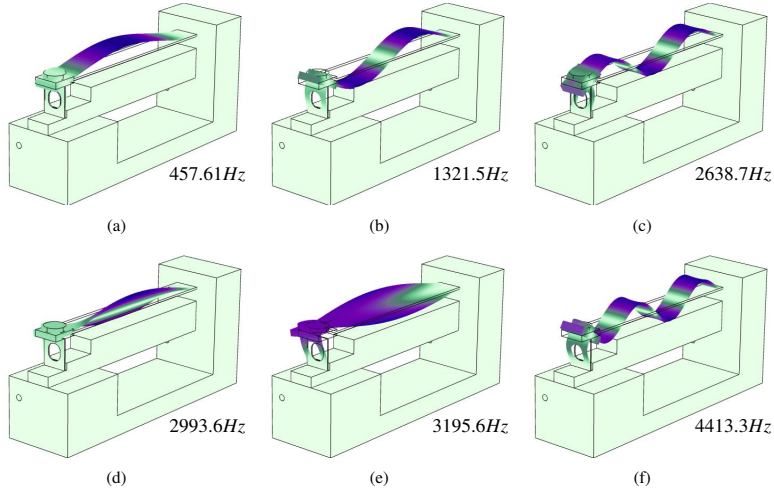


Figure 7: Modeshape of vibration at the 1<sup>st</sup> to 6<sup>th</sup> eigenfrequency.

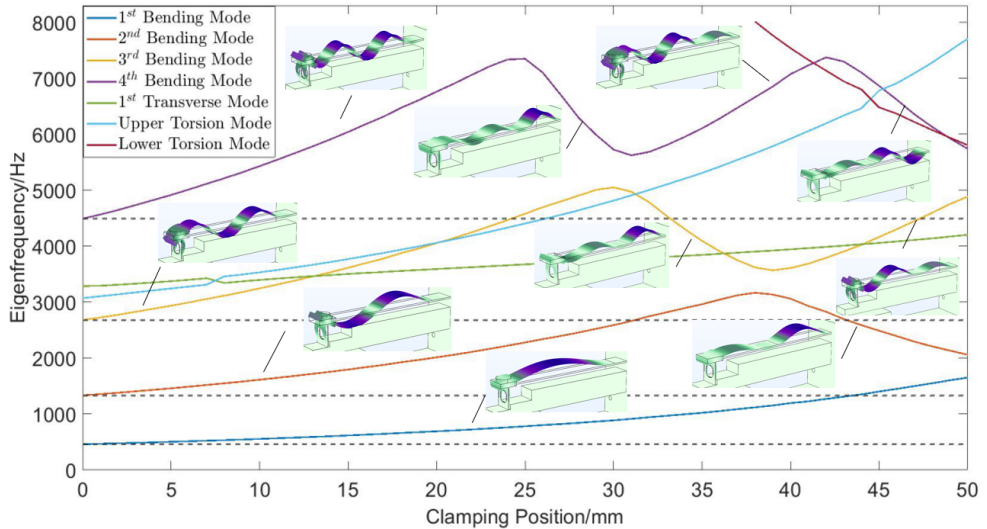


Figure 8: Modal behavior with respect to clamping position.

and with preload from the bottom (Bore B) and side (Bore C) to keep the block in position. This configuration is in an exact-constrained way, as shown in Fig. 6. After tuning, the block is locked by a flexible strut through hole A. Therefore, it is mounted in a statically determined way. The second part shown as Fig. 5(b) is to close the "E-shaped" block and strengthen it.

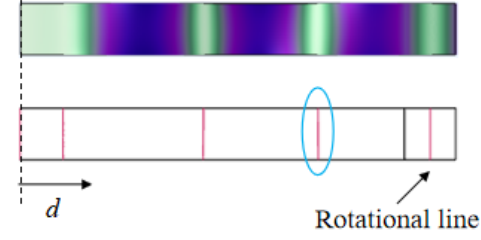
#### 2.4. Finite element modelling and analysis

In this section, the design is analyzed by finite element modelling, with the adopted material Al 7075 t6. A mirror would be placed at end effector, with material Fused Silica, and dimen-

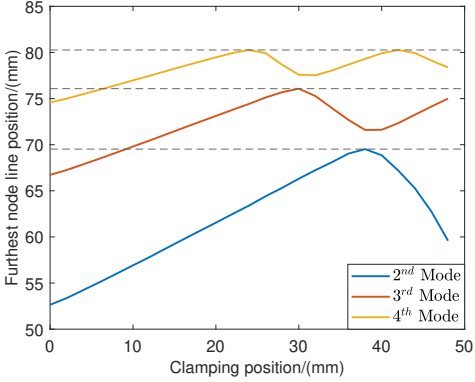
sion 10mm diameter, 2mm height. Modal behavior and dynamic performance have been simulated.

The first to sixth eigenmode of the scanner are shown as Fig. 7, where Fig. 7(a),7(b),7(c),7(f) is the 1<sup>st</sup>, 2<sup>nd</sup>, 3<sup>rd</sup> and 4<sup>th</sup> bending modes of the resonator respectively. One could also notice that there are other modes, which are torsional mode (Fig. 7(d)) and transverse mode (Fig. 7(e)), and these would lead to motion in unwanted DoF. Therefore, it is important to eliminate modal coupling so that scanning motion could be relatively pure.

It would be difficult to eliminate transverse mode and torsional mode (and their higher order modes) of a cantilever in



(a)



(b)

Figure 9: (a). Schematics of the furthest node line position from cantilever base. and (b) position of the furthest node line with respect to clamping position

the range of 500 to 5k  $Hz$  while its bending modes are in this range, especially when starting tuning the bending modes, other unwanted modes would also be tuned as well. Therefore, to avoid modal coupling, modal behavior with respect to clamping position is studied by modal analysis. The cantilever resonator is designed with length  $90mm$ , and the contact configuration is modelled as small plates, with width equal to the width of Hertzian contact area. Half of the contact width could be calculated as [19]

$$w = \sqrt{Rd} \quad (1)$$

where  $R$  is the radius of contact surface, and  $d$  is the indentation depth which could be expressed as

$$d \approx \frac{4F}{\pi E^* l} \quad (2)$$

where  $l$  is the contact length,  $E^*$  is effective Young's modulus calculated as

$$\frac{1}{E^*} = \frac{1 - \nu_1^2}{E_1} + \frac{1 - \nu_2^2}{E_2}, \quad (3)$$

with  $E_1$ ,  $E_2$  the elastic modulus and  $\nu_1$ ,  $\nu_2$  the Poisson's ratios of each body.  $F$  is the preload force and assumed to be  $80 N$  and clamping surfaces have radius of  $50mm$ . This corresponds to

$0.22 mm$  contact width, and  $354.3N/\mu m$  contact stiffness. Fig. 8 shows an estimation of modal behavior of bending and unwanted modes. One could notice that by moving the clamping block to around  $45mm$ , all four bending modes could connect or overlap with their higher ones. There are drops of eigenfrequency happening at some range of clamping position, and that is due to the elastic mode of the beam between the clamping block and the base, whose eigenfrequency decreases with increasing length by moving the clamping block further from the base. These regions could hardly cause amplitude at the end effector, and therefore should be avoided. 1<sup>st</sup> transverse and upper torsional mode (between the end effector and clamp) starts from around  $3000 Hz$ , and couples into the 3<sup>rd</sup> bending mode at clamping position around  $13$  and  $20mm$ . When the clamping block is near  $45 mm$  (half of the cantilever), lower torsional mode (between clamping block and base) starts to occur closing to the working frequency range. At this clamping position, coupling between transverse and 3<sup>rd</sup> bending mode is seen again. Therefore, one should be aware that modal coupling between bending and unwanted mode would happen at region between  $3$  to  $4k Hz$ , and larger input power could be expected since unwanted modes would consume energy. To minimize this coupling, accurate alignment of the actuator could be done such that the force is acting at the center line in the bending direction. And to ensure resonance cause scanning amplitude, only regions with positive slope could be considered as usable ones.

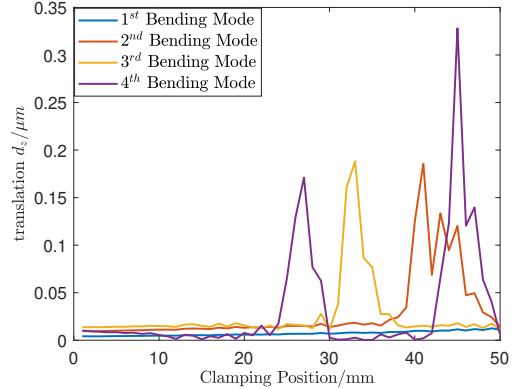


Figure 10:  $d_z$  at center of the end effector when scanner is operated at resonant frequency of the 1<sup>st</sup>, 2<sup>nd</sup>, 3<sup>rd</sup> and 4<sup>th</sup> mode with  $0.5mrad$  angular deflection at the end effector.

The scanner is actuated by a reluctance actuator which applies prescribed force as an excitation. This actuation point should not be located at the nodal line of any bending modes within  $500$  and  $5k Hz$  range. To select an actuation point, behavior of nodal line of 2<sup>nd</sup> to 4<sup>th</sup> bending modes within the moving range of clamp is studied, and the 1<sup>st</sup> bending mode is neglected since it coincides with the clamping position. As Fig. 9(a) shown, the position of the furthest nodal line on the cantilever beam with respect to the base is captured, and Fig. 9(b) shows that within the moving range of the clamping block, nodal line

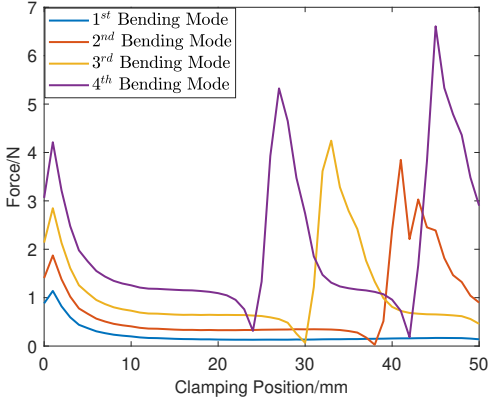


Figure 11: Reaction force at clamping position when scanner is operated at resonant frequency of the 1<sup>st</sup>, 2<sup>nd</sup>, 3<sup>rd</sup> and 4<sup>th</sup> mode with 0.5mrad angular deflection at the end effector.

of any 1<sup>st</sup> to 4<sup>th</sup> bending modes would not locate further than  $d = 80mm$ . The actuation point is then chosen at  $d = 84mm$ .

At the chosen actuation point, excitation at resonance frequency of first four bending modes is given such that the angular deflection of the end effector is 0.5mrad, and the corresponding translation  $d_z$  and reaction force at clamping position are studied. Since torsion and transverse modes are only possible to be excited due to misalignment of the actuator, thus in ideal case of this actuation configuration, they might not occur. Fig. 10 plots the  $d_z$  of 1<sup>st</sup> to 4<sup>th</sup> bending modes with respect to clamping positions. It shows that at the clamping regions that cause drop of eigenfrequency in Fig. 8,  $d_z$  is larger than others. This might be due to the fact that the resonance of these regions is mainly at the part between base and clamp, which hardly generates angular motion at the end effector, and to still push the cantilever for intended angular amplitude, a larger force is needed and thus larger  $d_z$ . It should be pointed out that for usable regions,  $d_z$  is expected to be lower than 40nm.

Fig. 11 shows reaction force of the 1<sup>st</sup> to 4<sup>th</sup> bending modes at clamping position in bending direction. There are some dips approaching zero, which are related to the nodal lines of the cantilever itself. When the clamping blocking moves from nodal lines to the right, a small increase could be expected and then drop to a relatively constant value until the next nodal line. While for the large peaks, they are corresponding to "frequency drop" regions mentioned above. Noting that the largest reaction force at clamping position would not exceed 7N, and due to large contact stiffness, movement at clamping position would not exceed 20nm, which is around 100 times less than the movement of edge of the end effector. This means clamping could function properly.

## 2.5. Conclusions on Design and Analysis

In this session, a design of tunable resonant scanner is proposed, where in scanner part a cantilever is taken as resonator,

together with a cut-leafspring as guiding hinge to provide 1 degree of rotation, and eigenfrequency is tuned by two clamping members with large radius of curvature, one fixated and the other preloaded. Preload force is 80N, much larger than estimated reaction force at clamping position, which means the clamping block could function. Key performances are studied by finite element analysis according to requirements:

- **Frequency range:** Fig.8 shows by moving the clamping block to around half length of the cantilever, resonant frequency could be tuned to cover the range of 500 - 5k Hz. Only usable regions should be considered for operation, and modal coupling should be aware.
- **Mirror motion in Unwanted DoF:** In the proposed design, torsion and transverse motion of the cantilever could cause rotation  $R_y$  about axis orthogonal to scanning motion, but this could be minimized by the actuation way which is a force in bending direction. Translation in optical axis  $d_z$  is related to constraint stiffness of the cut-leafspring, and simulation shows  $d_z$  would not exceed 40nm, much less than the maximum allowable value of 100 $\mu$ m.

## 3. Test Setup and Measurement

### 3.1. Experiment Design

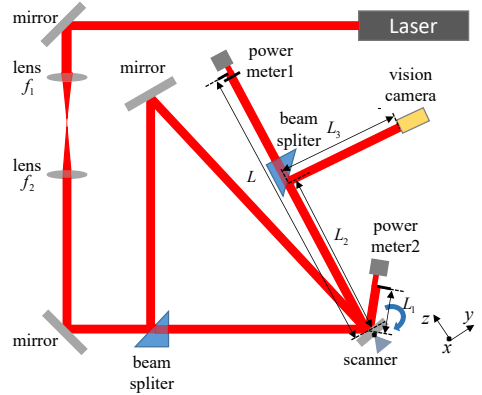


Figure 12: Schematics of optical measurement system.

Since the mirror on the scanner is a flat mirror, there are 3 DoF movements would change the reflected beam position (tip, tilt and translation along optical axis). The actual position of the reflected beam would be a result of a linear combination of these 3 DoF motions. To decouple it, an optical measurement setup is proposed as shown in Fig. 12. A laser beam with diameter  $d$  is directed to pass two lenses with focal length  $f_1$  and  $f_2$  respectively, which acts as beam expander to control the beam size. Outcoming beam diameter could be expressed as

$$d' = \frac{f_2 d}{f_1}. \quad (4)$$

This then is directed to a beam splitter, and the two splitted beams are the incoming beam of the scanner with two different incident angles  $\alpha_1$  and  $\alpha_2$ . Two power meters are placed on two outgoing beam paths, with knife-edge in front, a distance  $L$  and  $L_1$  from the scanner. The knife-edge in front of power meter 2 cut half of the beam from the side. Planar position of the beam at knife-edge could be inferred by measuring power change. For power meter 1, two knife-edges are placed, with one from the top into the paper plane and the other from the side, to measure out of plane and in plane position of the reflected beam respectively. One reflected beam is splitted and directed to a CCD camera to record the beam motion.

Assumed that the scanner rotates about  $x$  and  $y$  axis with an angle  $R_x$  and  $R_y$  respectively, and translates along  $z$  axis with a distance  $d_z$ . When the beam is only cut by knife-edge from the side, its position change  $P$  at knife-edge detected by power meter 1 and 2 could be expressed as

$$\begin{aligned} P_1 &= 2R_x L + 2d_z \sin(\alpha_1) \\ P_2 &= 2R_x L_1 + 2d_z \sin(\alpha_2) \end{aligned} \quad (5)$$

One could notice that, rotation about  $y$  axis  $R_y$  is decoupled by this measurement method, and to have a more sensitive measurement with less coupling, it is preferable to have a small incident angle with a long distance between scanner and power meter when measuring rotation, and vice versa when measuring translation, which could be inferred from eq. 5. This corresponds to Fig. 12, where  $L = 1053.74mm$ ,  $\alpha_1 = 15^\circ$  and  $\alpha_2 = 60^\circ$ .  $L_1$  would be discussed in the following measurement steps. Since  $R_y$  is expected to be at  $\mu rad$  level, and the reflected beam to power meter 1 corresponds to an incident angle  $\alpha_1 = 15^\circ$  to the scanner, therefore, at power meter 1, when the beam is only cut from top, position change  $P'_1$  could be approximated as

$$P'_1 \approx 1.9319R_y L \quad (6)$$

From finite element analysis, only torsion and transverse motion of the resonator beam could cause  $R_y$ , and one main factor that could lead to these is the misalignment of magnet and coil. And in the measurement system, misalignment between the scanner and the top knife-edge could be also detected as  $R_y$ . Meanwhile,  $d_z$  is expected to be movement in nanometer level. Therefore, measurement is divided into two parts:

- **1. Resonant scan and tuning performance test:** The measurement steps are conducted as follow: firstly clamp the beam at a certain position, and a frequency sweep is conducted to locate resonant frequencies. Secondly, apply an excitation such that scanning angle  $R_x$  is equal to  $0.5mrad$ , and use the same amplitude to locate frequencies with gain half of that at resonance to figure out Q factor, which could be calculated as [20]

$$Q = \frac{f_r}{\Delta f} \quad (7)$$

where  $f_r$  is the resonant frequency and  $\Delta f$  is the difference between two frequencies corresponding to half gain of

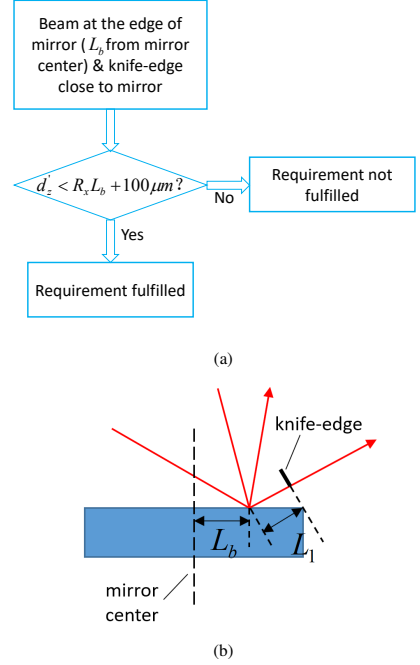


Figure 13: (a). Verification process for  $d_z$ . (b). Experiment schematic for  $d_z$  verification.

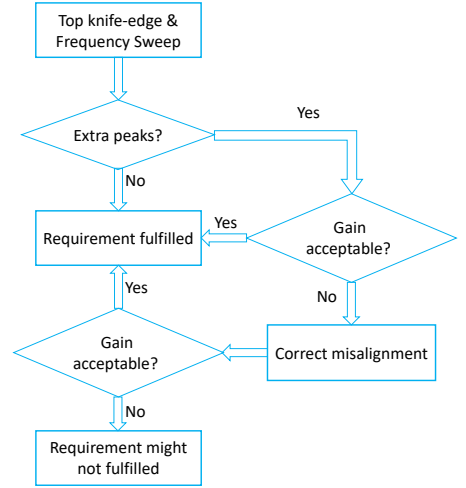


Figure 14: Verification process for  $R_y$ .

resonance. Then the clamping position would be changed and for each position, steps 1 to 2 are repeated.

- **2. Verification of unwanted motion:** Regarding  $d_z$ , the verification process is shown as Fig. 13(a). The scanner is



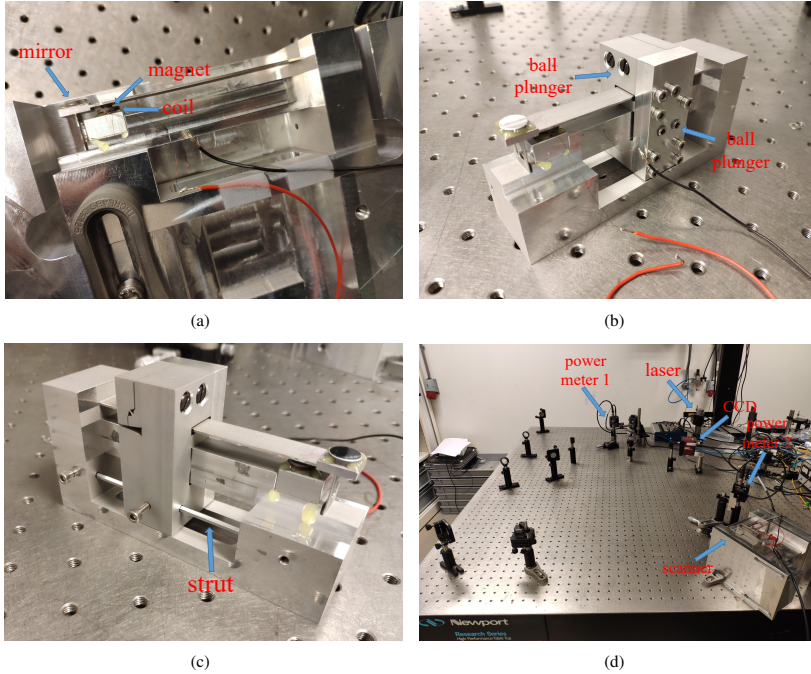


Figure 15: Photos of the the scanner and test setup.

aligned as shown in Fig. 13(b), such that the position of two incoming beams on the mirror has a distance  $L_b$  from the mirror center, where the translation is at micrometer level during scanning motion. At the same time the knife-edge of power meter 2 is placed perpendicular to the outgoing beam, with distance  $L_1 = (5 - L_b)\cos(30^\circ)$ . This is to reduce the effect of beam movement induced by  $R_x$ . The scanning angle is brought to around  $0.5\text{mrad}$ , and reflected beam position change at two knife-edges are recorded power meter 1 and 2. If measured  $d'_z$  at spot position on the mirror is less than  $R_x L_b + 100\mu\text{m}$ , then the requirement is fulfilled. The 4<sup>th</sup> mode at  $0\text{mm}$  clamping position is considered for verification.

Regarding  $R_y$ , verification process is shown as Fig. 14. The beam at power meter 1 is only cut by the top knife-edge, and a frequency sweep is conducted with a relatively large amplitude input. The beam power change measured by power meter is a combination effect of  $R_y$  and  $R_x$  due to misalignment of knife-edge. One could check if there would be more resonant peaks other than four bending modes. If no, then torsion and transverse mode would not be seen in this actuation; if yes, then the gain could be checked whether with maximum current needed for scanning, the amplitude would be smaller than requirement. If yes, then at other frequencies which are not at resonance of torsion and transverse mode,  $R_y$  would be even much smaller. This means the requirement is fulfilled, and mis-

alignment between magnet and coil is acceptable. If still no, one could infer misalignment by gain of four bending modes to correct measurement data for further check.

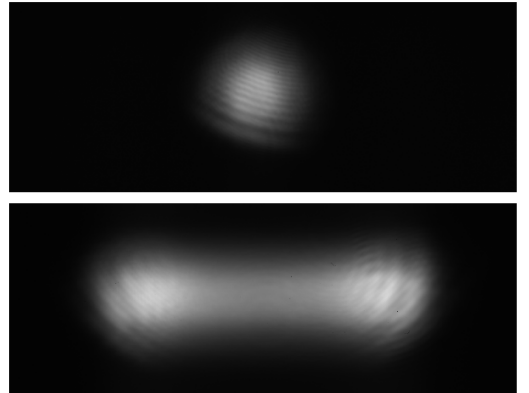


Figure 16: Comparison between still spot and scanning line pattern at resonance captured by vision camera.

### 3.2. Test Setup

The scanner mechanism and "E-shaped" block of frequency tuning mechanism are monolithically machined by spark erosion.

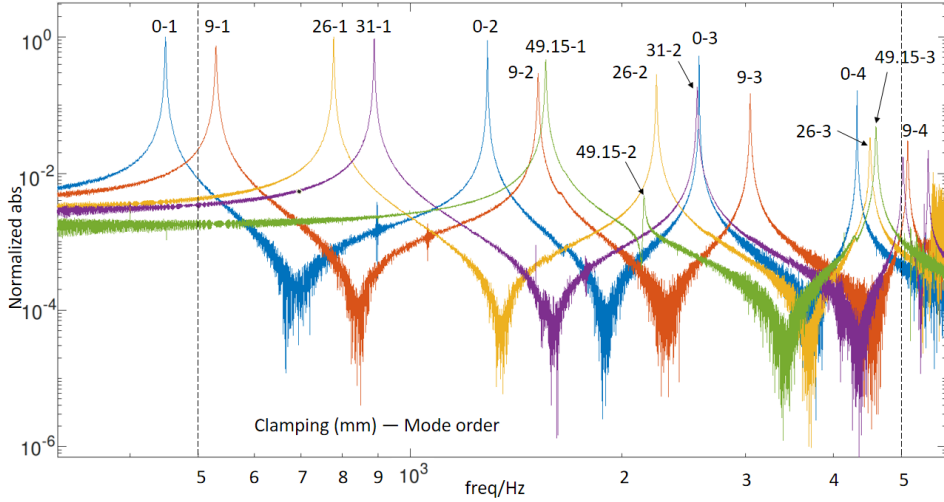


Figure 17: Frequency responses at several clamping positions within range of 500-5k Hz. Gain normalized by 1<sup>st</sup> peak at 0 clamping.

The assembled system is shown in Fig. 15(a). A mirror is glued on the end effector stage, and a magnet is glued on the bottom side of the resonator beam at the chosen actuation position. The coil is first placed on a block and then align according to the magnet position.

Preload is applied by ball plunger, shown as Fig. 15(b). Its tip is a ball connected to a spring, and the outside has thread. After tuning, a strut is used with screws perpendicularly tightened to lock, as shown in Fig. 15(c).

The measurement setup is built on an optical table, shown as Fig. 15(d). To integrate scanner setup into the measurement system, it is clamped on a block and the block is mounted on the table.

## 4. Results and Discussion

With an excitation at resonance, the scanning line pattern is captured by vision camera, with a comparison of the stationary spot when scanning is off, shown as Fig. 16. The scanning line has larger intensity at the edge than at the middle, which corresponds to sinusoidal motion at resonance.

### 4.1. Resonant scan and tuning performance test

Fig. 17 shows results of frequency response within 500 - 5k Hz at clamping positions at 0, 9, 26, 31 and 49.15mm (maximum stroke) from the base, and the gain is normalized by the gain of the first peak at 0 clamping position. This is the 1<sup>st</sup> bending mode of the resonator beam itself. At 0mm clamping, the measured current for 1mrad angular movement of reflected beam at 1<sup>st</sup> to 4<sup>th</sup> mode is around 20mA, 24mA, 64mA and 224mA peak to peak respectively. One could observe that the frequency range of 500-5k Hz could be covered by moving the frequency tuning mechanism within its range. At around 26, 31 and 49mm clamping position, 3<sup>rd</sup>, 2<sup>nd</sup>, 1<sup>st</sup> bending mode could

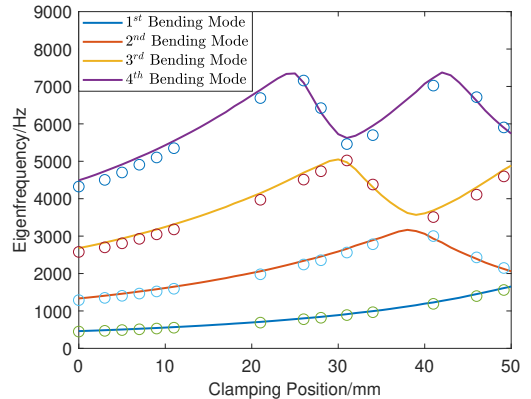
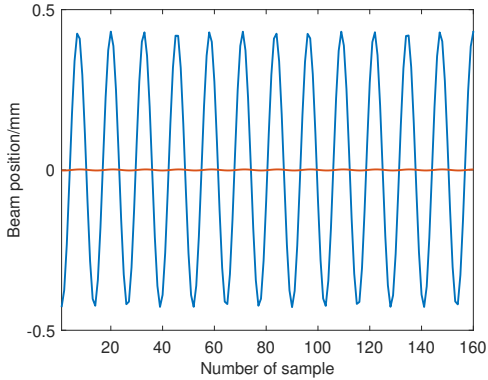
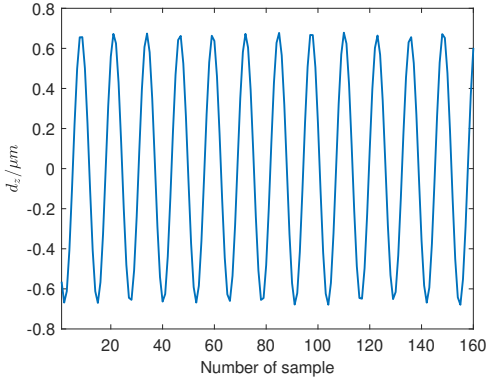


Figure 18: Comparison between the measured (circular dot) and simulation (curve) results of resonant frequencies with respect to clamping position.

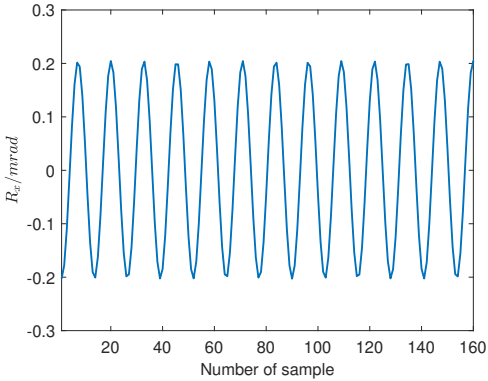
connect to 4<sup>th</sup>, 3<sup>rd</sup>, 2<sup>nd</sup> bending mode of resonator beam itself respectively, and at 9mm clamping position, 4<sup>th</sup> bending mode is at 5102.3 Hz. The measured Q factor stays within the range of around 200 to 500 (see Chapter 8.1), but no clear regular pattern could be found. It could be pointed out that starting from the 2<sup>nd</sup> peak of resonator itself, amplitudes of frequency response drop with a certain negative slope is seen (see Chapter 8.1), and this could be partly due to the cutoff frequency of the actuator, because of limited accuracy and a relatively large gap between coil and magnet remained by hand alignment. An improvement could be done by adding an iron core inside the coil to strengthen magnetic field and reduce magnetic reluctance. While the air gap between magnet and coil could be reduced by more sophisticated alignment.



(a)

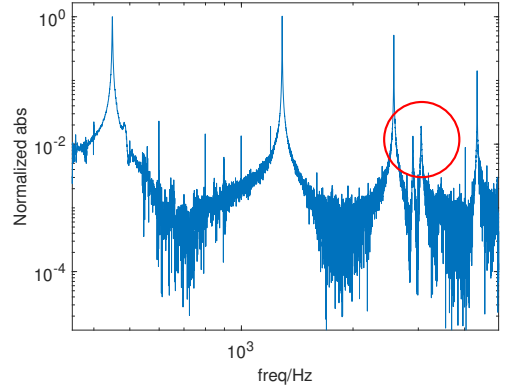


(b)

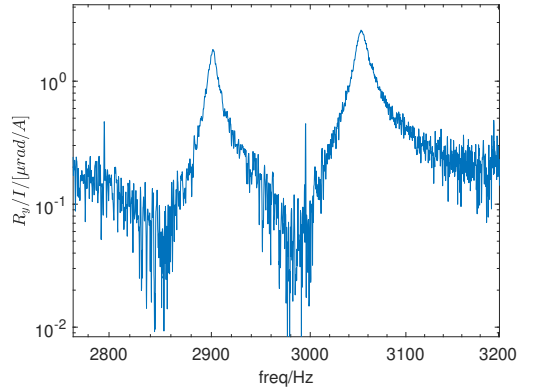


(c)

Figure 19: (a). Beam position change measured by power meter 1 (blue curve) and power meter 2(orange curve). (b) Calculated  $d_z$  and (c). calculated  $R_z$ , at the beam position on the mirror. Sampling frequency 55000 Hz.



(a)



(b)

Figure 20: (a). Frequency response of power change measured by power meter 1 with the top knife-edge. Gain normalized by 1<sup>st</sup> peak. and (b) Zoomed version of (a) at frequency near 3k Hz.

Fig. 18 compares the resonant frequencies of the 1<sup>st</sup> to 4<sup>th</sup> bending modes between the measurement (circular dot) and simulation (line). At 0 clamping position, the measured resonant frequency of first four bending mode is 448.8, 1288.8, 2577.6 and 4324.1 Hz respectively, with error 1.93%, 2.47%, 2.32% and 2.02%. This could be mainly due to manufacturing accuracy. With hand positioning of the frequency tuning mechanism, the accuracy of the clamping position could achieve 50 $\mu$ m. Regarding error between measured data and simulation, it could be bounded within 5% (see Chapter 8.1).

#### 4.2. Verification of unwanted motion

To verify  $d_z$ , the beam position on the scanning mirror is measured as  $L_b = 3.6$ mm. An input signal is given at 4324.1Hz to excite the 4<sup>th</sup> bending mode with angular movement of the scanner around 0.5mrad. Beam position at the knife-edge mea-

sured by power meter 1 and 2 are shown as Fig. 19(a) as blue and orange curve respectively. By solving eq. 5, one could obtain  $d_z$  and  $R_x$  information as shown in Fig. 19(b) and 19(c).  $d_z$  is around  $1.4\mu\text{m}$ , corresponding to translation due to  $R_x$  with  $0.4\text{mrad}$  at a distance of  $L_b = 3.6\text{mm}$ . Therefore, requirement on  $d_z$  is fulfilled.

To verify  $R_y$ , clamping position is set at  $0\text{mm}$ , and the top knife-edge cuts half of the beam spot. Fig. 20(a) shows the frequency response of sensor output of power meter 1. Response amplitude is ratio between measured power changed and input current, then normalized by gain at  $1^{\text{st}}$  peak. The four obvious peaks of power change are due to misalignment between knife-edge and scanner. Other than those, there are still two small peaks observed at around  $3\text{k Hz}$ , which are marked by the red circle. Fig. 20(b) shows a zoomed version at around  $3\text{k Hz}$  region. These two peaks have eigenfrequency at  $2901$  and  $3053\text{Hz}$  respectively.

According to Fig. 7, they are torsion and transverse mode. Noting that this frequency region is closing to zero of bending mode, thus one could assume that these two peaks are mainly induced by  $R_y$ . Measured gain is  $1.813$  and  $2.602\mu\text{rad}/\text{A}$ . This means even at resonance of torsion and transverse mode, to reach the maximum allowable value of  $25\mu\text{rad}$ , current needed is around  $500$  times larger than that for  $1^{\text{st}}$  bending mode to achieve  $0.5\text{mrad}$ , and if not at their resonance,  $R_y$  is even less, which fulfills the requirement. While an important remark for operation is to try to avoid coupling region between bending and unwanted modes. Even  $R_y$  stays within the required value, but coupling might lead to higher input power since unwanted modes also consume energy.

An essential recommendation is to connect the frequency tuning block to an actuator controlled by closed-loop such that a smaller step of movement could be achieved with high accuracy. In this way, one could find out a more detailed modal behavior with respect to clamping positions on the real prototype, which can serve as a reference for clamping position selection with intended frequency, and avoid the regions that cause unwanted motion if possible, or hardly produce scanning amplitude.

## 5. Conclusions

This paper presents a flexure mechanism design of a tunable resonant scanning mirror. The scanner mechanism contains a bending cantilever as resonator and a cut-leafspring as hinge guiding to provide  $1$  degree of rotation. The tuning method is to change the effective length of resonator beam, and this is realized by two clamping surfaces with large radius of curvature, in which one is fixated and the other is preloaded. This provides large contact stiffness and low hysteresis clamping. Sliding would be enabled by DLC coating and therefore clamping position could be changed easily. A novel tuning concept is proposed by exciting higher order modes of resonator, so that the scanner could achieve resonant motion in a wide frequency range.

Finite element analysis shows that by clamping from  $0$  to around half length of the proposed dimension of the cantilever, the  $1^{\text{st}}$  to  $4^{\text{th}}$  bending modes could cover the intended frequency

range of  $500 - 5\text{k Hz}$ . However, some regions that cause coupling or hardly generate scanning amplitude should be aware.

The design is realized into hardware. Measurement is attempted to figure out  $R_x$ ,  $R_y$  and  $d_z$  according to the requirement by the presented setup.

- **Frequency Range:** By moving the frequency tuning mechanism from  $0$  to around  $46\text{mm}$  from the base, resonant frequency of the scanner could cover the range of  $500 - 5\text{k Hz}$
- **Range of Motion:** The reflected beam could achieve a scanning angle of  $1\text{mrad}$ , although at high frequency a relatively large current amplitude is needed, which is partly due to the cutoff frequency of the actuator.
- **Mirror Motion in Unwanted DoF:** For resonant scanner itself,  $d_z$  at the  $4^{\text{th}}$  bending mode is verified much less than  $100\mu\text{m}$  when  $R_x$  is around  $0.4\text{mrad}$ ;  $R_y$  has gain of  $2.602\mu\text{rad}/\text{A}$  even at resonance of transverse mode.
- **Beam Size:** The end effector stage has dimension  $12 \times 12\text{mm}$ , where a mirror with  $12\text{mm}$  diameter could be placed on.
- **Size:** The prototype would occupy a space of  $127 \times 35 \times 68.9\text{mm}$ .

In the future work, the coil could be improved to increase its bandwidth. It is also recommended to position the frequency tuning mechanism by an actuator to get a more detailed modal behavior of the prototype for avoiding modal coupling and making frequency tuning strategy.

## References

- [1] H. Cho, *Optomechanronics: Fusion of Optical and Mechatronic Engineering*, CRC Press, Boca Raton, USA, 0-8493-1969-2, 2006.
- [2] Zhou. et al, *Design of Fast Steering Mirror Systems for Precision Laser Beams Steering*, 2008 International Workshop on Robotic and Sensors Environments, 978-1-4244-2594-5, 2008.
- [3] M. Hafeza et al, *Design, simulations and experimental investigations of a compact single mirror tip/tilt laser scanner*, *Mechatronics*, vol. 10, pp. 741-760, 2000.
- [4] R. P. Aylward, *Advanced galvanometer-based optical scanner design*, *Sensor Review*, vol. 23, pp. 216-222, 2003.
- [5] S. Xiang et al, *Study on fast linear scanning for a new laser scanner*, *Optics & Laser Technology*, vol. 42, pp. 42-46, 2010.
- [6] J. Xiang et al, *The precision improvement of the scanner in optical scanning imaging system*, *Optics & Laser Technology*, vol. 30, pp. 109-112, 1998.
- [7] G. F. Marshall and G. E. Stutz, *Handbook of Optical and Laser Scanning*, Second Edition, Boca Raton, USA: CRC Press, 978-1-4398-0880-1, 2012
- [8] M. Burdenko et al, "Resonant scanner:", *U.S. Patent 5,528,411*, issued June 18, 1996.
- [9] D. B. Murphy "Confocal Laser Scanning Microscopy," in *Fundamentals of Light Microscopy and Electronic Imaging*, New Jersey: Wiley, 2001, pp.218.
- [10] L.B. Kheng et al., *Design optimization and fatigue testing of an electronically-driven mechanically-resonant cantilever spring mechanism*, *Materials and Design*, vol. 31, pp. 4023-4028, 2010.
- [11] L. Koay and H. Gitano, *Design and Optimization of Mechanically Resonant Torsional Spring Mechanism for Laser Light Dispersion Applications*, *Journal of Mechanical Design*, vol. 133, 2011.

- [12] H. Urey et al. *Optical scanners for high resolution RSD systems*, *Proceedings of SPIE, AeroSense, Orlando, U.S.*, vol. 4711, August 5, 2002.
- [13] W. Reimels, *Low Wobble Resonant Scanners*, *Proceeding SPIE 0390, High Speed Read/Write Techniques for Advanced Printing and Data Handling, Los Angeles, U.S.*, September 20, 1983.
- [14] M. Burdenko, *Resonant Scanner*, *U.S. Patent 5,528,411*, issued June 18, 1996.
- [15] J. I. Montagu et al., "Tunable resonant mechanical system.", *U.S. Patent 4,874,215*, issued October 17, 1989.
- [16] J. B. Hopkins and M. L. Culpepper, *Synthesis of multi-degree of freedom, parallel flexure system concepts via Freedom and Constraint Topology (FACT) - Part I: Principles*, *Precision Engineering*, vol. 34, pp. 259-270, 2010.
- [17] J. B. Hopkins and M. L. Culpepper, *Synthesis of multi-degree of freedom, parallel flexure system concepts via freedom and constraint topology (FACT). Part II: Practice*, *Precision Engineering*, vol. 34, pp. 271-278, 2010.
- [18] H. Soemers, *Design for Stiffness*, in "Design Principle for Precision Mechanism", 978-90-365-3103-0, 2010.
- [19] Valentin L. Popov, *Contact Mechanics and Friction, Physical Principles and Applications*, 2nd ed. Springer, 2016, pp. 61-65.
- [20] E.I. Green, *The Story of Q*, *American Scientist*, vol. 43, pp. 584-594, 1955.



# 5

## SUPPLEMENTARY MATERIAL: CONCEPT DESIGN

### 5.1. SYSTEM CONCEPT

A tunable resonant scanner consists of two main parts, resonance and frequency tuning, and this leads to the system concept that consists of resonator and frequency tuning method selection. Regarding the tuning method, according to the Literature review in Chapter 2, only two candidates "changing effective length" and "adding axial load" are considered to have potential to easily achieve a wide range tuning. Considering easy implementation of the tuning action, the resonator is chosen to be a cantilever beam. The cantilever beam as resonator would not be free end in the scanner system, since it only constrains 3 DoF as a leaf spring, and the scanner is intended to have 1 degree of rotation. Cantilever beam in torsional motion or in bending motion with a hinged boundary condition could provide rotation during deflection.

There are mainly three criteria considered: ease of implementation, possibility to connect higher order modes, and influence of constrain stiffness of other flexure element. Evaluation is in combination of finite element analysis. Fig. 5.1 shows an example that compares the effect of frequency tuning by changing effective length and adding axial load on a cantilever beam in clamped-hinged boundary condition. Its original eigenfrequency of the first four bending modes is 452.2, 1422.6, 3065.6 and 5254.2 *Hz* respectively. In Fig. 5.1a and 5.1b, cantilever effective length is changed by full plate constraint and line constraint which is a more easily implementing alternative respectively. One could notice that by plate constraint, all first four bending modes could be easily connected. Even with line constraint, they could connect when the constrain line is at around 60% of the cantilever length. While in Fig. 5.1c, by applying axial load (compression to its buckling and tension to 50% yielding), all modes could just connect. Noting that the compression and tension is around 180 N and 1000 N respectively.

With some more trials on different dimensions of cantilever, one might conclude that

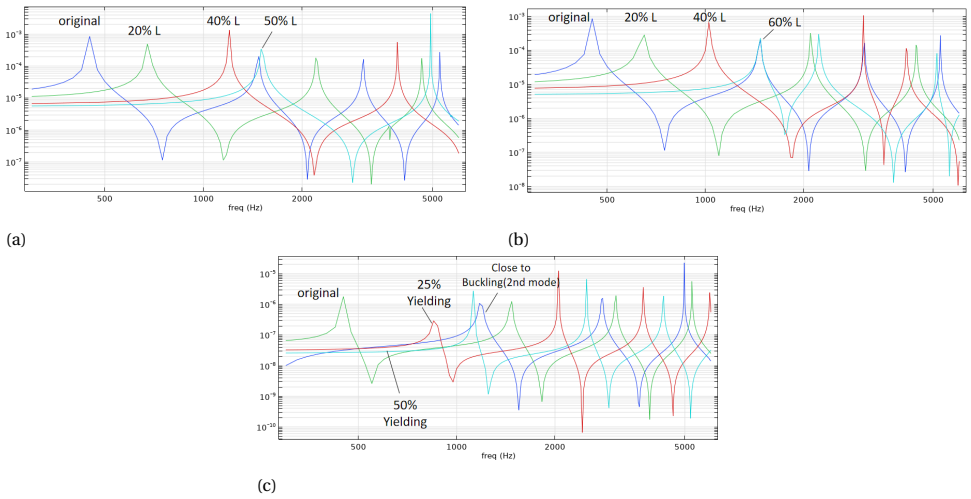


Figure 5.1: An example of comparison of eigenfrequency tuning by (a). plate constraint, (b). line constraint and (c). axial load.

5

it would be difficult to apply axial load to cover a wide frequency range by connecting higher order modes. Even there might exist some dimensions that are easier, but magnitude of load up to a few hundreds or even thousands Newton could be expected. This amount of load might be difficult to apply and maintain. From Fig. 5.1c, it should be noted that even the beam is compressed to buckle, tuning effect for higher order modes is limited. Furthermore, applying axial load would lead to deformation of the cantilever and other flexure elements that serve as constraints in the mechanism, and this pre-deformation could lead to reduction of constrain stiffness. Regarding changing effective length, it is possible to connect the first four bending modes, and this tuning action could be implemented by sliding a clamping mechanism along the cantilever, which in principle does not influence any other flexure elements. Fig. 5.2 summarizes the evaluation regarding the three criteria. In this sense, the system concept with a cantilever beam as resonator and its resonant frequency tuned by changing effective length is more preferable.

|                  | <b>Ease of implementation</b>              | <b>Possibility to connect higher order modes</b> | <b>Influence of constrain stiffness</b> |
|------------------|--|--|---|
| Axial Load       | High load expected                         | High load up to 50% yielding                     | Could influence                         |
| Effective Length | Sliding along cantilever (line constraint) | constrain up 60% of length (line constraint)     | In principle does not                   |

Figure 5.2: Concept evaluation of tuning methods.



## 5.2. 1 DOF RESONANT SCANNER MECHANISM

### 5.2.1. RESONATOR

#### RESONATOR INTEGRATION

The scanner is intended to achieve 1 degree of rotation in resonance, and there are two strategies to integrate the resonator into the mechanism. The first one is to synthesize a 1 degree of rotation mechanism according to FACT method [1,2], where some constraints inside the constrain space serve as resonator. The other is to choose some typical mechanisms with 1 degree of rotation originally, and resonance is generated by a separated resonant actuator.

Regarding the first one, the constrain space of 1 degree of rotation is shown as blue figure in Fig. 5.3, and the mechanism should contain at least five independent constraints from it. Since the proposed resonator is chosen as a cantilever, it is equivalent to a leaf spring which constrains 3 DoF. Fig. 5.4 shows two concepts corresponding to utilizing the bending and torsional deflection of the cantilever respectively for rotation, where the other two constraints are two flexible struts. This forms an exact-constrained mechanism.

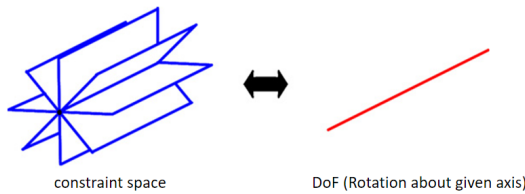


Figure 5.3: Reciprocal system of 1 degree of rotation (red) and set of constraint space (blue)[?].

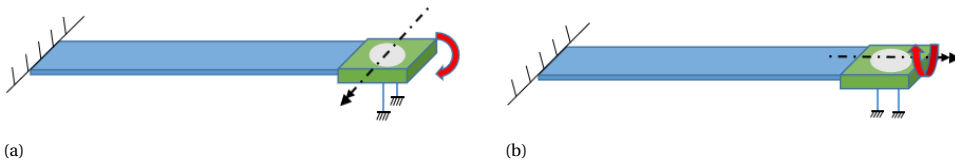


Figure 5.4: Schematic of concept of strategy one with a. bending and b. torsion beam.

Regarding the second one, there are some existing flexure mechanisms with 1 degree of rotation that are widely used. For example notch flexure with rotational axis at the notch place, and crossed flexure with rotational axis at the intersection of two leaf springs. They both have low rotational stiffness and high rigidity at other DoF, therefore, by designing proper dimension, their eigenfrequency of rotation mode could be much lower than 500 Hz, and other modes are higher than 5k Hz. This means they could be used as guiding. To provide resonance in the intended working frequency range, with the chosen resonator as cantilever, it is not a proper way to directly connect cantilever to guiding,

since this would lead to over-constraint. The proposed concept, shown as Fig. 5.9, is to choose a parallel leaf spring guiding as resonant actuator, which has 1 degree of translation and the leaf spring could be treated as a resonator. It is placed at the edge of the end effector, and connected by a notch hinge to be able to actuate rotation of the end effector. The length of two leaf springs could be changed to achieve eigenfrequency tuning. Fig. 5.5a and 5.5b corresponds to crossed flexure and notch flexure as guiding.

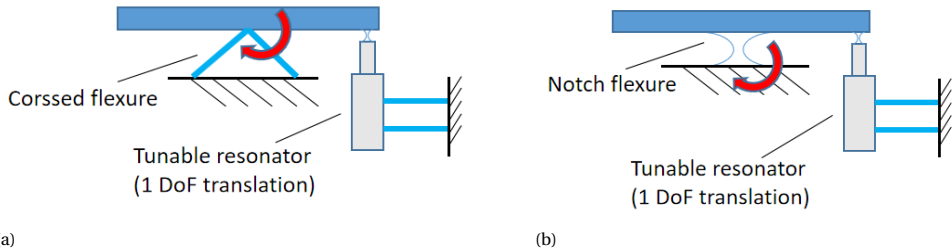


Figure 5.5: Schematic of concept of strategy two with a. crossed flexure and b. notch flexure as guiding.

5

There are two main criteria considered in concept evaluation, ease of tuning and complexity, shown as Fig. 5.6. One might notice that, for the first category, it is easy to tune only one cantilever. While for the second category, it would be quite difficult to maintain two cantilevers with exactly the same length, or otherwise these two would be slightly different in resonant frequency. This might lead to beating, or different amplitude of vibration, which influences dynamic performance or even induces unwanted motion. Furthermore, the concept in the first category with no subsystem, in principle would be less complicated than the second one that contains two separated subsystems. Therefore, the first strategy is more preferable.

|                                   | Ease of tuning | Complexity | Total |
|-----------------------------------|----------------|------------|-------|
| Resonator inside constraint space | +              | +          | ++    |
| 1 DoF guiding + resonant actuator | -              | 0          | -     |

**Ease of tuning:** + means could be easily tuned without affecting performance a lot; 0 means might be difficult to tune but performance could be maintained; - means difficult to tune and difficult to maintain performance

**Complexity:** + means concept does not have subsystem; 0 means concept has 2 subsystem; - means concept have more than 2 subsystem

Figure 5.6: Harris profile of strategies of resonator integration.

|         | Mode Coupling | Sensitivity to Disturbance | Actuation of Unwanted Mode | Scanning Accuracy | Total |
|---------|---------------|----------------------------|----------------------------|-------------------|-------|
| Bending | o             | +                          | +                          | o                 | ++    |
| Torsion | -             | -                          | -                          | +                 | --    |

**Mode Coupling:** + means no mode coupling effect would occur; o means mode coupling would occur but could be easily avoided; - means mode coupling would occur and difficult to avoid

**Sensitivity to Disturbance:** + means no other mode has low resonant frequency than the first intended mode; o means there would be 1 mode with lower resonant frequency than the first intended mode; - means there would be more than 1 mode with lower resonant frequency than the first intended mode

**Actuation of Unwanted Mode:** + means ideally the actuation would not excite other modes; o means ideally the actuation would excite other modes but could be avoided; - means ideally the actuation would excite other modes and might be difficult to avoid

**Scanning Accuracy:** + means no parasitic motion/rotational center would not shift during deflection; o means parasitic motion could be expected but could be limited to acceptable range/rotational center would shift but negligible; - means parasitic motion could be expected but difficult to limit to acceptable range/rotational center would shift noticeably

Figure 5.7: Harris profile of resonator motion.

## MOTION OF RESONATOR

For the first strategy (Fig. 5.4), there is another choice between bending and torsion. There are mainly three considerations. The first one is mode coupling, which could lead to unwanted motion. This is an important issue that needs to be dealt with when making use of resonance. In the application of a 1 DoF scanning mirror, torsional and bending mode are unwanted resonant mode towards each other. It would be quite difficult to maintain all intended modes within 500 to 5k Hz and at the same time keep all other unwanted modes outside this range. The idea is to avoid the coupling region, and this means the less number of unwanted mode stay inside working frequency range, the better the concept. Generally speaking, torsional motion of a cantilever often has higher stiffness than bending, and therefore has higher resonant frequency.

According to [3], there are some empirical numbers for engineering estimation of eigen-frequency of higher order modes based on the first mode. As Fig. 5.4 shown, Fig. 5.4a is clamped-hinged for bending and clamped-clamped for torsion, and Fig. 5.4b is clamped-free for torsion and clamped-clamped for bending. Regarding the bending case, for a clamped-hinged cantilever, ratio of the 1<sup>st</sup> to 4<sup>th</sup> bending modes is 15.42:49.97:104.25:178.27, and for a clamped-clamped torsion beam, ratio of the 1<sup>st</sup> to 4<sup>th</sup> torsion modes 1:2:3:4. If the first bending mode is set at 400 Hz, the higher order modes would be around 1296.3 Hz, 2704.6 Hz and 4624.9 Hz. And if the dimension is designed properly such that the first torsional mode is higher than 2500 Hz, then there would be only one torsional mode stay in the intended frequency region. While regarding the torsional case, for a clamped-free torsion beam, ratio of the 1<sup>st</sup> to 4<sup>th</sup> torsion modes 1:π:2π:3π, and for a clamped-clamped cantilever, ratio of the 1<sup>st</sup> to 4<sup>th</sup> bending modes is 22.37:61.67:120.90:199.86. If the 1<sup>st</sup> torsion mode is set at 400 Hz, the 1<sup>st</sup> bending

mode would expect to be lower than that, and at least more than two higher order bending modes might stay within 500 - 5k *Hz*. And during the tuning action, the 1<sup>st</sup> bending mode would be brought into the working frequency range as well. Therefore, for the torsional concept, mode coupling issue would be expected to be more complicated. Since both concepts cannot eliminate the possibility of mode coupling, and bending motion is easier to avoid that, thus "o" for bending and "-" for torsion in this criteria.

The second consideration is sensitivity to disturbance. Followed by the first consideration, if torsional motion is chosen and the first mode is set to around 500 *Hz*, then the first bending mode might be lower than that with lower stiffness, and hence this would be sensitive to disturbance. While if the first bending mode is set to 500 *Hz*, generally there would be no modes with eigenfrequency lower than that, and eigenfrequencies of the torsional modes would be way higher than that as well. Therefore, with bending as scanning motion, unwanted mode would have higher stiffness and be less sensitive to disturbance ("+" for bending and "-" for torsion).

5

The third consideration is actuation of unwanted modes. The actuation configuration of bending motion could be a force acting on the center line of the cantilever, and This line is also the nodal line of torsional mode. While for torsion, its excitation should be a torque at the center line, which corresponds to force at the edge of cantilever. Hence, in principle actuation of bending motion would have less possibility to excite unwanted mode, especially closing to the mode coupling frequency region, and this might reduce the coupling effect ("+" for bending and "-" for torsion).

The last consideration is scanning accuracy. Since flexure mechanism is involved, parasitic motion could be expected during deflection of flexure, and this might cause shift of rotational center and thus influence the scanning accuracy. For the two shown concepts, ideally, torsion beam itself has a rotational axis, which is the center line of the beam, and therefore, the deflection of the two-strut constraint would not lead to shift of rotational axis. While for bending motion, deflection of the flexure would lead to this shift, but would be negligible for small motion [4]. Furthermore, bending of cantilever would also exert load on the two-strut constraint in its longitudinal direction. This load could be large at high frequency such that two struts might lose constraint due to limited stiffness and the motion of end effector would be a coupling between bending and translation. However, they could be designed properly or even replaced by other equivalent flexure elements with high stiffness in longitudinal direction such that the unwanted translation could be limited to an acceptable range ("o" for bending and "+" for torsion).

From above discussion, the proposed concept adopt a bending cantilever as the resonator and it is integrated into the constraint space. Fig. 5.8 summarizes above design flow.

### 5.2.2. GUIDING HINGE

The chosen concept with two struts underneath the end effector might not be enough to support high frequency resonance. This issue could be shown as Fig. 5.9a, which is a displacement field close to the end effector at around 5k *Hz*, and the motion of

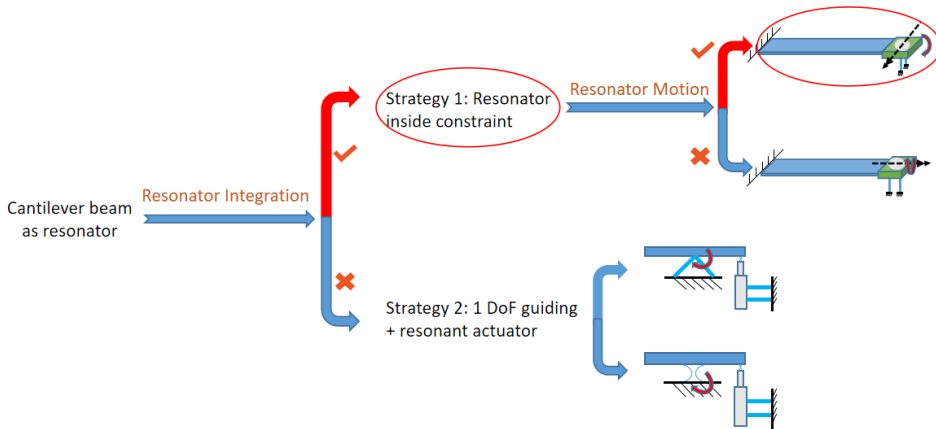


Figure 5.8: Design flow of resonator for 1 degree of rotation.

the end effector is a coupling between translation in  $z$  axis and rotation about  $x$  axis. This two struts could be treated as a hinge joint, shown as Fig. 5.9b, and the problem becomes to design a flexure hinge that has low rotational stiffness about  $x$  axis and high stiffness in  $z$  direction. And it is preferable to constrain 2 DoF, and release translation in  $x$  and  $y$  direction to cope with misalignment, manufacturing error and to realize an exact-constrained mechanism.

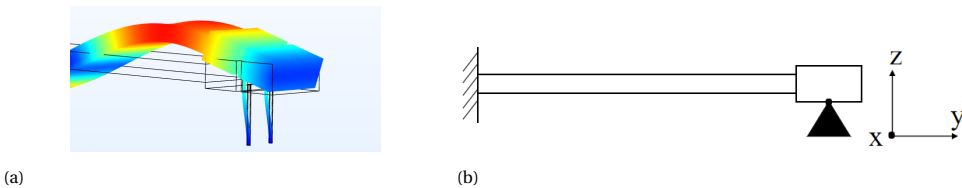


Figure 5.9: (a). Displacement field close to strut at around  $5k$  Hz resonance. (b). Equivalent cantilever beam with clamped-hinged boundary condition

All generated concepts are shown as Fig. 5.10. To make concept evaluation easier, some of them are even strengthened to have a higher support stiffness in  $z$  direction, and if they still lose constraint then those concepts would be excluded. Concept descriptions are as followed:

- A. Two folded leaf springs are equivalent to two flexible struts, and their height are increased to strengthen the constraint stiffness
- B. One side of the folded leaf spring is extended to further enhance the constraint stiffness.
- C. Folded leaf spring is strengthened by another leaf spring in parallel, but the end effector is over-constrained.

- D. One side of the folded leaf spring is replaced by a block with two notch, but the end effector is over constrained 2 times.
- E. Four notch flexures in series is equivalent to a flexible strut, and two pairs of them are used to replace the two struts with same constraint space but higher constrain stiffness, and the end effector is exact-constrained
- F. Two leaf springs in series is equivalent to a flexible strut. Two pairs are used and the end effector is exact-constrained but there are two under-constrained parts.
- G. A leaf spring is used as a guiding, together with the resonator beam to forms a crossed-flexure, but the end effector is 1 time over constrained.
- H. A cut is introduced to the leaf spring guiding in concept G to reduce the effect of over constraint.

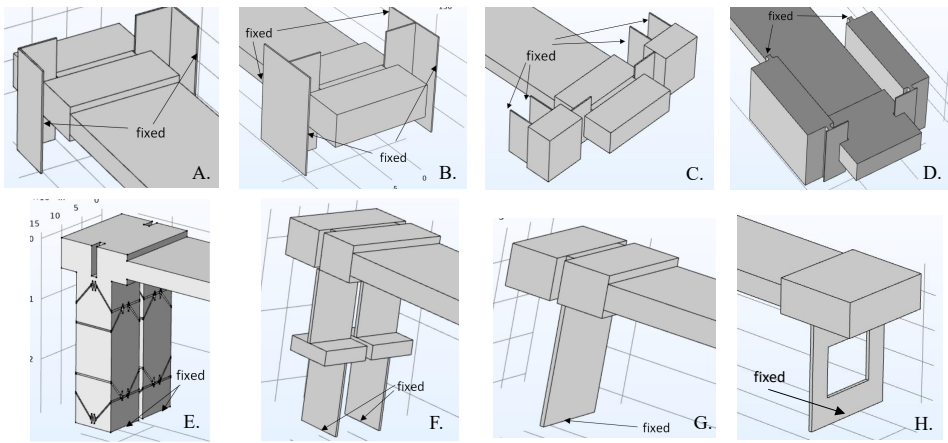


Figure 5.10: Schematics of guiding concept.

#### Evaluation Steps:

1. Dimension parameters are tuned such that the mechanism has the 4<sup>th</sup> bending mode with eigenfrequency around 5k Hz. Then apply an 5k Hz excitation such that the angular deflection is around 0.5 mrad, and the displacement field is captured to see whether guiding hinge would lose constraint.
2. Select those concepts that does not lose constraint, and further evaluate with other important criteria.

#### STEP 1

A rough simulation estimation results is shown as Fig. 5.11. One could obviously notice that, concept A, B, and C lose constraint, even their constrain stiffness is strengthened for simulation. Therefore, concept D, E, F, G, H would be proceed to step 2.

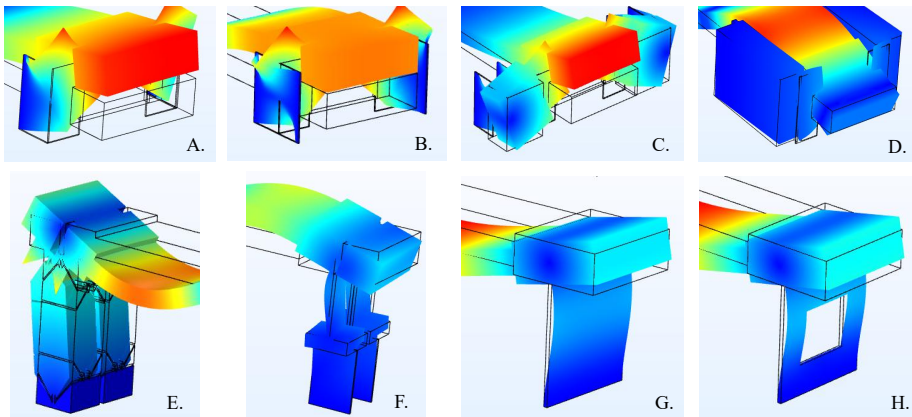


Figure 5.11: Displacement field close to guiding at around  $5k\text{ Hz}$  resonance.

## STEP 2

There are three criteria are considered to evaluate concepts, with Harris profile shown as Fig. 5.12.

- Exact constraint:** This criterion is related to predictability of flexure. It is preferable to have the end effector exact-constrained without other under/over-constrained parts. + means the end effector is exact-constrained and the mechanism has no other under/over-constrained parts. o means end effector is exact-constrained but mechanism contains under/over-constrained parts. - means end effector is under/over-constrained.
- Ease of manufacturing:** This criterion is related to manufacturability of flexure. It is better to have a simple design that is easily machined. + means concept could be machined by wire EDM only from one side combining with a little amount of milling. o means concept should be machined by wire EDM from more than one side or combine with a large amount of milling. - means concept should be machined by wire EDM from more than one side and combine with a large amount of milling.
- Stress concentration**(at angular deflection  $0.5\text{ mrad}$ ): This criterion is related to fatigue of material. Since mechanism is expected to operate at high frequency oscillation, it is preferable to keep the maximum stress much lower than yielding stress and get rid of stress concentration. This is investigated with combination of rough finite element simulation. + means maximum stress could be lower than 30% of yielding stress. o means maximum stress would be higher than 30% but lower than 60% of yielding stress. - means maximum stress would be higher than 60% of yielding stress.

From above discussion, the concept of 1 DoF resonant scanner mechanism is designed

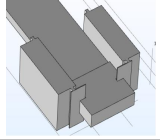
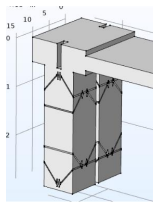
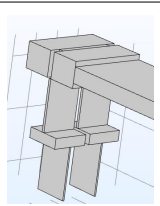
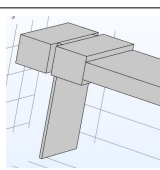
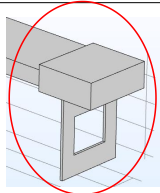
|  | Exact constraint | Ease of Manufacturing | Stress Concentration | Total |
|--|------------------|-----------------------|----------------------|-------|
|   | -                | -                     | +                    | -     |
|   | +                | 0                     | -                    | 0     |
|   | 0                | 0                     | +                    | +     |
|   | -                | +                     | +                    | ++    |
|  | +                | +                     | +                    | +++   |

Figure 5.12: Harris profile of hinge guiding concept selection.

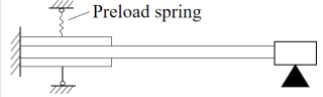
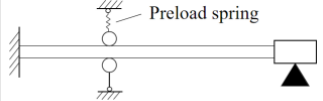
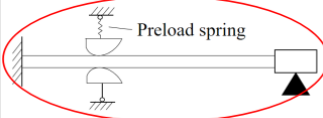
as a bending cantilever in clamped-hinged boundary condition, and the hinge guiding is a leaf spring with a cut at the middle.

### 5.3. FREQUENCY TUNING MECHANISM

To change the effective length of the cantilever beam, clamping could be an option. There are three criteria considered to evaluate concepts: ease of implementation, mechanical wear and tolerance. Fig. 5.13 shows three concepts utilizing clamping. All of



the three concepts use two identical members for clamping, with one fixated and the other preloaded. If the reaction force at clamping position during oscillation is lower than the preload force then ideally the clamping could function.

|   | Ease of Implementation | Mechanical Wear | Tolerance | Total |
|---|------------------------|-----------------|-----------|-------|
|  | -                      | -               | +         | -     |
|  | +                      | +               | -         | +     |
|  | +                      | 0               | +         | ++    |

**Ease of implementation:** This criterion is mainly implied by how easy the preload could be applied (in 2 D configuration). + means preload could be applied through point, o means preload needs to be applied through several points, - mean preload needs to be equally distributed over a certain area.

**Mechanical Wear:** + means sliding does not or cause negligible wear, o means sliding cause wear but (contact) area is small, - means sliding cause wear and (contact) area is large.

**Tolerance:** + means little amount of assembly is needed and accuracy could be easily maintained, o means large amount of assembly is needed or accuracy is difficult to maintained, - mean large amount of assembly is needed and accuracy is difficult to maintained.

Figure 5.13: Harris profile of frequency tuning mechanism concept selection.

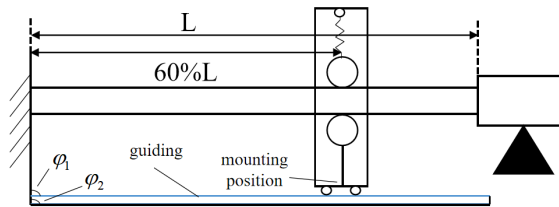
The first concept uses plate clamp. This could be effective and the effective length is equal to distance between clamping end and the end effector. But for the implementation, the preload might require to be equally distributed over the surface to ensure proper contact of the full surface. And with DLC coating, it could reduce friction of coefficient and enable sliding, but this could still cause mechanical wear for the whole contact area.

The second concept is to use roller bearing for clamping in Hertz line contact. The preload could be applied through the center of the bearing downward to the contact place, which is easy to implement. Instead of sliding, the bearing could be rolled along the cantilever and therefore much less mechanical wear could occur. However, line contact might prefer to have large radius for the curve surface, which could enable larger preload force and further increase the contact stiffness. It should be noted that bearing with large radius would be bulky.

Followed by the second concept, the third one adopts two curve surfaces (parts of a large circle) with large radius of curvature to keep the size small and at the same time enable

large preload and contact stiffness. But the sliding could induce wear.

Regarding the criteria of tolerance, an example dimension of cantilever is taken for analysis. Error of position change in height of the clamping would cause deflection of the beam, and the mirror would have an initial angle. Considering the allowed space, a cantilever in  $140 \times 12 \times 2.5\text{mm}$  in clamped-hinged boundary condition has the first bending mode close to  $500\text{Hz}$ . According the previous simulation, when the line constraint is at 60% of total length, all the first four bending modes could connect to higher order ones to cover  $500 - 5\text{kHz}$  range, which means this would be the maximum stroke. Therefore, the error would have maximum effect at  $84\text{mm}$ . Tolerance analysis is shown as Fig. 5.14. By finite element calculation, the sensitivity of the angle change in end effector per unit height position change is  $25.396\ \mu\text{rad}/\text{um}$ . This could be induced by guiding itself, mounting position of the bearing and tolerance of the bearing diameter. Machining of the base platform and assembly of guiding could also cause angular deviations  $\phi_1$  and  $\phi_2$ . This induces a height variation of  $0.6L\phi$  at 60%L clamping position, and therefore leads to a sensitivity of  $2.133\ \mu\text{rad}/\mu\text{rad}$ . Some relatively tight values are assigned in tolerance, which leads to the fact that pre-deflection of the cantilever due to error could cause rotation at end effector is around  $\pm 0.38\text{mrad}$ , even larger than the intended scanning angle ( $\pm 0.25\text{mrad}$ ).



(a)

| Parameter                                | Sensitivity | unit        | Tolerance( $\pm$ ) | unit   | Effect on initial angle/[urad] |
|--|-------------|-------------|--------------------|--------|--------------------------------|
| Height variation of guiding              | 25.39632233 | [urad/um]   | 10                 | [um]   | 253.9632233                    |
| Angle deviation of guiding ( $\phi_1$ )  | 2.133291076 | [urad/urad] | 10                 | [urad] | 21.33291076                    |
| Diameter of bearing                      | 12.6982     | [urad/um]   | 10                 | [um]   | 126.982                        |
| Bearing mounting position deviation      | 25.39632233 | [urad/um]   | 10                 | [um]   | 253.9632233                    |
| Angle deviation of platform ( $\phi_2$ ) | 2.133291076 | [urad/urad] | 10                 | [urad] | 21.33291076                    |
| RMS/[urad]                               |             |             |                    |        | 382.1377396                    |

(b)

Figure 5.14: (a). Schematics and (b). tolerance analysis of bearing clamping.

While it is possible to specify lower manufacturing error when machining monolithically for concept 1 and 3. This could ensure high accuracy clamping. Furthermore, there would be little amount of assembly needed, which means less error parameters need to be taken into account.

# 6

## SUPPLEMENTARY MATERIAL: DIMENSION DESIGN

In this session, the detail design of key features are presented with combination of finite element analysis. The design flow is shown as Fig. 6.1.

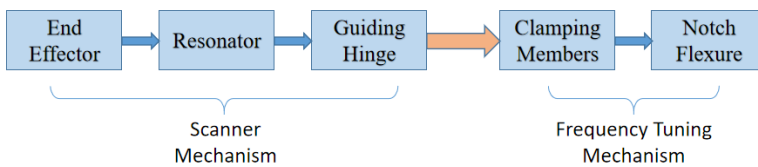


Figure 6.1: Design flow of detailed dimension.

### 6.1. SCANNER MECHANISM

#### End Effector

According to the requirement of beam size of  $11\text{ mm}$  in diameter, the end effector is designed in a square shape in  $12 \times 12 \times 3\text{ mm}$ . Modal analysis is conducted with an ideal hinge constrain at the center of the block, with model shown as Fig. 6.2a. The first eigenmode related to scanning motion is shown as Fig. 6.2b, with frequency higher than  $50\text{ k Hz}$ .

#### Resonator

There are several considerations of the resonator design.

- **1. Design space:** The design should be able to fit into allowed space  $70 \times 70 \times 150\text{ mm}$ , where  $150\text{ mm}$  would be related to cantilever length.

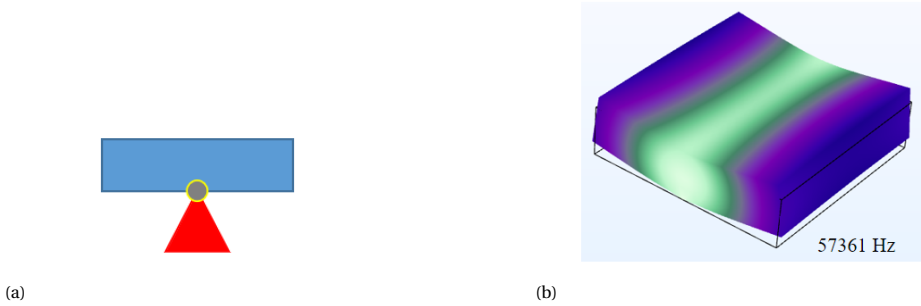


Figure 6.2: a. Schematic of concept of strategy one with a. bending and b. First eigenmode of the end effector related to scanning motion.

- **2. Eigenfrequency of bending and torsional mode:** According to the discussion in Chapter 5, the first four bending modes of resonator should be located close to 500 - 5kHz range for ease of tuning, and the first torsional mode should be higher than 2500Hz for less possibility of modal coupling.
- **3. Ratio between constraint and motion stiffness:** Ratio between constraint and motion stiffness should be larger than 150 [5] to be considered as a "good flexure".
- **4. Tuning sensitivity:** It is preferable to have a longer cantilever so that the tuning sensitivity is lower which allows for more accurate tuning.
- **5. Bending stiffness:** Cantilever with a higher bending stiffness could achieve a better performance of disturbance rejection.

There are three parameters for the resonator beam: width, height and length. For ease of manufacturing, width is set 12mm, equal to that of the end effector. And the cantilever should be shorter than 140mm such that it can fit into design space together with the end effector. Estimated ratio of the first four bending modes of a clamped-hinged cantilever is 15.42:49.97:104.25:178.27. Therefore, the 1<sup>st</sup> bending mode should be at the range of 350 - 450Hz. Noting that the guiding hinge would also add some extra stiffness which might lead to a few tens of Hz increase in eigenfrequency.

A quick analysis is conducted with Al 7075 T6. Based on the criteria of the 1<sup>st</sup> bending mode, possible solution set of cantilever dimension is obtained. The length is in the range of 50 - 140mm, and step for length and height change is 10mm and 0.1mm respectively. Stiffness ratio between  $x$  and  $z$ , and  $y$  and  $z$  direction are estimated. Since  $l \gg w$ , they could be calculated as

$$\frac{c_x}{c_z} = 4 \left( \frac{l}{h} \right)^2 \quad (6.1)$$

and

$$\frac{c_y}{c_z} \approx \left( \frac{w}{h} \right)^2. \quad (6.2)$$

Stiffness at the middle of the cantilever is also estimated. The results are shown in Table B.1 (P82). One could notice that, as the length increases, to keep the 1<sup>st</sup> bending mode within the intended range, height would increase as well. This lead to an increase of mass and therefore an increase of bending stiffness. To keep the ratio between constraint and motion stiffness larger than 150, cantilever length should not exceed 90mm. The dimension  $90 \times 1 \times 12\text{mm}$  is chosen. Even  $c_y/c_z$  is a bit lower than 150, but this could be strengthened by the leaf spring guiding hinge. And all the three dimension parameters are integers, which could be easier for machining.

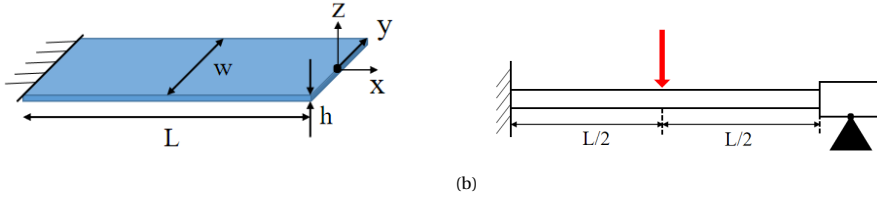


Figure 6.3: a. Flexure parameters and coordinate for stiffness ratio estimation and b. Position for bending stiffness estimation.

### Guiding Hinge

Considerations for the guiding hinge design:

- 1. Low bending stiffness.
- 2. High longitudinal stiffness (translation of end effector along optical axis less than  $100\mu\text{m}$ ).
- 3. 1<sup>st</sup> eigenfrequency related to scanning should be higher than 5k Hz.
- 4. Could be fitted into design space.

The cut at the leaf spring would have a 3mm radius filleted corner due to milling tool used in manufacturing. Therefore, the performance is evaluated by finite element analysis. The chosen dimension is  $12 \times 15 \times 0.5\text{mm}$  for width, height and thickness respectively, shown in Fig. 6.4a. The cut is 7mm in width and 8mm in height from center. Simulation are conducted with a mirror (10mm diameter and 2mm height) on the end effector, and estimated eigenfrequency of the 1<sup>st</sup> to 4<sup>th</sup> bending mode of cantilever is 457.61Hz, 1321.5Hz, 2638.7Hz, and 4413.3Hz respectively, which are all closed to or within 500 - 5k Hz. The 1<sup>st</sup> mode of guiding leaf spring is 14594Hz, shown as Fig. 6.4b, around 3 times higher than 5k Hz. With excitation at the 1<sup>st</sup> to 4<sup>th</sup> eigenfrequency of bending mode of cantilever, and angular deflection of the end effector is brought to 0.5mrad, the maximum stress, shown as Fig. 6.5, is 1.32MPa, 1.34MPa, 1.59MPa and 2.21MPa respectively, which is much smaller than yielding stress (around 503MPa). Translation of the end effector in z direction is measured as around 4nm, 9.8nm, 14.2nm and 13.3nm respectively, which is much less than  $100\mu\text{m}$ .

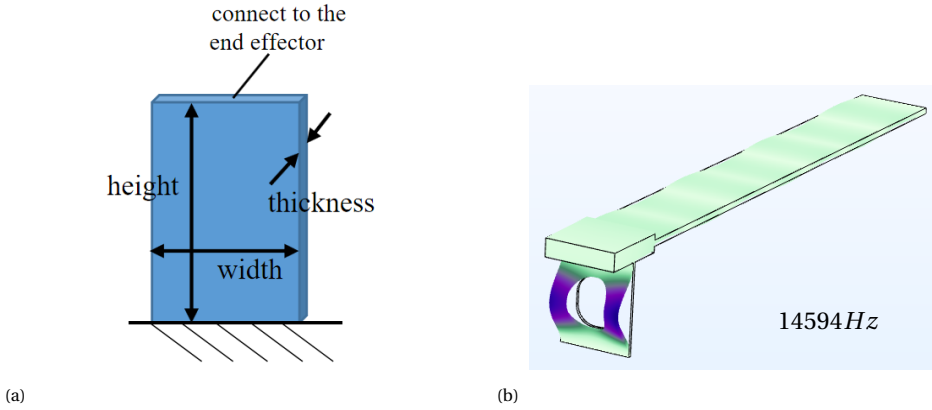


Figure 6.4: a. Dimension parameters of hinge guiding, and b. The 1<sup>st</sup> mode of the guiding hinge.

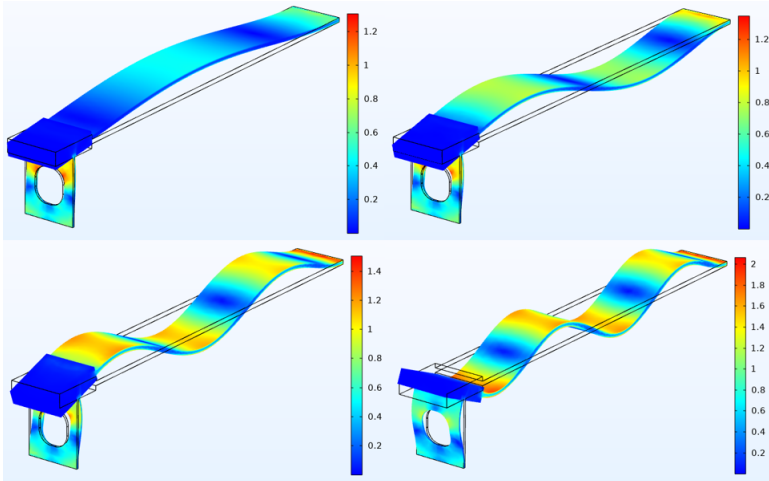


Figure 6.5: Stress field of scanner at the 1<sup>st</sup>, 2<sup>nd</sup>, 3<sup>rd</sup> and 4<sup>th</sup> bending with  $0.5\text{ mrad}$  angular amplitude at the end effector/[MPa].

Clamping is modelled as a small plate with width  $0.22\text{ mm}$  as presented in Chapter 4. After obtaining eigenfrequencies with respect to the clamping position, tuning sensitivity  $S$  could be estimated as a function of clamping position  $C$ ,

$$S(C) = \frac{f_{C+\delta} - f_C}{\delta}, \quad (6.3)$$

where  $f_C$  and  $f_{C+\delta}$  is eigenfrequency at clamping position  $C$  and  $C + \delta$ . Fig. 6.6a shows the tuning sensitivity of the 1<sup>st</sup>, 2<sup>nd</sup>, 3<sup>rd</sup> and 4<sup>th</sup> bending mode, where the negative ones are neglected since those regions are not considered for operation. Noting that for intended frequency range  $500 - 5\text{ k Hz}$ , clamping position for the 4<sup>th</sup> bending mode would not exceed  $8\text{ mm}$ . Therefore, with around  $10\mu\text{ m}$  positioning accuracy for the tuning

mechanism, eigenfrequency could be tuned with resolution less than  $1\text{Hz}$ . This could be easily achieved by a spindle drive. Fig. 6.6 shows the maximum stress with respect to clamping position when the scanner is operated at resonant frequency of the  $1^{\text{st}}$  to  $4^{\text{th}}$  bending mode with angular deflection of the end effector  $0.5\text{mrad}$ . Even not at usable regions, it would not exceed  $40\text{MPa}$ , which is much less than 30% of yielding stress (around  $503\text{MPa}$ ).

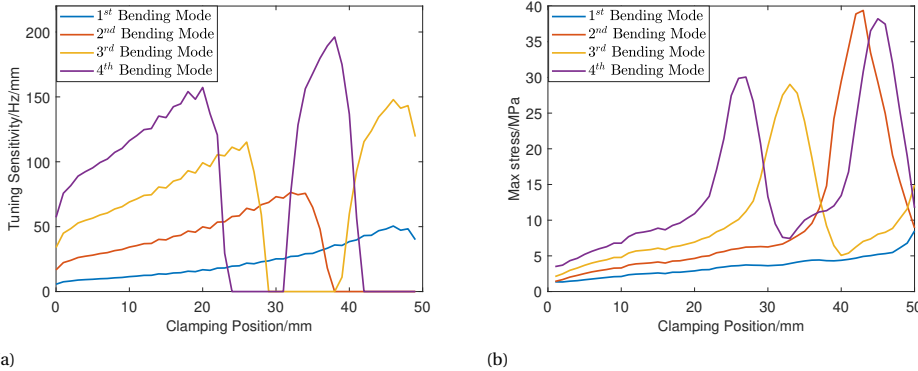


Figure 6.6: a. Tuning sensitivity of the  $1^{\text{st}}$  to  $4^{\text{th}}$  bending mode. and b. maximum stress of  $1^{\text{st}}$  to  $4^{\text{th}}$  bending mode with respect to clamping position when angular deflection of the end effector is  $0.5\text{mrad}$ .

### Guiding rail

Another important part is the guiding rail that defines the position of the frequency tuning mechanism. To enable around  $45\text{mm}$  stroke for the tuning, designed length is  $73\text{mm}$  (dimension of the tuning mechanism is taken into account). The  $1^{\text{st}}$  mode is found at  $8994.3\text{Hz}$ , as shown in Fig. 6.7a. Performance is estimated at its middle where the stiffness is relatively low. According to Chapter 4, when the clamping position is at around  $36\text{mm}$ , at usable regions, the clamping reaction force would not exceed  $2\text{N}$ . Fig. 6.7b shows a negligible displacement.

## 6.2. FREQUENCY TUNING MECHANISM

Design consideration for the Frequency tuning mechanism:

- 1. Large radius of curvature for contact
- 2. High Hertz contact stress for low hysteresis clamping
- 3. With the given preload force, contact stress should be less than yielding stress

The parameter design and contact features are also estimated by HertzWin (<https://www.vinksa.com/en-2/>). The proposed design is  $50\text{mm}$  radius for clamping surface with  $80\text{N}$  preload. Estimated Hertz contact stress is  $41.32\text{MPa}$ , which is acceptable.

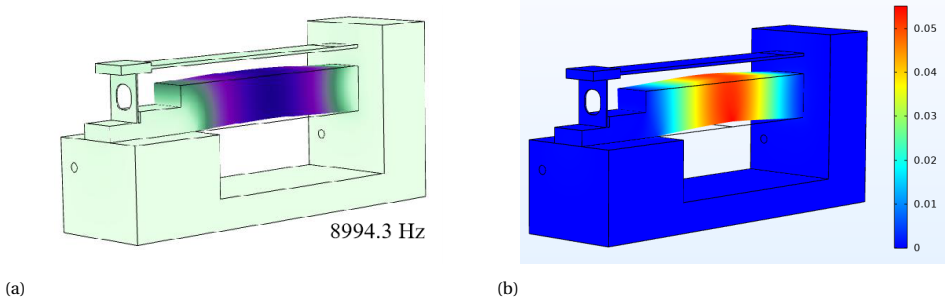


Figure 6.7: a. Mode shape of guiding rail. and b. displacement field of guiding rail with excitation  $2N$  and  $5k$   $Hz$  at middle/ $[\mu m]$ .

To save space, preload spring is placed parallel to the longitudinal direction of the cantilever, and force is applied via a notch hinge. Stiffness is estimated by formulas from JPE website (<https://www.jpe-innovations.com/precision-point/flexure-hinge-elastic-hinge/>). Dimension is shown as Fig. 6.8, with  $h = 0.15mm$  and  $D = 4mm$  and this give stiffness at the preload application point (distance  $L=5.5mm$  to the notch point)  $1.11 \times 10^5 N/m$ .

## 6

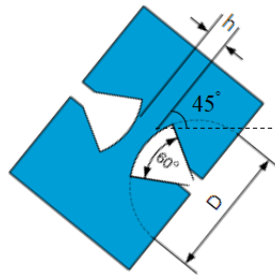


Figure 6.8: Dimension design of the notch hinge.

Free body diagram of the upper clamping surface is shown as Fig. 6.9. Noting that the center point of the curvature is located on the dashed line, with a distance of  $1mm$  to the edge of the block. The reaction force at the contact place is supposed to be on this line as well. Stroke of upper the clamping surface to contact the cantilever is  $0.1mm$ , and this needs  $F = 11.1N$  for the upper clamping surface to just contact the cantilever. This causes a reaction moment  $M = FL$  and a force  $F_1 = F$  at the notch hinge. After that,  $F$  would increase  $80N$  more which adds as preload force, and this induces  $F_c = 80N$ . Since the distance between the notch point to the contact point and to the preload point is equal. Therefore, reaction force  $F_1 = 91.1N$  and  $F_2 = 80N$ . Its angle between horizontal line is  $41.28^\circ$ . For ease of manufacturing,  $45^\circ$  is chosen.

From Session A.3, an issue of pre-deflection of the cantilever caused by tolerance of bearing and assembly is discussed. To ensure the performance of the frequency tuning mechanism, tolerance analysis is conducted. According to the modal behavior analysis



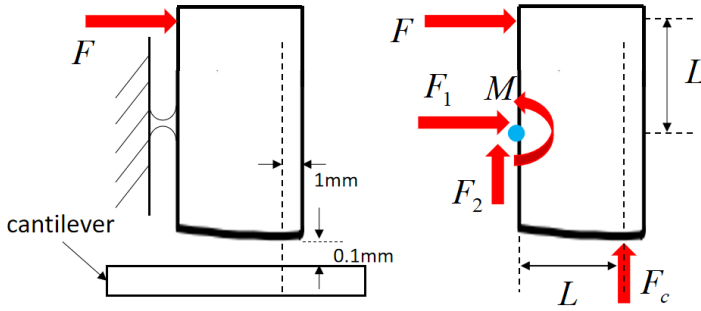
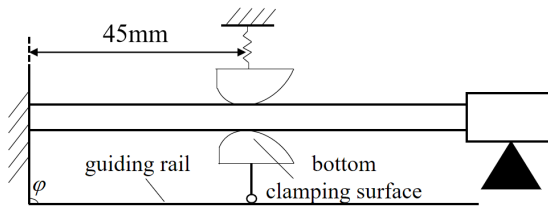


Figure 6.9: Free body diagram of the upper clamping surface.



(a)

| Parameter                                   | Sensitivity | unit        | Tolerance( $\pm$ ) | unit   | Effect on initial angle/[urad] |
|---|-------------|-------------|--------------------|--------|--------------------------------|
| Height variation of guiding rail            | 36.53931028 | [urad/um]   | 1                  | [um]   | 36.53931028                    |
| Angle deviation of guiding (phi)            | 1.6443      | [urad/urad] | 10                 | [urad] | 16.443                         |
| Height variation of bottom clamping surface | 36.53931028 | [urad/um]   | 1                  | [um]   | 36.53931028                    |
| RMS/[urad]                                  |             |             |                    |        | 54.22743439                    |

(b)

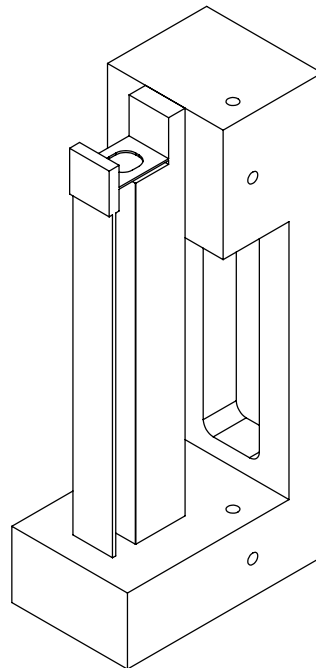
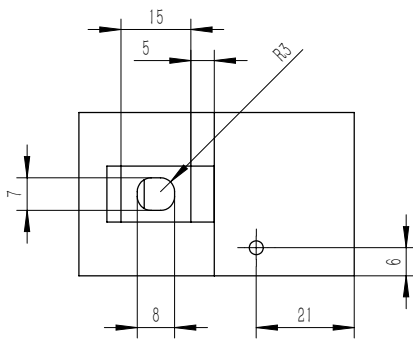
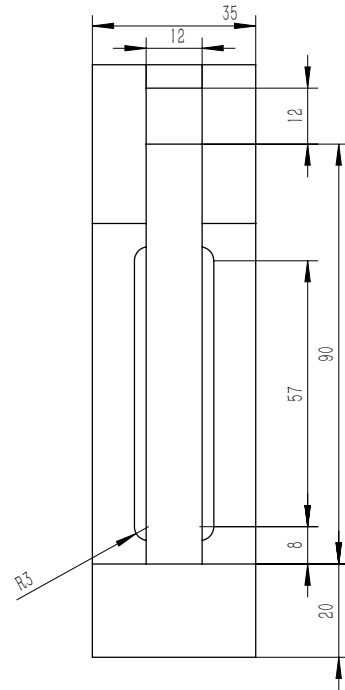
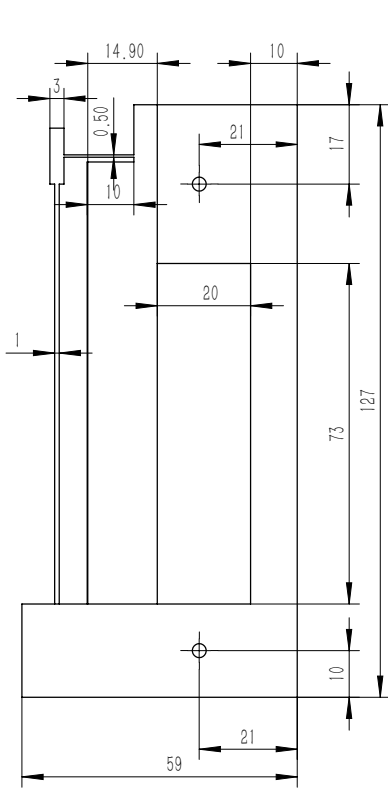
Figure 6.10: (a). Schematics and (b). tolerance analysis of clamping mechanism.

in Chapter 4, needed stroke for frequency tuning mechanism is  $45\text{mm}$ . Since spark erosion is used for manufacturing, less assembly work is needed. As Fig. 6.10a shows, height and angle variation of the guiding rail, and height variation of the bottom clamping surface could cause pre-deflection. With achievable accuracy by wire-EDM ( $\approx \pm 1\mu\text{m}$ ), rotation of the end effector due to pre-deflection could be limited 5 times less than the scanning angle. Noting that from requirement, the maximum allowable  $d_z$  is  $100\mu\text{m}$ , and the incoming fluorescence light from samples has an incident angle of  $45^\circ$  to scanner. In this configuration, focal point movement induced by the maximum  $d_z$  is  $P = 2d\sin(45^\circ) = 0.14\text{mm}$ . Since negligible  $d_z$  of the scanner is expected according to Session 4, this tolerance could be used for pre-deflection angle. At a distance  $L = 0.14 / (2 \times 108.45 \times 10^{-6}) = 654.7\text{mm}$ , focal point movement induced by the maximum allowable  $d_z$  and pre-deflection are equal. Therefore, it is recommended to place the detector array close to the scanner, while if a large distance is needed, it could be positioned by a 1 DoF alignment mechanism.

Design drawings are included in the following Figures.

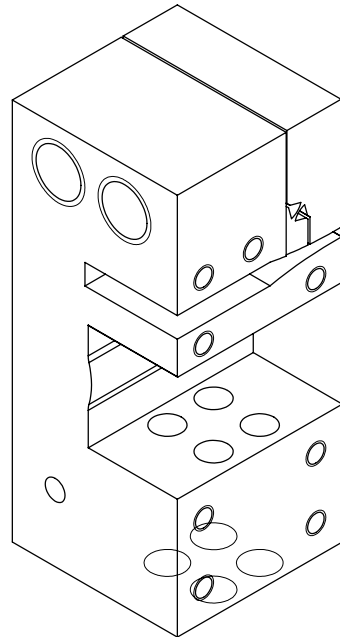
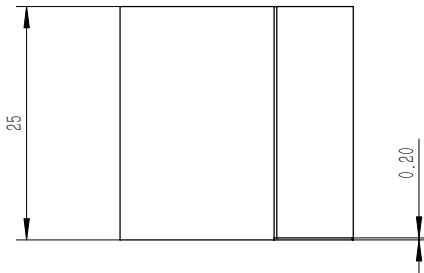
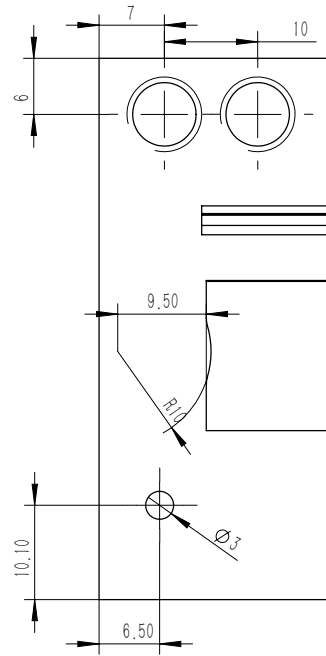
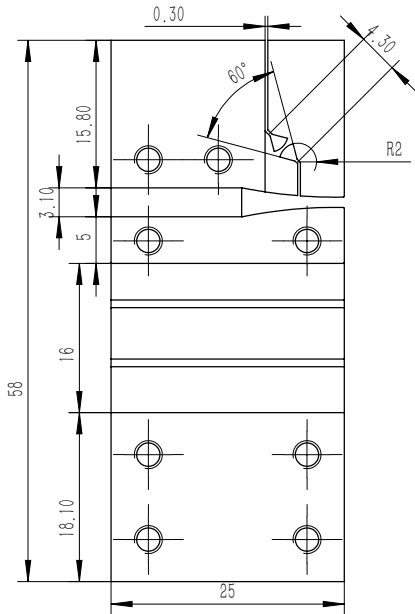
|                  |         |        |         |         |         |         |         |        |         |         |         |         |         |         |         |         |         |     |
|------------------|---------|--------|---------|---------|---------|---------|---------|--------|---------|---------|---------|---------|---------|---------|---------|---------|---------|-----|
| L/mm             | 50      | 60     | 70      | 70      | 80      | 80      | 80      | 80     | 90      | 90      | 90      | 90      | 100     | 100     | 100     | 110     | 110     | 110 |
| h/mm             | 0.4     | 0.5    | 0.6     | 0.7     | 0.7     | 0.8     | 0.9     | 0.9    | 0.9     | 1       | 1       | 1.1     | 1.1     | 1.2     | 1.3     | 1.4     | 1.4     | 1.5 |
| w/mm             | 12      | 12     | 12      | 12      | 12      | 12      | 12      | 12     | 12      | 12      | 12      | 12      | 12      | 12      | 12      | 12      | 12      | 12  |
| c_x/c_z          | 62500   | 57600  | 54444.4 | 40000   | 52244.9 | 40000   | 31604.9 | 40000  | 32400   | 26776.9 | 33057.9 | 27777.8 | 23668.6 | 20408.2 | 28639.1 | 24693.9 | 21511.1 |     |
| c_y/c_z          | 900     | 576    | 400     | 293.9   | 293.9   | 225     | 177.8   | 177.8  | 144     | 119     | 119     | 100     | 85.2    | 73.5    | 85.2    | 73.5    | 64      |     |
| F_bending/Hz     | 435.3   | 406.4  | 373.8   | 437.7   | 343.0   | 392.8   | 442.5   | 355.5  | 395.4   | 435.3   | 357.1   | 389.8   | 422.4   | 277.8   | 352.7   | 379.9   | 407.1   |     |
| F_torsion/Hz     | 2396.1  | 2421.7 | 2437.8  | 2831.6  | 2447.8  | 2784.4  | 3118.0  | 2745.5 | 3038.5  | 3323.5  | 2968.9  | 3226.7  | 3473.8  | 3728.1  | 3142.6  | 3372.6  | 3589.4  |     |
| Stiffness (N/mm) | 3.3     | 3.8    | 4.3     | 6.8     | 4.6     | 6.9     | 9.8     | 7.0    | 9.6     | 12.8    | 9.4     | 12.2    | 15.5    | 19.4    | 11.8    | 14.7    | 18.1    |     |
| L/mm             | 110     | 120    | 120     | 120     | 120     | 130     | 130     | 130    | 130     | 130     | 140     | 140     | 140     | 140     | 140     | 140     | 140     |     |
| h/mm             | 1.6     | 1.6    | 1.7     | 1.8     | 1.9     | 1.8     | 1.9     | 2      | 2.1     | 2.2     | 2.3     | 2.1     | 2.2     | 2.3     | 2.4     | 2.5     | 2.6     |     |
| w/mm             | 12      | 12     | 12      | 12      | 12      | 12      | 12      | 12     | 12      | 12      | 12      | 12      | 12      | 12      | 12      | 12      | 12      |     |
| c_x/c_z          | 18906.3 | 22500  | 19930.8 | 17777.8 | 15955.7 | 20864.2 | 18725.8 | 16900  | 15328.8 | 13966.9 | 12778.8 | 17777.8 | 16198.3 | 14820.4 | 13611.1 | 12544.1 | 11597.6 |     |
| c_y/c_z          | 56.3    | 56.3   | 49.8    | 44.4    | 39.9    | 44.4    | 39.9    | 36     | 32.7    | 29.8    | 27.2    | 32.7    | 29.8    | 27.2    | 25      | 23.04   | 21.3    |     |
| F_bending/Hz     | 434.2   | 367.9  | 391.0   | 414.0   | 437.2   | 355.3   | 375.1   | 394.8  | 414.5   | 434.2   | 454.0   | 359.5   | 376.5   | 393.8   | 410.9   | 427.8   | 445.1   |     |
| F_torsion/Hz     | 3799.5  | 3471.5 | 3675.3  | 3864.6  | 4044.7  | 3558.5  | 3726.5  | 3900.6 | 4057.6  | 4238.2  | 4399.8  | 3267.5  | 3932.1  | 4080.8  | 4223.9  | 4362.7  | 4504.8  |     |
| Stiffness (N/mm) | 21.9    | 17.0   | 20.4    | 24.2    | 28.5    | 19.2    | 22.6    | 26.3   | 30.4    | 35.0    | 40.0    | 24.5    | 28.2    | 32.2    | 36.6    | 41.3    | 46.5    |     |

Table B.1: Analysis for solution set of cantilever dimension.

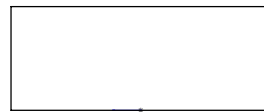
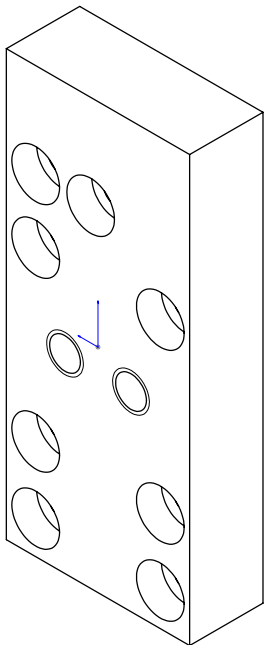
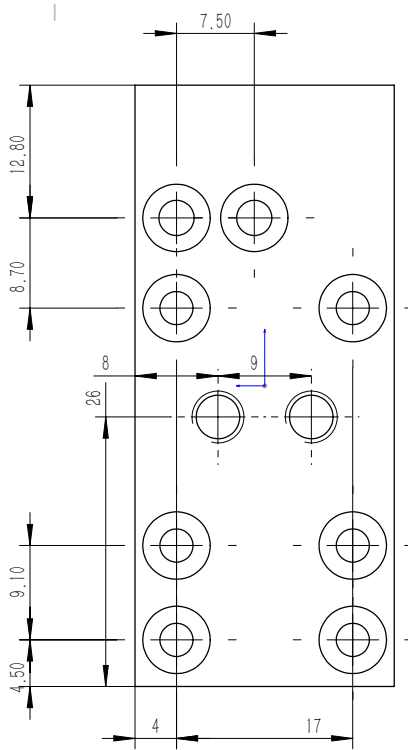
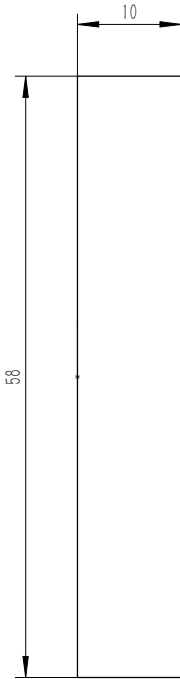


Scanner Mechanism

6



Clamping Mechanism



Closing Unit



# 7

## SUPPLEMENTARY MATERIAL: PROTOTYPE AND TEST SETUP

### 7.1. SCANNER SETUP

The scanner mechanism and the clamping mechanism are monolithically machined by spark erosion. Preload are applied by ball plungers as shown in Fig. 7.1. Since its tip is a ball, it should be pointed out that the Hertz contact stress is better to be lower than the yielding stress, especially for the ones to keep frequency tuning mechanism to stay in position. Part number Misumi BPRJ 5 is chosen. Its tip ball ( $2.4\text{mm}$  diameter) is made by Polyacetal, with Young's Modulus  $3.15\text{GPa}$  and Poisson's ratio  $0.44$ . The maximum load could be applied by one is  $20\text{N}$ , and this lead to a maximum contact stress of  $202.6\text{MPa}$  on guiding rail, which is acceptable. However, due to large expected preload and limiting space at the clamping mechanism, part number Misumi BP-8-H is chosen, with tip ball ( $4.6\text{mm}$  diameter) material 100cr6 steel and the maximum load  $62\text{N}$ . This could lead to a maximum contact stress of  $1197\text{MPa}$  at one arm of the notch hinge. Since this preload is supposed to apply one-off and remain, therefore could be acceptable.

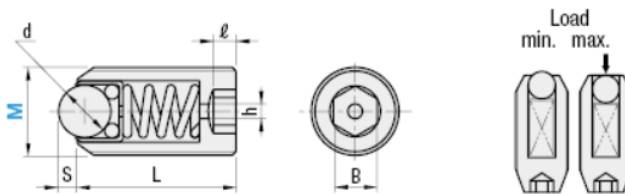


Figure 7.1: Schematic of ball plunger (from Misumi website).

Photos of the scanner setup with technical details are shown in Fig. 7.2. Coil and magnet for actuation could be seen in Fig. 7.2a. The ball plungers that apply preload for

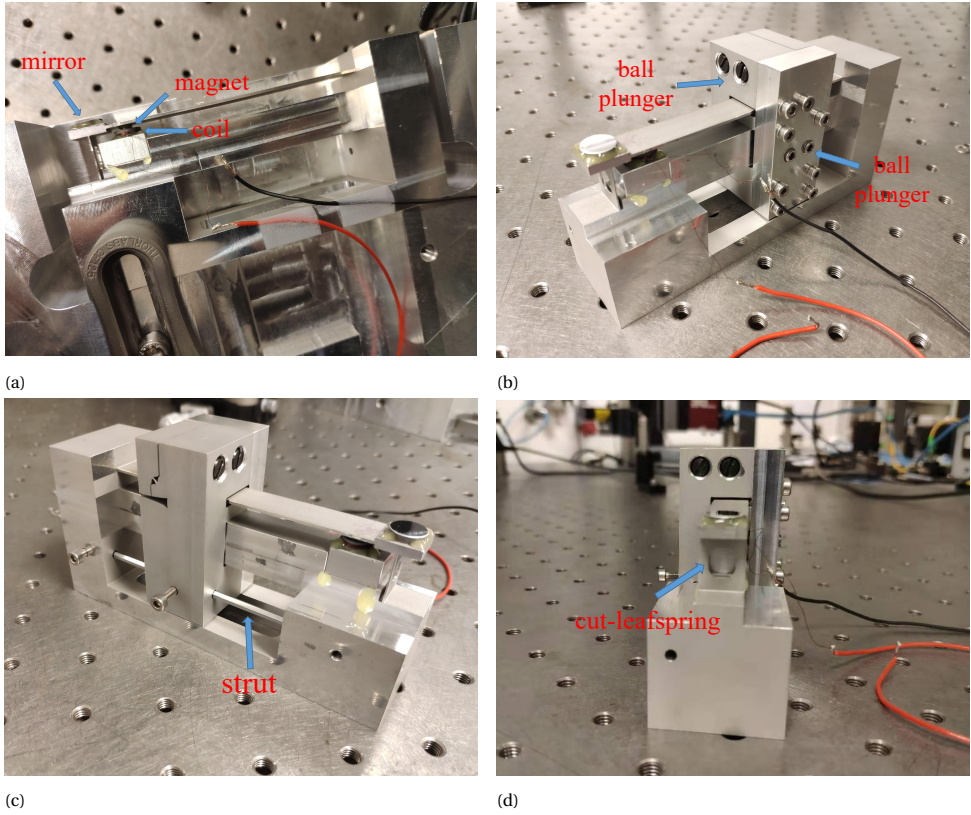


Figure 7.2: Photos of the the scanner and test setup.

clamping through the notch hinge and for positioning from the side and bottom of the frequency tuning mechanism could be observed in Fig. 7.2b. The locking strut could be seen in Fig. 7.2c, and In Fig. 7.2d, the cut-leafspring as the hinge guiding could be seen.

## 7.2. COIL DESIGN

The chosen magnet is S-04-01-N (from Supermagnet), with dimension  $4\text{mm}$  diameter,  $1\text{mm}$  height and Residual magnetism around  $1.3\text{ T}$ . To have a thin coil such that the wire could stay in the magnetic field of the magnet, it is designed with a small height but large number of layer to keep the number of turns. Coil parameters are designed as  $0.1\text{mm}$  wire diameter (Copper),  $1\text{mm}$  inner coil diameter,  $5$  turns in height, and  $20$  layer of turns. Its inductance is estimated by "Multilayer coil inductance calculator" (<https://coil32.net/>), which is around  $20\mu\text{H}$ . Resistance could be calculated as

$$R = \rho \frac{L}{A}. \quad (7.1)$$



The total wire length is  $L = 0.942m$ , cross-sectional area  $A = 0.0079mm^2$ , and resistivity of Copper is  $\rho = 0.0171\Omega mm^2/m$ . This gives a motor constant around 1.22, and the corresponding resistance of the coil is  $2.04\Omega$ . Therefore, the cutoff frequency is estimated at around 15.9k Hz. After alignment of the coil and the magnet, an air gap of 0.5mm is remained.

### 7.3. TEST SETUP

The schematic of the test setup is shown in Fig. 7.3. The input signal to the coil is generated by a function generator which also contains a current source inside. To obtain the actual current acting on the coil, a resistor with  $1\Omega$  resistance is connected in series, and its voltage difference is sampled by data acquisition device. The vision camera is accessed via Ethernet. The total setup is shown as Fig. 7.4. Fig. 7.5 shows the test setup in operation.

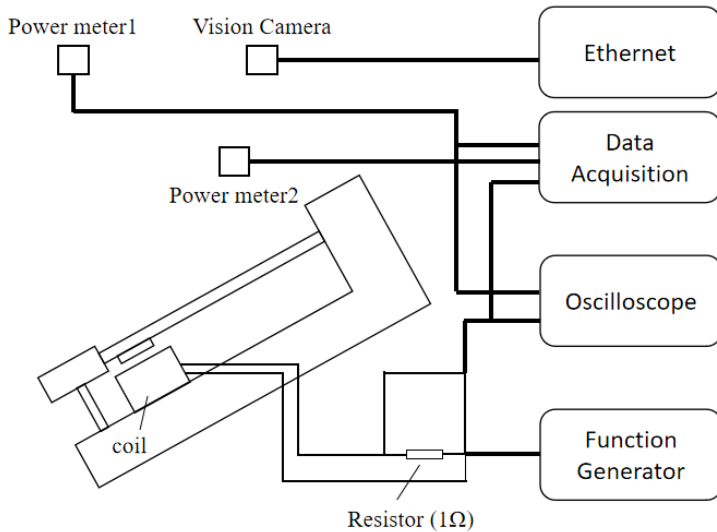


Figure 7.3: Schematic of test setup.

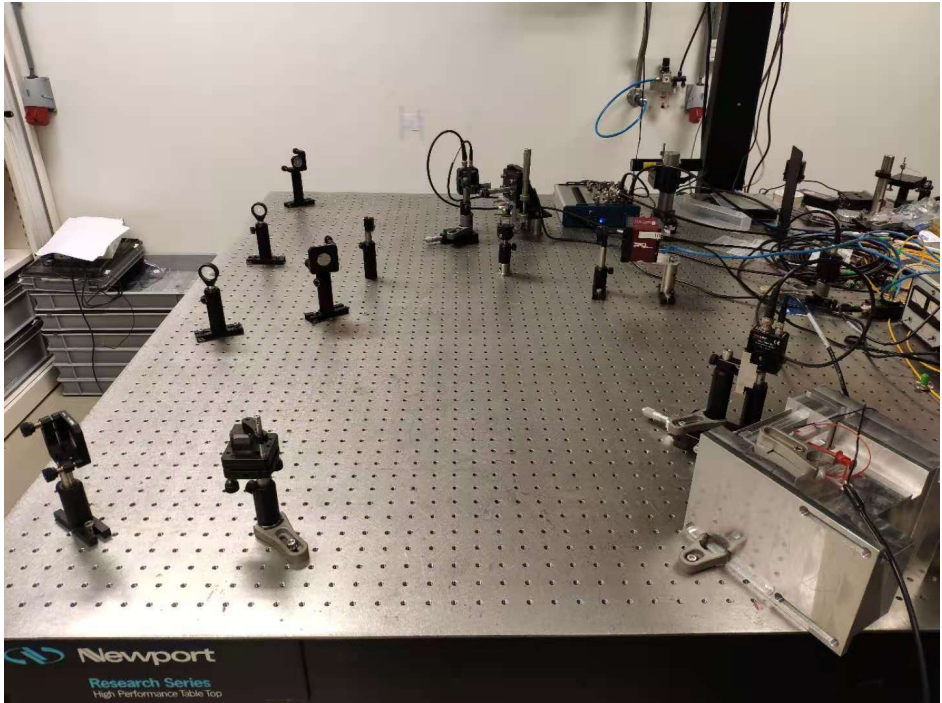


Figure 7.4: Total test setup.

7

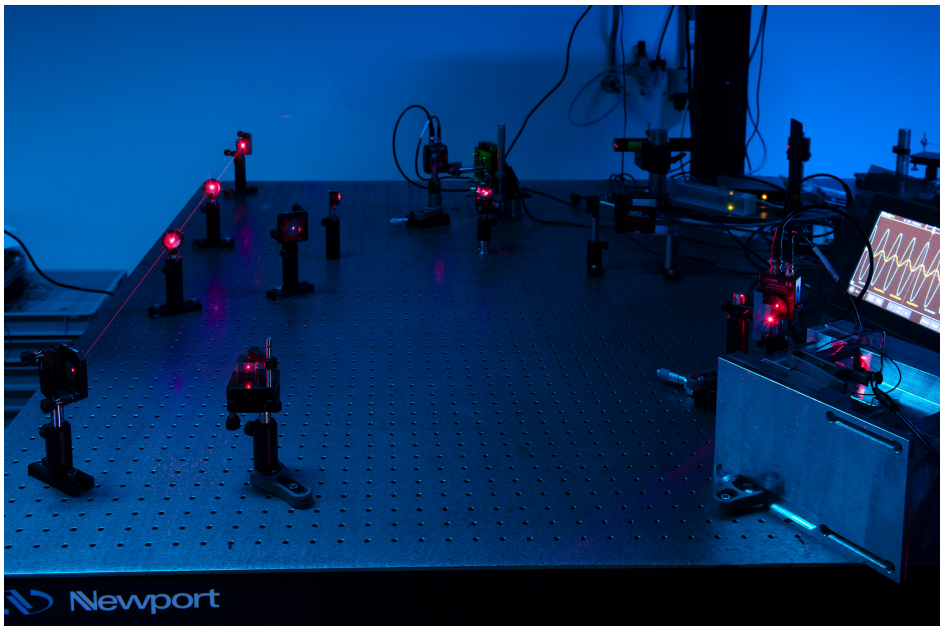


Figure 7.5: Test setup in operation.

# 8

## SUPPLEMENTARY MATERIAL: TEST RESULT

The data obtained from the power meter output are voltage change due to position change of the reflected beam. To convert this voltage information to position information, the relation between voltage and knife-edge position are obtain before measurement. This is done by moving the knife-edge with small steps and recording the voltage output from the power meter when the beam is stationary. The knife-edge is clamped by a post and then mount on a stage. It is positioned by an adjustment screw with resolution  $10\mu m$ . Fig. 8.1 shows an example when the knife-edge moves from left (negative) to right (positive) to block the beam. Fig. 8.2a shows data obtained from power meter output, and by interpolation into the data set in Fig. 8.1, one could get the beam position change at knife-edge as shown in Fig. 8.2b.

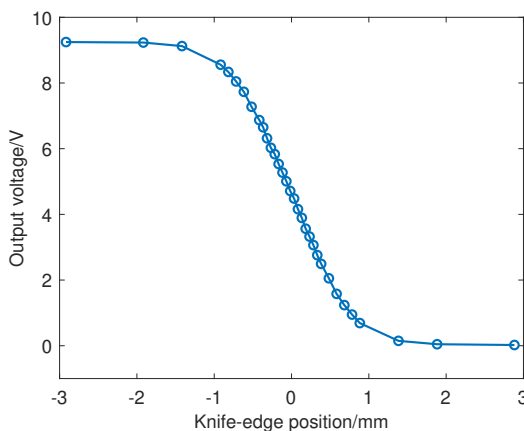


Figure 8.1: Power meter output with respect to knife-edge position.

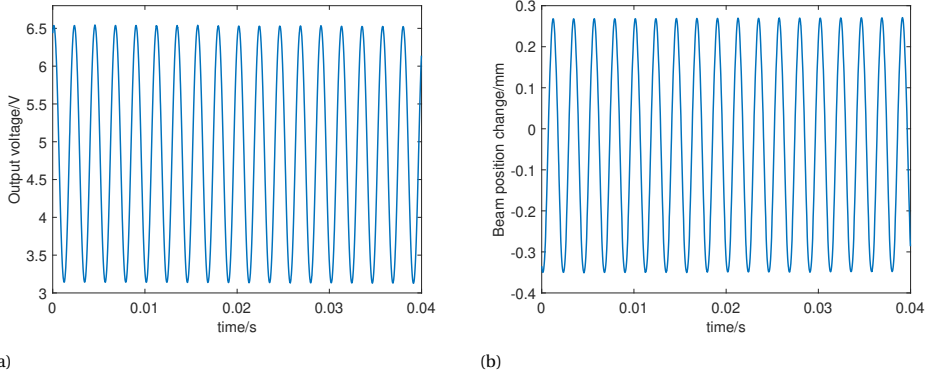


Figure 8.2: a. Power meter output. and b. corresponding beam position change by interpolation

To locate the resonant frequencies, the input signal is triggered in oscilloscope. When the output signal has a relatively large amplitude and a phase difference of  $90^\circ$  with respect to the input, the frequency is recorded as resonant frequency. Fig. 8.3 shows an example on the oscilloscope where the yellow curve is the input and blue curve is the output.



Figure 8.3: Resonance shown on oscilloscope with input (yellow) and output (blue) signal.

## 8.1. RESONANT SCAN AND TUNING PERFORMANCE TEST

Frequency response of the scanner mechanism without clamping is shown as Fig. 8.4, and the intended frequency range of 500 - 5k Hz could be divided by the four resonant peaks into four regions.

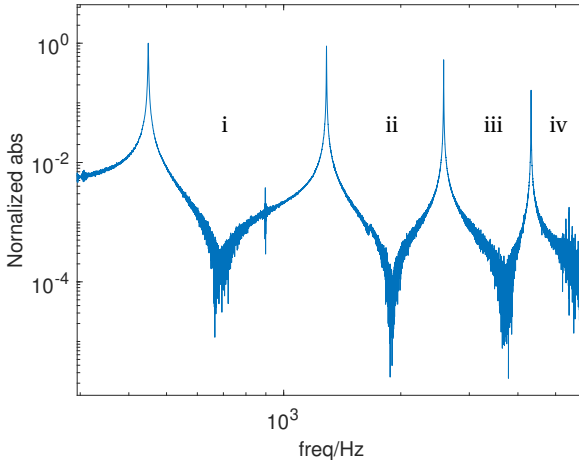


Figure 8.4: Frequency response of scanner mechanism without clamping. Gain normalized by the 1<sup>st</sup> peak.

Tuning strategy could be based on the analysis of modal behavior with respect to clamping position in Chapter 4. Test results show that frequency range iv, iii, ii, i could be covered by moving clamping to around 9, 26, 31 and 46mm from the base, shown as Fig. 8.5a, 8.5b, 8.5c and 8.5d respectively. Noting that gain at high frequency range would be relatively low, this could be partly due to the cutoff frequency of actuator. In Fig. 8.6, starting from around 2k Hz, amplitude drops with a certain slope is observed. Normalized gain at the 2<sup>nd</sup> and 4<sup>th</sup> peak is 0.8964 and 0.1627, with frequency 1288.8 and 4324.1 Hz. This corresponds to 5.5 time change over around a half decade, which could be partly related to a -1 slope when passing the cutoff frequency of the actuator. Therefore, its cutoff frequency could be estimated at around 2k Hz.

Detailed test results are shown in Table. D.1, where  $f_{FEM}$  and  $f_{test}$  corresponds to the simulation and the test results respectively.  $f^-$  and  $f^+$  is frequency lower and larger than resonant frequency with gain half of that at resonance, and therefore,  $\Delta f = (f^+) - (f^-)$ . Error  $e$  is calculated as

$$e = \frac{abs(f_{FEM} - f_{test})}{f_{FEM}} \times 100\%.$$

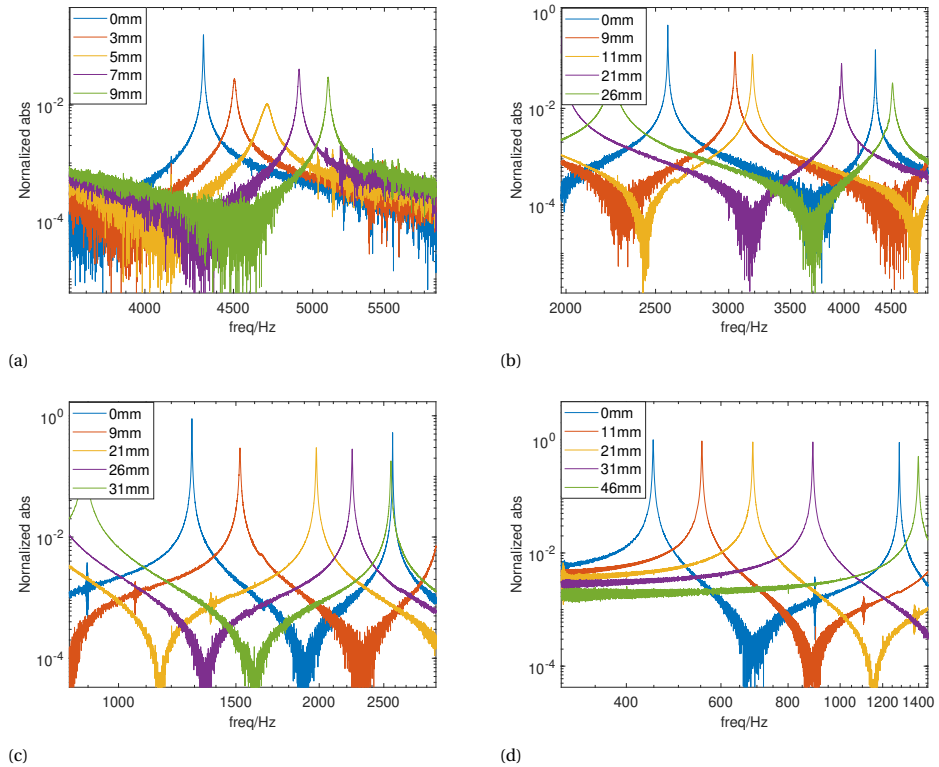


Figure 8.5: Tuning action to cover frequency range iv, iii, ii and i. Gain normalized by the 1<sup>st</sup> peak without clamping.

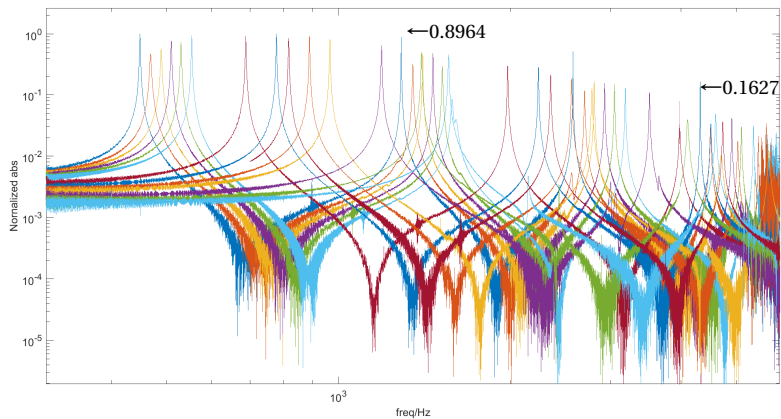


Figure 8.6: Tuning action to cover frequency range of 500 - 5k Hz. Gain normalized by the 1<sup>st</sup> peak without clamping.

| clamping/mm | 0                     | 3       | 5      | 7       | 9      | 11     | 21     | 26     | 31     | 41     | 46     | 49.15  |        |
|-------------|-----------------------|---------|--------|---------|--------|--------|--------|--------|--------|--------|--------|--------|--------|
| model       | $f_{FEW} / \text{Hz}$ | 457.61  | 485.73 | 503.84  | 524.06 | 544.55 | 567.57 | 707.59 | 802.62 | 914.01 | 1227.2 | 1450.6 | 1603.7 |
|             | $f_{REV} / \text{Hz}$ | 448.8   | 468.4  | 489     | 509.3  | 529.7  | 551.9  | 687.86 | 778.8  | 889.7  | 1189.9 | 1397.3 | 1560   |
|             | e                     | 1.93%   | 3.57%  | 2.95%   | 2.82%  | 2.73%  | 2.76%  | 2.79%  | 2.97%  | 2.66%  | 3.04%  | 3.67%  | 2.72%  |
|             | $f_{-} / \text{Hz}$   | 448.1   | 466.2  | 487     | 508    | 528.2  | 550.6  | 686.46 | 776.8  | 887.7  | 1186.9 | 1393.3 | 1556   |
|             | $f_{+} / \text{Hz}$   | 449.5   | 470.6  | 491     | 510.6  | 531.2  | 553    | 689.26 | 780.8  | 891.3  | 1192.9 | 1401.3 | 1564   |
|             | Q                     | 320.57  | 106.45 | 122.25  | 195.88 | 176.57 | 229.96 | 245.66 | 194.70 | 247.13 | 198.32 | 174.66 | 195.00 |
|             | $I_{p-B} / \text{mA}$ | 10      | 26     | 26      | 12     | 22     | 12     | 12     | 12     | 54     | 64     | 72     | 80     |
|             | $f_{FEW} / \text{Hz}$ | 1321.5  | 1406.8 | 1460.3  | 1519.7 | 1580.2 | 1647.7 | 2060.6 | 2339.8 | 2661.9 | 2931.9 | 2392.8 | 2134.1 |
|             | $f_{REV} / \text{Hz}$ | 1288.8  | 1349.5 | 1405.2  | 1464.5 | 1521.4 | 1593   | 1979.8 | 2241.3 | 2561.3 | 3001   | 2431.3 | 2148   |
|             | e                     | 2.47%   | 4.07%  | 3.77%   | 3.63%  | 3.72%  | 3.32%  | 3.92%  | 4.21%  | 3.78%  | 2.36%  | 1.61%  | 0.65%  |
| model2      | $f_{-} / \text{Hz}$   | 1287.4  | 1345.5 | 1403    | 1462.5 | 1518   | 1583   | 1976.8 | 2237.3 | 2556.3 |        |        |        |
|             | $f_{+} / \text{Hz}$   | 1290.2  | 1353.5 | 1407.4  | 1466.5 | 1524.8 | 1603   | 1982.8 | 2245.3 | 2566.3 |        |        |        |
|             | Q                     | 460.289 | 168.69 | 319.369 | 366.13 | 223.74 | 79.65  | 329.97 | 280.16 | 256.13 |        |        |        |
|             | $I_{p-B} / \text{mA}$ | 12      | 56     | 30      | 30     | 60     | 224    | 88     | 90     | 104    |        |        |        |

cont'd

| clamping/mm | 0                             | 3      | 5      | 7      | 9      | 11     | 21     | 26     | 31     | 41     | 46     | 49,15  |        |
|-------------|-------------------------------|--------|--------|--------|--------|--------|--------|--------|--------|--------|--------|--------|--------|
| mode3       | $f_{FEM} / \text{Hz}$         | 2638.7 | 2827.3 | 2935.8 | 3055.8 | 3178.5 | 3314.8 | 4147   | 4695.8 | 4973.7 | 3686.8 | 4303.8 | 4752.3 |
|             | $f_{\text{test}} / \text{Hz}$ | 2577.6 | 2699   | 2807.5 | 2927.2 | 3047.3 | 3179   | 3971   | 4510.3 | 5022.3 | 3508.9 | 4108.3 | 4596   |
|             | e                             | 2.32%  | 4.54%  | 4.37%  | 4.21%  | 4.13%  | 4.10%  | 4.24%  | 3.95%  | 0.98%  | 4.83%  | 4.54%  | 3.29%  |
| mode4       | $I_{p-p} / \text{mA}$         | 32     | 166    | 90     | 116    | 122    | 244    | 260    | /      | 220    | 352    | 350    |        |
|             | $f_{FEM} / \text{Hz}$         | 4413.3 | 4734.7 | 4914.9 | 5114   | 5318.2 | 5544.6 | 6907.1 | 7100.3 | 5622.6 | 7229.6 | 6616.6 | 5926.4 |
|             | $f_{\text{test}} / \text{Hz}$ | 4324.1 | 4503   | 4701   | 4908   | 5102.3 | 5350   | 6690   | 7158.2 | 5460.3 | 7022.9 | 6714   | 5905   |
|             | e                             | 2.02%  | 4.89%  | 4.35%  | 4.03%  | 4.06%  | 3.51%  | 3.14%  | 0.82%  | 2.89%  | 2.86%  | 1.47%  | 0.36%  |
|             | $I_{p-p} / \text{mA}$         | 112    | /      | /      | /      | /      | /      | /      |        |        |        |        |        |

1. Potting of the frequency tuning mechanism is done by hand with caliper (accuracy 50  $\mu\text{m}$ )
2. Frequencies that covered the region i, ii, iii and iv are marked by blue color
3. Frequencies that are not at usable regions are marked by gray color
4. Due to the estimated cutoff frequency of the actuator at around 2k Hz, Q factor of frequencies larger than 2.5k Hz are not tested
5. At some clamping positions, higher order modes cannot achieve above scanning angle with the maximum output current of the function generator (around 354mA peak to peak), and therefore marked by “/”.

Table D.1: Detailed test results.



## 8.2. VERIFICATION OF UNWANTED MOTION

$d_z$

According to the verification method and process presented in Chapter 4, corresponding setup is shown as Fig. 8.7, with the two beam positions  $3.6\text{mm}$  from the mirror center. Output from the power meter 2 with respect to the knife-edge position is shown in Fig. 8.8. Noting that since the expected beam movement at this knife-edge would be micron level, therefore only a small range of knife-edge movement is measured, with the step size  $10\mu\text{m}$  (resolution of the adjustment screw).

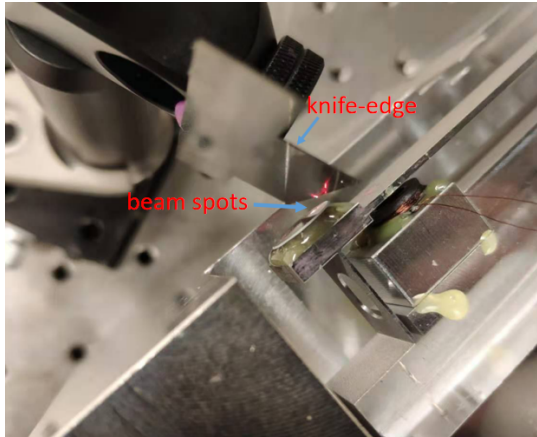


Figure 8.7: Setup of knife-edge of the power meter 2 for  $d_z$  verification.

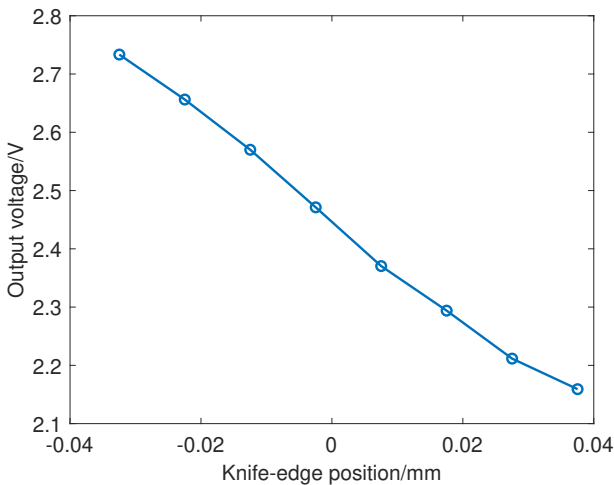


Figure 8.8: Power meter 2 output with respect to knife-edge position

Beam position changes are inferred by interpolating output from power meter 1 and 2, and they are shown in Fig. 8.9a (blue and orange respectively). Fig. 8.9b is zoomed to beam position change measured by power meter 2.  $d_z$  and  $R_x$  at the measured point of mirror could be obtained as shown in Fig. 8.9c and 8.9d. Measured  $d_z$  is around  $1.4\mu m$ , corresponding translation stroke at a distance  $3.6mm$  from the rotational axis with an angle around  $0.4mrad$ .

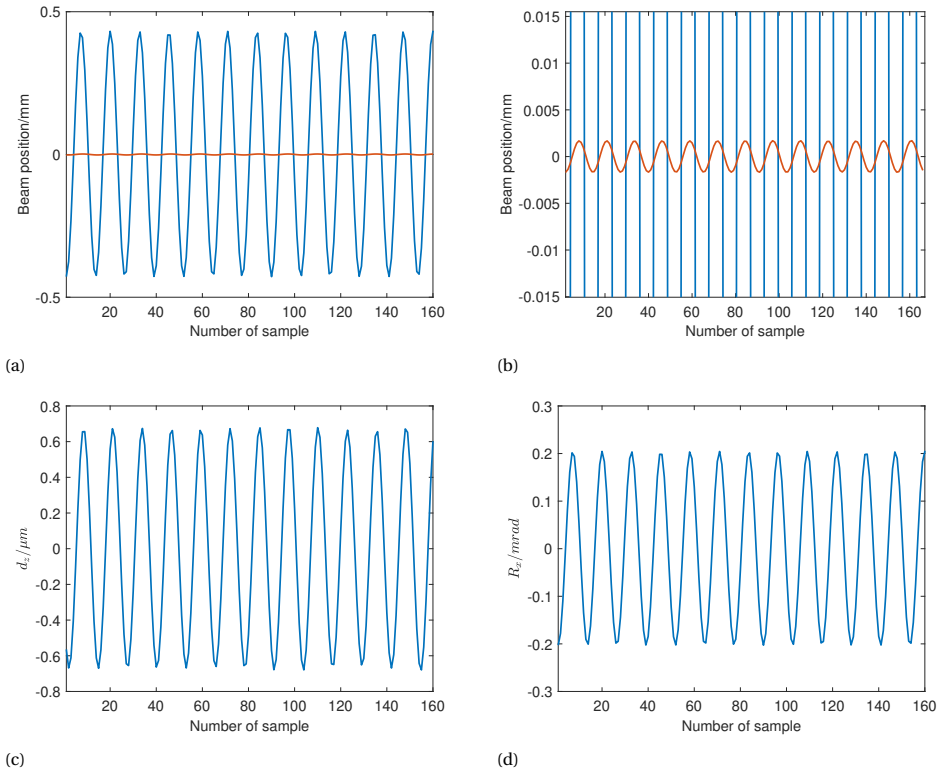


Figure 8.9: a. Beam position change measured by power meter 1 (blue curve) and power meter 2 (orange curve). b. Zoomed version of beam position change measured by power meter 2. c. Calculated  $d_z$  and d. calculated  $R_x$  at beam position on mirror. Sampling frequency  $55000 Hz$ .

### $R_y$

Corresponding setup is shown as Fig. 8.10 based on the verification process discussed in Chapter 4. Only the top knife-edge block parts of beam, and the output with respect to the knife-edge position ( $10\mu m$  step size) is shown as Fig. 8.11a. Measured gain at the peak of the transverse mode is  $2.602\mu rad/A$  (presented in Chapter 4). This corresponds to Fig. 8.11b, where an input current with  $354mA$  peak to peak at  $3053 Hz$  is given, and the measured  $R_y$  is around  $0.9\mu rad$ .

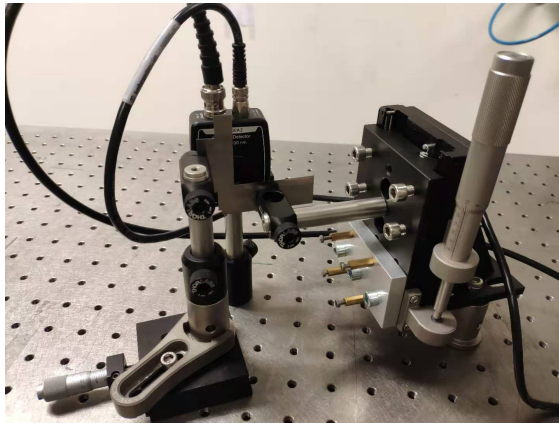


Figure 8.10: Setup of knife-edge of the power meter 1 for  $R_y$  verification.

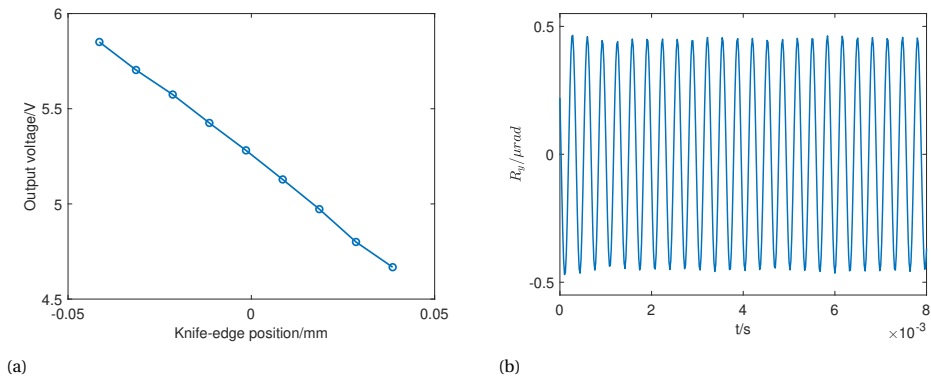


Figure 8.11: a. Power meter 1 output with respect to the top knife-edge position. and b. measured  $R_y$  with current  $354\text{mA}$  peak to peak at  $3053\text{ Hz}$ .



# 9

## CONCLUSIONS AND RECOMMENDATIONS

In this thesis, a flexure mechanism design of a tunable resonant scanning mirror is presented. This is based on a well-rounded evaluations of a variety of concepts of the whole system and detailed components. The proposed design of the scanner mechanism contains a bending cantilever as resonator and a cut-leafspring as hinge guiding to provide 1 degree of rotation. The selected tuning method is to change the effective length of the resonator beam, and this is realized by two clamping surfaces with large radius of curvature, in which one is fixated and the other is preloaded. This provides large contact stiffness and low hysteresis clamping. Sliding would be enabled by DLC coating and therefore clamping position could be changed easily. A novel resonant frequency tuning concept is proposed by exciting higher order modes of the resonator, so that scanner could achieve resonant motion in a wide frequency range.

Finite element analysis shows that by clamping from 0 to around half length of the proposed dimension of the cantilever, the 1<sup>st</sup> to 4<sup>th</sup> bending modes could cover intended frequency range of 500 - 5k Hz. However, some regions that cause coupling or hardly generate scanning amplitude should be aware. The proposed design is estimated to have nanometer level of  $d_z$  movement, and  $R_y$  would assumed to be induced by misalignment of the actuator.

The design is realized into hardware. With the presented measurement setup,  $R_x$ ,  $R_y$  and  $d_z$  are verified according to the requirement.

- **Frequency Range:** By moving the frequency tuning mechanism from 0 to around 46mm from the base, resonant frequency of scanner could cover the range of 500 - 5k Hz
- **Range of Motion:** The reflected beam could achieve a scanning angle of 1mrad, although at high frequency a relatively large current amplitude is needed. This

is partly due to the cutoff frequency of the actuator, since amplitude drop of the frequency response with a certain slope is observed starting at around  $2\text{kHz}$ .

- **Mirror Motion in Unwanted DoF:** For resonant scanner itself,  $d_z$  at the 4<sup>th</sup> bending mode is verified much less than  $100\ \mu\text{m}$  when  $R_x$  is around  $0.4\text{mrad}$ .  $R_y$  has gain of  $2.602\ \mu\text{rad}/A$  even at resonance of transverse mode, and would be much less if not at resonance. This means unwanted motions could be negligible for operation.
- **Beam Size:** The end effector stage has dimension  $12 \times 12 \times 3\ \text{mm}$ , where a mirror with  $12\text{mm}$  diameter could be placed on.
- **Size:** The prototype would occupy a space of  $127 \times 35 \times 68.9\text{mm}$ .

The actual cutoff frequency of the reluctant actuator shows a large difference compared to the estimated value. This could be related to a relatively large air gap remained between magnet and coil due to hand alignment. A recommendation is to add an iron core inside to close the magnetic circuit. This could reduce the reluctance and hence the inductance, which could increase the cutoff frequency.

Due to the use of clamping for resonant frequency tuning, a relatively tight tolerance for the bottom clamping surface is found, since this defines the reference position for clamping. Noting that some tolerance on  $d_z$  is specified in the requirement, and  $d_z$  of the proposed design is estimated to be nanometer level. Therefore, a recommendation is to place the detector array close to the scanner such that the reflected beam movement induced by the initial angle of the mirror caused by pre-deflection due to clamping error is less than that induced by  $d_z$  at the maximum tolerance. If a large distance is needed, a 1 DoF alignment mechanism could be used for the detector array.

Another essential remark to position the frequency tuning mechanism by an actuator to get a more detailed modal behavior of the prototype for avoiding modal coupling and making frequency tuning strategy. Noting that with a spindle drive ( $\approx 10\ \mu\text{m}$  positioning accuracy), tuning accuracy less than  $1\ \text{Hz}$  could be achieved.

It should be pointed out that in the test setup, the scanner is operated in open-loop. This might not have high performance for reference tracking and disturbance rejection. Therefore, some resonant controllers could be added to close the control loop if necessary. One should be aware that controller might need to be updated after each time of frequency tuning.

## REFERENCES

- [1] J. B. Hopkins and M. L. Culpepper, *Synthesis of multi-degree of freedom, parallel flexure system concepts via Freedom and Constraint Topology (FACT) - Part I: Principles*, *Precision Engineering*, vol. 34, pp. 259-270, 2010.
- [2] J. B. Hopkins and M. L. Culpepper, *Synthesis of multi-degree of freedom, parallel flexure system concepts via freedom and constraint topology (FACT). Part II: Practice*, *Precision Engineering*, vol. 34, pp. 271-278, 2010.
- [3] R. D. Blevins, *Formulas for Natural Frequency and Mode Shape*, ISBN: 0442207107, 1979.
- [4] W. Reimels, *Low Wobble Resonant Scanners*, *Proceeding SPIE 0390, High Speed Read/Write Techniques for Advanced Printing and Data Handling*, Los Angeles, U.S., September 20, 1983.
- [5] H. Soemers, *Design Principle for Precision Mechanism*, 978-90-365-3103-0, 2010.

